

# Design of a Biaxial Device for Measuring Cell Contractile Forces

A Major Qualifying Project Proposal:  
Submitted to the Faculty  
of the  
WORCESTER POLYTECHNIC INSTITUTE



In partial fulfillment of the requirements for the  
Degree of Bachelor of Science

Submitted by:

---

Todd Bitner

---

Lindsay Deitelbaum

---

Tim Ebner

---

Hristina Srbinoska

Date: April 24, 2008

Approved by:

---

Prof. Kristen Billiar

---

Prof. Marsha Rolle

## Table of Contents

Table of Contents .....	i
Table of Figures.....	iv
Acknowledgements .....	vi
Authorship.....	viii
Abstract .....	ix
1.0 Introduction .....	1
2.0 Background .....	4
2.1 Contraction in the Extracellular Matrix .....	4
2.2 Force Sensitivity and Regulation of Cellular Contractile Forces.....	4
2.3 Importance of Cellular Contractility .....	5
2.4 Culture Force Monitors .....	6
2.5 Gaps in Current Research.....	8
3.0 Project Design .....	10
3.1 Client Statement .....	10
3.2 Objectives.....	11
3.3 Functions .....	12
3.4 Constraints.....	12
4.0 Design Approach.....	13
4.1 Published Methods for Cycling Tissue Cultures.....	13
4.1.1 Spinning Disk .....	13
4.1.2 Vacuum Cycling.....	14
4.1.3 Insertion of Stainless Steel Balls .....	15
4.1.4 Linear Cycling.....	16
4.2 Proposed Design #1.....	19
4.2.1 Necessary Iterations to Proposed Design #1 .....	21
4.3 Proposed Design #2.....	22
4.3.1 Necessary Iterations to Proposed Design #2 .....	25
4.4 Proposed Design #3.....	25
4.4.1 Necessary Iterations to Proposed Design #3 .....	28
5.0 Methodology .....	30
5.0 Construction .....	30
5.1.1 Fixed Hooks .....	30
5.1.2 Vascular Clamps.....	30
5.1.3 U-beams.....	31
5.1.4 Collets.....	31
5.1.5 Horizontal Actuator Extension Beams .....	31
5.1.6 Actuator Mounts.....	32
5.1.7 Frame.....	33
5.1.8 Isolation Feet .....	33
5.1.9 Isolation Feet Attachment .....	34

5.2 Control System Overview .....	34
5.3 Verification of Subsystems .....	35
5.3.1 Actuator Motion .....	36
5.3.2 Load Cell Calibration .....	36
5.4 Bench-Top Testing of Sub-Systems.....	37
5.4.1 Fixed-Hook Testing.....	37
5.4.2 Uniaxial Tensile Test with Rice-Craft Paper .....	38
5.5 Incubator Testing of Sub-Systems .....	39
5.5.1 Thermal Drift Measurements .....	40
5.5.2 Acellular Collagen Gel.....	40
5.6 Validation .....	40
5.6.1 Uniaxial Cell Force Measurement.....	41
5.6.2 Experimental Data.....	42
6.0 Results .....	44
6.1 Verification of Sub Systems.....	44
6.1.1 Actuator Motion .....	44
6.1.2 Verification of Load Cell Calibration .....	44
6.1.3 Rice Paper Test.....	45
6.2 Validation.....	46
6.2.1 Thermal Drift.....	46
6.2.2 Acellular Collagen Testing.....	47
6.2.3 Validate Uniaxial Cell Force Measurement in Populated Gels.....	48
6.2.4 Noise Testing.....	49
6.3 Experimental Testing .....	59
6.3.1 Fetal Fibroblast and IPF .....	59
7.0 Analysis and Discussion.....	61
7.1 Verification of Sub Systems.....	61
7.2 Validation.....	63
7.3 Experimental Testing .....	65
8.0 Future Recommendations.....	65
8.1 Biaxial Force Trials .....	65
8.2 Visual Strain Analysis.....	66
8.3 Sterile System for the Purpose of Prolonged Testing .....	67
9.0 References .....	68
10.0 Appendices .....	72
Appendix A: Typical Literature Contraction Graphs.....	72
Appendix B: Objective Tree .....	74
Appendix C: Pairwise Comparison Charts.....	75
Appendix D: Morphological Chart .....	79
Appendix E: Further Importance of Cell Contraction.....	80
Wound Healing.....	80
Phenotypic Shifts.....	82
Appendix F: Motor Systems .....	84

DC Motor .....	84
Servo Motor.....	85
Hydraulic Motor.....	86
Pneumatic Motor.....	87
Stepping Motor.....	87
Appendix G: Methods for Achieving Linear Motion.....	90
Pulley System.....	90
Mechanical Sliders.....	90
Actuators.....	91
Appendix H: Measure Forces Uniaxially and Biaxially.....	94
Strain Gauge.....	94
Torque Transducer.....	95
Transducer Class Strain Gauge.....	96
Load Cell.....	97
Appendix H: Brainstorming Sketches.....	98
Appendix I: Parts List and Specifications.....	103
Portescap Digital Linear Actuator.....	104
Futek Miniature S Beam Load Cell.....	108
Air Incorporated Aluminum Extruded Framework.....	109
National Instruments 4-Axis Integrated Stepper Driver Power.....	110
National Instruments Signal Conditioning Carrier.....	111
Isonoe Isolation Feet.....	112
Appendix J: Manufactured Parts.....	113
Actuator Base.....	113
Horizontal Extension Beam.....	114
U-Beam.....	115
Foot Plate.....	116
Appendix L: Methodology Protocols.....	117
Acellular Collagen Gel Contraction.....	117
Validation of Uniaxial Force Measurement in Cell Populated Collagen Gels.....	118
Protocol and Procedure for Fetal Fibroblast vs. IPF.....	119

## Table of Figures

Figure 1: MIT CFM.....	6
Figure 2: First CFM.....	7
Figure 3: Uniaxial CFM.....	8
Figure 4: Spinning Disk.....	14
Figure 5: Vacuum Cycling.....	15
Figure 6: Stainless Steel Balls.....	16
Figure 7: Linear Cycling.....	17
Figure 8: WPI Biaxial Testing Device.....	18
Figure 9: Proposed Design #1.....	20
Figure 10: Proposed Design #2.....	24
Figure 11: Proposed Design #3.....	27
Figure 12: Fixed Hook Prototypes.....	30
Figure 13: Schematic of Final Device.....	35
Figure 14: Load Cell Calibration.....	37
Figure 15: Fixed-Hook, Two Hook Prototype.....	38
Figure 16: Proof-of-Concept Testing.....	39
Figure 17: Validation Testing.....	42
Figure 18: Preparation of Flexcell Gel.....	42
Figure 19: Uniaxial Testing.....	42
Figure 20: Load Cell Calibration.....	45
Figure 21: Proof-of-Concept Testing.....	46
Figure 22: Thermal Drift.....	47
Figure 23: Uniaxial Acellular Validation.....	48
Figure 24: Uniaxial Cellular Validation.....	48
Figure 25: Cytochalasin-D Application.....	49
Figure 26: Force v. Time Noise Reading – No Feet & No Noise.....	51
Figure 27: FFT Plot – No Feet & No Noise.....	51
Figure 28: Force v. Time Noise Reading – No Feet & Noise Created.....	52
Figure 29: FFT Plot – No Feet & Noise Created.....	52
Figure 30: Force v. Time Noise Reading – Standard Feet & No Noise.....	53
Figure 31: FFT Plot – Standard Feet & No Noise.....	53
Figure 32: Force v. Time Noise Reading – Standard Feet & Noise Created.....	54
Figure 33: FFT Plot – Standard Feet & Noise Created.....	54
Figure 34: Force v. Time Noise Reading – Isonoe Isolation Feet & No Noise.....	55
Figure 35: FFT Plot – Isonoe Isolation Feet & No Noise.....	55
Figure 36: Force v. Time Noise Reading – Isonoe Isolation Feet & Noise Created.....	56
Figure 37: FFT Plot – Isonoe Isolation Feet & Noise Created.....	56
Figure 38: FFT Plot – Incubator with No Load.....	57
Figure 39: FFT Plot – Incubator with Acellular Collagen Gel Loaded.....	58
Figure 40: FFT Plot – Incubator with Acellular Collagen Gel Loaded and Actuating.....	58

Figure 41: Force per Area .....	59
Figure 42: Force per Cell.....	60
Figure 44: Cruciate-Shaped Acellular Test.....	66
Figure 45: Eastwood/Brown Contractile Curve.....	72
Figure 46: Kolodney Contractile Curve.....	73
Figure 47: Kolodney Cyto-D Findings.....	73
Figure 48: DC Motor.....	85
Figure 49: Hydraulic Motor.....	86
Figure 50: Stepping Motor.....	88
Figure 51: Mechanical Sliders.....	91
Figure 52: Motor/Actuator.....	92
Figure 53: Versatile Beams.....	98
Figure 54: Bending Beams.....	98
Figure 55: Punch.....	99
Figure 56: “Cookie Cutter”.....	99
Figure 57: Punch with Hooks.....	100
Figure 58: Spiked Wall.....	100
Figure 59: Stud Gun Attachment Method.....	101
Figure 60: Preliminary Clamping Sketch.....	101
Figure 61: Teflon Rollers.....	102
Figure 62: Manufactured Clamp.....	102

## Acknowledgements

We would like to thank the following persons for their assistance throughout the design process:

Haseeb Ali – undergraduate Mechanical Engineering student at Worcester Polytechnic Institute

- Haseeb was working on an Independent Study Project (ISP) for Billiar labs in an attempt to measure cell contractile force in Professor Rolle’s blood vessel equivalents. Through his efforts, we were able to take pictures of smooth muscle arterial grafts with cell-derived matrices that had been attached to our device.

Jenna Balestrini – doctoral Biomedical Engineering researcher at Worcester Polytechnic Institute

- Jenna served as a co-advisor for our project and assisted us with any procedure or protocol that our team had never performed before. She served as strong moral support and twenty-four hour assistance. We owe a large portion of our results to Jenna’s efforts.

Raymond Dunn, M.D. – resident surgeon at UMass Medical School

- Dr. Dunn obtained all of the vascular clamps which were used for the attachment methods in the final device design.

Jeff John – graduate Biomedical Engineering student at Worcester Polytechnic Institute

- Jeff assisted our team with trouble-shooting of the LabView VI. His expertise made the process of creating a complicated iterative VI much easier.

Will Johnson – graduate of Worcester Polytechnic Institute and currently employee of National Instruments

- Will was integral to the load cell calibration process. He came into Gateway Park on a weekend by request and resolved all of the calibration issues that were plaguing our device.

Angela Throm – doctoral Biomedical Engineering researcher at Worcester Polytechnic Institute

- Angie assisted in some of our cell culturing and admittance into Gateway Park.

Lisa Wall – employee of the Biomedical Engineering department at Worcester Polytechnic Institute

- Lisa purchased all of our materials used in the construction of the final device design. She also accepted delivery of said items.

Lynn Worobey – undergraduate Biomedical Engineering student at Worcester Polytechnic Institute

- Lynn provided our group with rat tail collagen that she had isolated for her own MQP's experiments. This collagen was used in all of the validation tests.



## **Authorship**

This major qualifying project was completed through equal efforts from all four team members. The authors for each portion of the final submission are:

Abstract: Tim Ebner

Introduction: Todd Bitner, Lindsay Deitelbaum

Background: Todd Bitner, Tim Ebner, Hristina Srbinoska

Project Design: Todd Bitner, Lindsay Deitelbaum

Design Approach: Todd Bitner, Hristina Srbinoska

Methodology: Todd Bitner, Tim Ebner

Results: Tim Ebner, Hristina Srbinoska

Discussion and Analysis: Tim Ebner, Hristina Srbinoska

Future Recommendations: Todd Bitner

Appendices: Todd Bitner, Lindsay Deitelbaum, Tim Ebner, Hristina Srbinoska

## Abstract

In the body, cells are constantly subjected to changing levels of tension within their surrounding tissue. Fibroblasts have the ability to sense this tension and apply a reactive tension to their extra cellular matrix (ECM) to maintain an equilibrium known as homeostatic tension. Cell contractility is critical in wound closure, regeneration and plays a large role in determining the morphology of certain tissue types [19]. Homeostatic tension can be measured in vitro by placing cell-seeded scaffolds into devices called culture force monitors (CFM) [3]. Studies using CFMs have shown fibroblasts migrate through the ECM and change their shape by extending cell processes. This phase is known as traction due to the tractional forces imparted on the ECM. After the cells have elongated and formed attachments to the ECM they apply a contractile force to the ECM. A thorough understanding of these intracellular forces is essential to engineer tissue for wound healing applications that can integrate into the body.

Previous devices cycled tissue uniaxially while measuring forces along one axis [7-9, 12, 27]. Although these measurements can be used to understand the traction and contractile forces exhibited in the cellular matrix, this uniaxial design causes alignment of collagen and cellular components which is dissimilar to natural planar tissue (e.g., dermal, heart, and lung tissue, etc.). The goal of this project was to design and validate a system for measuring the contractile forces of cells cultured within three-dimensional ECMs. In addition, its simple, inexpensive and easily adjustable design enables the device to be compatible with matrices of varying composition and geometries in order to accommodate the research conducted by multiple labs. This device will be used to model cell contractile forces in skin substitutes and vascular patches, and can be used in future applications with many other types of tissue constructs.

## 1.0 Introduction

The goal of this project was to design and build a device for measuring cell contractile forces in soft tissue samples. This device will be used to understand the significance of changing cellular forces in the body. Fibroblasts, for example, impart contractile forces on their extracellular matrix (ECM) by elongating, anchoring to their surrounding tissues, and contracting the ECM inward. This contracture is critical in wound closure and tissue remodeling and frequently will determine cell morphology. Disease states, such as hypertrophic scarring – a painful and disfiguring skin condition caused by too much contracture by the fibroblasts – can be studied through *in vitro* testing. The ability to distinguish the differences in cell forces present in disease states as compared to healthy tissue is important for understanding the mechanobiology of these diseased cells. Once the cellular modeling processes of these diseases are recognized, steps can be taken to mechanically or chemically induce normal tissue remodeling.

Measuring cell forces *in vitro* is a necessary step in engineering tissues that closely mimic native tissue. Living tissue equivalents, such as the skin replacement Apligraf marketed by Organogenesis, have been FDA approved and already used for wound healing applications. In order to be compatible and functional, these implants must exhibit similar mechanical properties as the native tissue they will be replacing. This can be achieved by applying varying stimuli *in vitro* while the LTE is growing, producing a more compatible implant.

The cell contractile forces that the device is expected to measure are extremely small. Literature values suggest that collagen gels seeded with ten million fibroblasts will only contract with a force equal to the weight of ten grains of rice (approximately 0.1mN). Designing a system that can isolate these forces is difficult. In addition to biocompatibility constraints, mechanical and environmental disturbances create noise in the acquisition signal, which will

completely mask the desired forces. Previous research efforts have developed uniaxial stretching and measuring devices called culture force monitors (CFMs). Many of these CFMs cast cell-populated collagen gels in a well in the center of the device between two porous bars. These bars are attached by stainless steel suture wire to an actuator and a force transducer. The actuator ensures that the gel remains at its original dimensions, while the force transducer measures the contractile forces produced by the gel. All validation testing for the new design was first compared to the contractile force findings reported in the literature for CFMs, which were measured uniaxially and statically for 24-48 hours.

There are several major limitations with the previous CFMs. The applied gel must be cast directly into the device. This prevents the same gel from undergoing multiple mechanical tests. Additionally, the well where the gel is cast restricts the size and geometry of the matrix to be tested, which limits the testing that can be performed. Finally, and most importantly for our design, current CFMs cannot cycle and measure forces biaxially. These devices cycle tissue uniaxially while measuring forces along only one axis. Although these measurements can be used to understand the traction and active contractile forces exhibited in the cellular matrix, the uniaxial design causes improper alignment of collagen and cellular components. This alignment is dissimilar to natural tissue and, therefore, not an ideal representation of the biaxial forces expected in tissues such as dermal and cardiac tissues. These models are only capable of measuring one type of model tissue, which is typically a collagen gel. A device that could be adjusted to measure multiple types of cells in a variety of ECM scaffolds would be useful in labs investigating the tissue mechanics of several kinds of tissue.

In this project, the team was to design and validate a system for measuring the contractile forces of cells cultured within three-dimensional ECMs. It will also address the major

limitations of previous CFMs. This device will apply a load and measure the resulting contractile forces biaxially, allowing for a more accurate model of tissue loading and cellular tension *in vitro*. In addition, the device will be compatible with matrices of varying composition and geometries in order to accommodate the research conducted by multiple labs. This device will be used to model cell contractile forces in skin substitutes and vascular patches, and can be used in future applications with many other types of tissue constructs.

## **2.0 Background**

### ***2.1 Contraction in the Extracellular Matrix***

Collagen gels seeded with dermal fibroblasts undergo a reconfiguration of their extracellular matrix (ECM). During this remodeling stage, also referred to as traction, the fibroblasts slowly migrate throughout the matrix, eventually altering its shape from a spheroid into an elongated form that can create attachments to the ECM. ECM remodeling occurs during the first eight hours following the polymerization of the collagen gel [26]. Once the fibroblasts have firmly anchored themselves to the ECM, the cells begin to pull inward. This cell contraction produces a force on the matrix, which slowly realigns the ECM along the direction of applied force. A thorough understanding of these intercellular forces is needed in order to accurately model tissue engineered skin equivalents after native tissue. It is imperative that the forces produced by the collagen gels mimic those in natural skin, otherwise normal wound healing will not occur. Extensive *in vitro* studies were previously completed attempting to accurately determine these cellular forces [13]. It is important to note that cell contractile forces are not only important for the creation of tissue engineered fibroblast-seeded gels, but are pivotal mechanical forces which occur in all tissues, such as smooth muscle cell-seeded blood vessels.

### ***2.2 Force Sensitivity and Regulation of Cellular Contractile Forces***

There are two contradictory hypotheses on the mechanisms involved in the regulation of cellular contraction. One hypothesis suggests that external force on the matrix alters actin-myosin and microtubule assembly within the cells [3]. These internal cell forces are transferred to the ECM, which preserves cell shape. In this way, when a force is applied *in vitro* to a fibroblast-populated collagen gel, the fibroblasts react by producing an opposite force on the ECM. For example, an increase in external mechanical loading would be expected to be

followed by a decrease in cell contractile force, while a decrease in external loading would signal an increase in cellular contractility. Brown's study also suggests that the rate of load application is a critical factor in determining cellular response: a higher rate of loading (strain rate) is followed by a greater cell response [3].

A second hypothesis was proposed by Freyman and Gibson. This theory states that cell contractility is a 'force-limited process.' It is hypothesized that cellular contractile force is not dependent on external load, but is a standard physiological level of force applied by myofibroblasts. Freyman and Gibson normalized matrices for ECM stiffness and cellular density and found that force/cell, regardless of ECM stiffness, approached an asymptotic level of tension.

A thorough understanding of the cellular effect of applied stimuli is the basis behind the field of mechanobiology. Previous designs of CFMs used by both Brown and Freyman measured contractile forces in the matrix in a uniaxial fashion. In order to confirm either of these hypotheses on cellular responses, it is important to model CFMs after the applied strains placed on native tissue. For this reason, the ability to biaxially vary load and strain is imperative for the creation of a device to measure contractile forces.

### ***2.3 Importance of Cellular Contractility***

Understanding the process of cell contractility is critical for the study of wound closure and healing, organ regeneration, and tissue engineering. Theories on wound contracture suggest that fibroblast locomotion within the connective tissue induces wound contraction. Additionally, forces generated by myofibroblasts are transmitted to other cells and surrounding connective tissue through their gap junctions and basement membranes [30]. The magnitude of wound contraction is influenced by cell number, cell types, and culture conditions [30]. The level of

tension caused by contractile cells will lead to either the formation of fibrous scar tissue or the regeneration of healthy tissue. For an in depth description of the process of wound healing, see Appendix E.

## 2.4 Culture Force Monitors

There are many published methods for measuring cell contractile forces using strain gauges. One common method employed by labs at the University of Pittsburgh and the Massachusetts Institute of Technology involves a single fixed beam cast inside of collagen-glycosaminoglycan (GAG) matrices. When the collagen matrix begins to exhibit contraction, the deflection of the beam is measured by attached strain gauges [12]. In further experiments, multiple beams are polymerized around the collagen-GAG matrix to allow for biaxial measurement of contractile forces [35]. This method is illustrated in the diagram below:

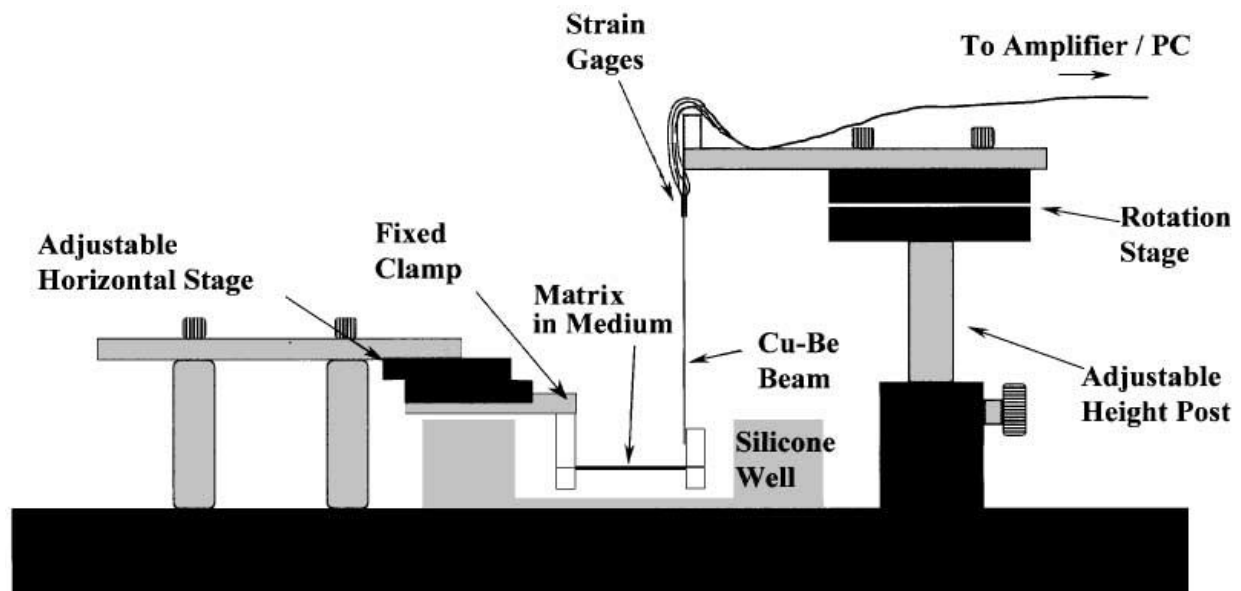


*Figure 1: MIT CFM*

A schematic of the culture force monitor being used in the Freyman labs at the Massachusetts Institute of Technology to measure contractile forces in collagen matrices. The force is measured through the Cu-Be beam by strain gauges that are attached to its top. [13]

There have been many attempts at performing biaxial stretch using novel methods. These methods will be described in brief in the Design Approach. They include, but are not limited to:



the spinning disk method created at MIT, a vacuum cycling method created by the Flexcell Corporation, and the insertion of stainless steel balls in an effort to create strain using magnetic fields.

While these methods are proven, our research was concentrated around the first published contractile monitor, now often referred to as the “typical” method of cell contraction measurement [4]. In 1994, Eastwood, Brown and McGregor conceived a device in order to measure uniaxial contractile forces in collagen matrices populated by dermal fibroblasts [8]. Their device employed four bars that had been polymerized into the collagen structure at the corners of the matrices [9]. Two of the bars were tied to a shaft, which was cycled with a microstepper motor. The other two bars were connected to a static force transducer.

A picture of the machine can be seen below.

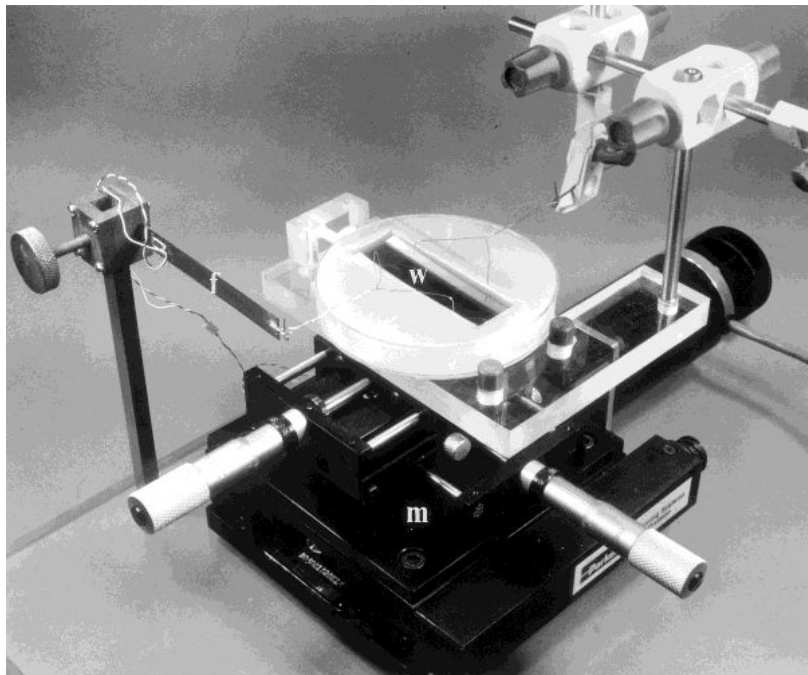


*Figure 2: First CFM*

**The first cell contractile force monitor as engineered by Eastwood, McGregor and Brown. The letter “f” denotes the force transducer, the letter “w” denotes the cell well, and the letter “m” denotes the motor system. [9]**

The wire system is much easier to distinguish in the following diagram, created by Peperzak, Gilbert and Wang for a similar system used in their labs at the University of Pittsburgh [27]:

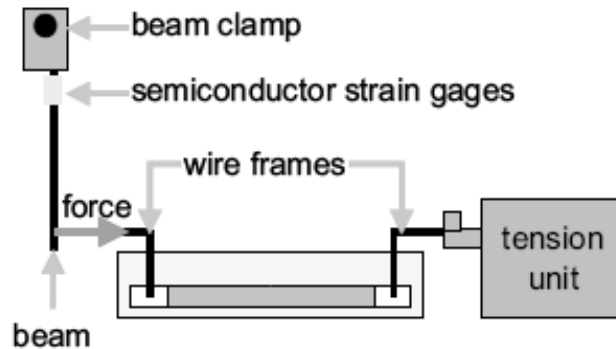


*Figure 3: Uniaxial CFM*

A simplified schematic of a “typical” uniaxial cell contractile force monitor. [27]

The collagen matrix is cycled for fifteen minutes following eight hours of culturing. Mechanical cycling is used to align the seeded fibroblast along the axis of applied force and remove stiction in the gel. The gel then not cycled for the next fifteen minutes. During this period, static uniaxial tensile forces were measured. This thirty minute process is then repeated for a period of sixteen hours to produce a tensile force v. time curve.

## ***2.5 Gaps in Current Research***

The samples used for the “typical” cell force monitors must be polymerized around porous beams attached to suture wire. These gels can only be measured inside of the CFM, and no other measurements or tests can be completed on the sample. Additionally, gels cannot be preconditioned in another device and then placed into the CFM to measure contractile forces. Due to the need for polymerized beams, current CFMs are not ideal for measuring any matrix not populated by collagen and fibroblasts. If a device were to be created to measure multiple types

of matrices – smooth muscle-seeded arterial grafts for example – new attachment methods must be examined.

Over the past decade this device has been refined in labs across the world. During this time, new methods of mimicking natural *in vivo* forces have surfaced. Current models cycle uniaxially while measuring tensile forces along two axes. They are also housed in miniature incubators to maintain *in vivo* conditions [4]. Although this explains more about the cell contractile forces placed on the cellular matrix, it does not accurately mimic homeostatic tension. There is need of a device that can both cycle and measure contractile forces along two axes. This design would be an ideal method of mimicking the forces experienced by *in vivo* collagen structures.

### **3.0 Project Design**

The purpose of the design process is to assess the client's needs and expectations. This was completed by interviewing the client and expected users and developing a client statement. Once the client statement was cemented, the device's objectives, functions, constraints and requirements were determined. Several design techniques were utilized, such as pairwise comparison charts (PCC), objective trees and a morphological chart. These steps were necessary for guiding future design approaches.

#### ***3.1 Client Statement***

Interviews were completed with the clients: our advisors Dr. Kristen Billiar and Dr. Marsha Rolle. Through these meetings, the problems with current iterations of culture force monitors (CFM) were fully explained, as well as the expectation for the design of this device. Interviews were also conducted with the expected users: Jenna Balestrini and Jeff John. Both persons were completing graduate research in Dr. Billiar's lab at Worcester Polytechnic Institute. These interviews were vital in determining future alterations to user interface and gel attachment methods. Graduate students were currently displeased with the attachment methods employed in a biaxial device used to measure gel stiffness present in the lab. Their suggestions were a major contribution to our attachment method iterations over the next six months.

A client statement was constructed that addressed all of the client's needs. The initial statement read:

*Create a device that measures cell contractile forces for the purpose of testing multiple cell matrices in a laboratory setting. The device must operate in at least a uniaxial direction, cycle a minimum of ten times, and be contained in an incubator. The project must be completed in 21 weeks.*

Following months of iterations, the final client statement was shortened to read:

*Create a device that measures cell contractile forces for the purpose of testing multiple types of cellular matrices in a laboratory setting.*

### **3.2 Objectives**

The client statement was used to identify the principle objectives expected of the device. The objectives were ranked using PCCs. To view these charts, refer to Appendix C. The initial objectives were ranked from most important to the design to least important. These objectives were:

- Reliable
- Stretching and Measuring of the Tissue
- Versatility of the Device with Concerns to Multi-Matrix Testing
- Durable
- Easy to Use
- Inexpensive

We expanded on the objectives to produce sub-objectives. These were organized into an objective tree, which can be seen in Appendix B.

Following six months of iterations to the device, these objectives were altered to reflect the final product. The final objectives were:

- Accommodate Cell-Populated Matrices of Different Geometries, Sizes and Origins
- Capable of Stretching and Measuring Force Biaxially
- Collect Reproducible and Reliable Data
- Easy to Use Interface
- Durable Construction

### ***3.3 Functions***

A morphological chart was used to identify and analyze potential functions and means for our device. The six principle functions of the device are:

- Measure Forces Uniaxially and Biaxially
- Stretch Tissue Using Computer Control
- Keep Cells at Physiological Conditions for 48 Hours
- Stabilize Itself from Internal and External Interference
- Record Data for 48 hours
- Attach Tissue without Harming Matrix and Cells

To view this morphology chart, refer to Appendix D.

### ***3.4 Constraints***

The design team was placed under several constraints involving cost, time, and the expected forces that were to be measured. The identified constraints were:

- \$5000 Budget
- 21 Week Time Frame
- Fits in an Incubator
- Capable of Accurate Measurement with Tolerable Error at the Force of 1mN

## **4.0 Design Approach**

### ***4.1 Published Methods for Cycling Tissue Cultures***

The purpose of this function is to produce tension along two axes in an attempt to naturally align the cells inside of the surrounding matrix. This will be accomplished by cycling the tissue approximately ten times immediately after it has been attached to the device. This multi-axis tension will mimic the forces occurring naturally in the body, and theoretically create the most ideal *in vitro* model for measuring cell contractile forces.

Before creating a preliminary design for the device, it was necessary to take a step back and consider which of the many methods would be optimal for loading a cell culture into the device and cycling the sample. Four plausible designs are highlighted below. Eventually, the linear cycling design was chosen as the method the device utilized to stretch the applied tissue.

#### ***4.1.1 Spinning Disk***

A design for measuring ultimate tensile strength and strain to failure of butterfly-shaped cellular specimens created by Mohr and Doyoyo at the Massachusetts Institute of Technology was examined to determine if the centripetal force being applied by their device could be used to cycle tissues. In this design, centripetal forces produce strain along the cellular matrix while the device is in motion. Once the device ceases spinning, the tissue returns to equilibrium. Figure 4 details a schematic of this cycling method.

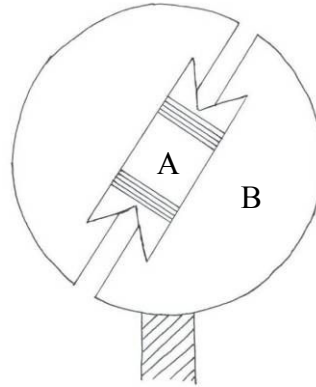


**Figure 4: Spinning Disk**

**In order to cycle tissue using centripetal force, a tissue is attached to the butterfly-shaped specimen tray (A). The device is rotated at a high velocity using a motor attached to the back of the disc. The tissue is pulled outward and its displacement is measured against notches in the butterfly tray (B).**

While this design appears to be a plausible solution for how to stretch the device using computer control, it has never been used for measurement of cell contractile forces. In fact, the paper referenced above is the only mechanical testing ever attempted on soft tissue using centripetal forces. It was feared that the majority of the time spent creating this device would be spent perfecting the cycling method, leaving little time to validate the force measurement techniques. Due to time constraints and limited literature on the spinning disk system, this method was not chosen to cycle soft tissue.

#### **4.1.2 Vacuum Cycling**

A simple method for producing strain on the cellular matrix in multiple directions is to create a vacuum below the tissue. This vacuum will pull on the tissue, often creating a large amount of displacement. The tissue can also be pulled around an object, whose shape and size can be altered to provide the desired strain on the matrix. Figure 5 is a schematic detailing the steps in this process.



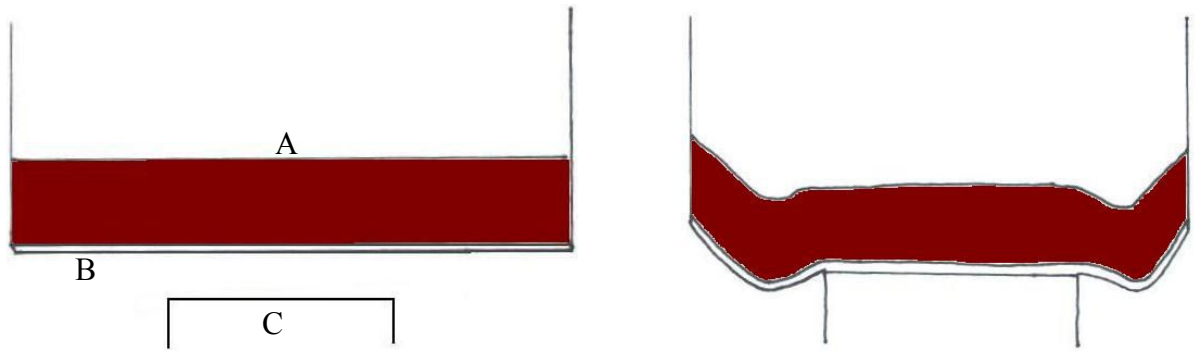


**Figure 5: Vacuum Cycling**

**In this example of vacuum cycling, a fibrin gel (A) is grown on top of a semi-permeable membrane (B). The membrane and gel are sucked down around a cylinder (C) that aids in the multi-axis cycling process. The fibrin gel is shown both before a vacuum is created beneath the membrane, and then after.**

Vacuum pressure is used to intermittently cycle the fibroblast-seeded collagen gels which will eventually be tested on our device. These gels are grown in six-well plates on a semi-permeable silicone membrane. The cycling procedure requires placing the six-well plate on top of six cylinders which match up with the semi-permeable membranes that the collagen tissue is grown on (similar to the cylinders seen in figure 5). The tissue is then “sucked” down over these cylinders with a vacuum.

A Flexcell culture system which employed this method of tissue cycling was already present in the Billiar labs, which makes this cycling process advantageous. However, it is incredibly hard to measure cell contractile forces using this method without using displacement measurements. This is a poor way of measuring contractile forces, and may affect the reliability of the device. Also, it is impossible to cycle smooth muscle cells grown into the shape of blood vessels with this method. As one of the device’s objectives was the ability to measure multiple types of cell matrices, this cycling method was not chosen for the preliminary design.

#### **4.1.3 Insertion of Stainless Steel Balls**

The tissue may also be stretched by the creation of surrounding magnetic fields. Silicone coated stainless steel balls are seeded into the matrix, and an electro-magnetic force is applied

and regulated to provide controlled force and stretch of the matrix. Figure 6 shows the set up for this method.

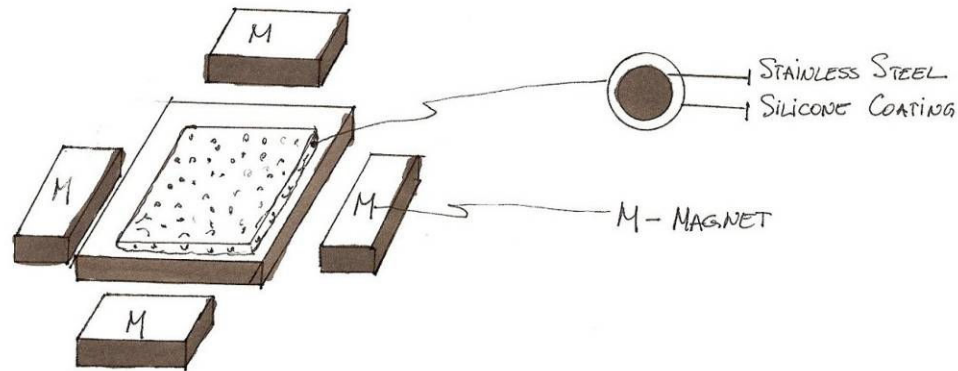


**Figure 6: Stainless Steel Balls**

The sketch shows the arrangement of the four magnets and the seeded stainless steel balls into the ECM.

Using this cycling method, all previous tissue attachment problems can be avoided and cycling can be achieved without damaging the matrix. However, there is not sufficient evidence that the seeded cells will not react erratically to magnetic fields. The cell contraction may be altered by applying these fields. There is also a possibility that the gel could rupture due to prolonged cycling of the small stainless steel balls. Due to these considerations, the use of magnetic forces to cycle soft tissue was not chosen for the preliminary design.

#### **4.1.4 Linear Cycling**

The majority of culture force monitors used in labs to measure cell contractile forces place strain on the matrix by way of uniaxial motor cycling. For this method, a stepping motor is attached to a device that converts its rotational motion into linear displacement. This may be accomplished by an actuator, a series of pulleys, or other means. The tissue is then gently “stretched” along the positive and negative axis, unloaded and allowed to return to equilibrium,

and then “stretched” again. This method can be simultaneously applied along two axes to create the desired effect of biaxial cycling. See Figure 7 for an early schematic of this form of cycling.

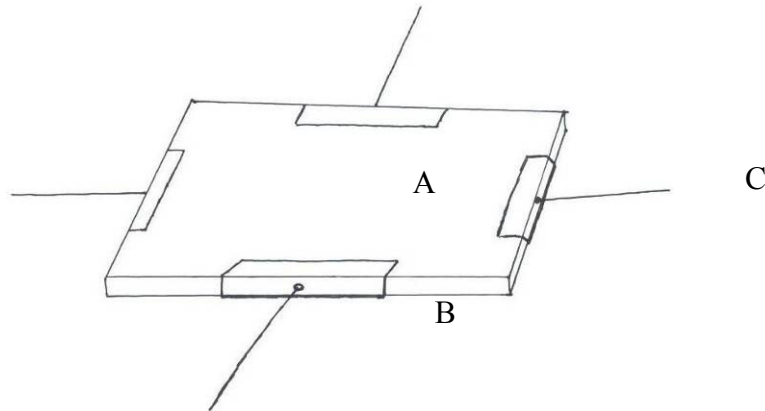


**Figure 7: Linear Cycling**

**In the linear cycling design, a tissue (A) is attached to the device by any means. In the above schematic, clamps (B) are used as the attachment method. The tissue is then stretched linearly along two axes. Above, this is performed by nylon wire (C) pulling on the clamps.**

As this is the most common method for cycling soft tissue, there is a large amount of literature providing specific ways to build this system. Additionally, the Billiar labs at Worcester Polytechnic Institute - where this project took place - contained a culture force monitor for use in measuring matrix stiffness. This device removed initial matrix tension from the attached tissue by way of linear cycling. The chief disadvantage of this design is the expected price of its components. Stepping motors and linear actuators are expensive, and would raise the anticipated cost.

The biaxial testing device for the purpose of measuring stiffness of the cellular matrix at Worcester Polytechnic Institute, applies tension and a strain rate of 10% along two axes. This procedure is chiefly used to stretch the tissue back to its original dimensions; however, it is also used to vary applied forces at a very low strain rate. Figure 8 gives a detailed schematic of the previous biaxial measurement device.

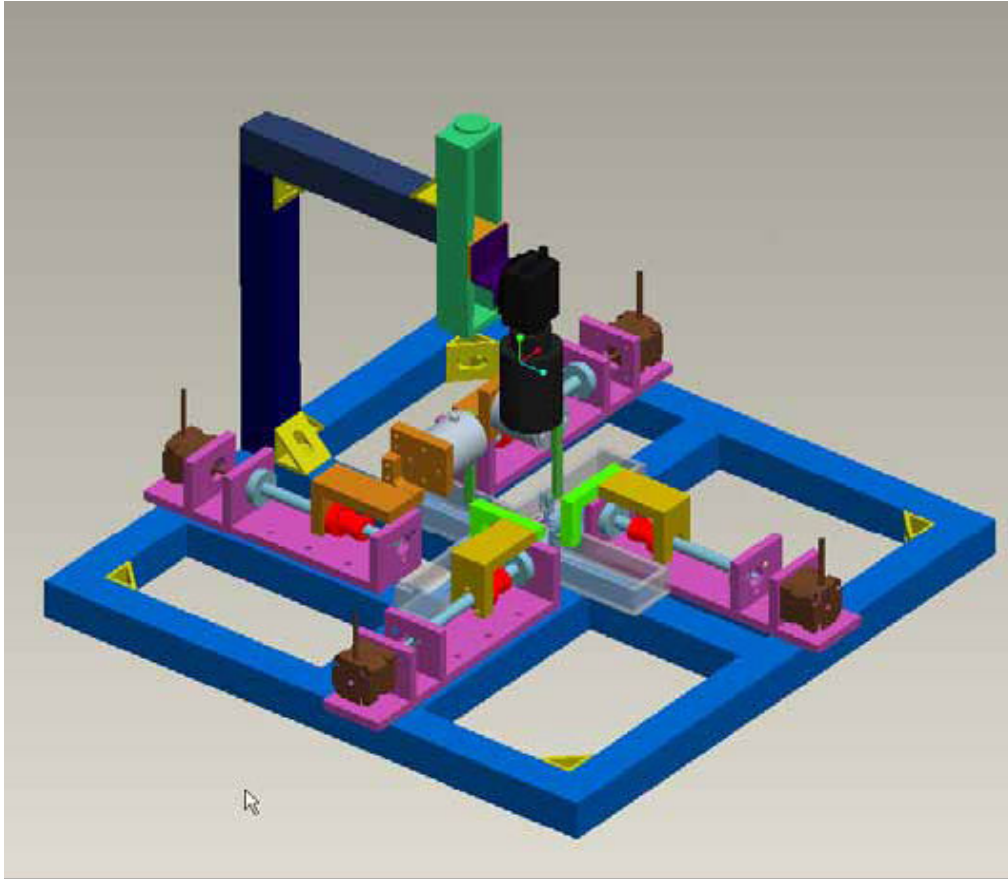


*Figure 8: WPI Biaxial Testing Device*

**This schematic shows four linear stepper motors (brown) attached to four Kerk rails (purple), two torque transducers (gray), acrylic bath (Plexiglas), and a camera (black). The sample is placed in the acrylic bath and attached to the transducers and motors by using hooks and sutures as method of attachment. The motors produce a stretching of the tissue, while the transducers measure the force applied by the tissue. The camera is used for taking images for later measuring of displacement.**

Limitations encountered with this device included difficult attachment of the gel with hooks and sutures and poor elimination of frictional forces, which can create shear stress that alter strain fields and produce inaccurate force measurements. Additionally, the device is bulky (approximately three feet by three feet) to be placed in the cell culture incubator for long-term experiments. Once these design flaws are addressed, this design is a good preliminary design for a contractile cell force monitoring device.

This linear cycling design was chosen for several reasons. The cycling system created by the previous MQP for stiffness measurement appeared promising if it could be compacted to fit

inside of an incubator. Also, utilization of a linear motor system offered a precise method of altering strain rate for different samples. These strain rates are reproducible, which will ensure accuracy of the device.

The device components used to place strains on the applied gel consist of: a motor, a method for transforming the rotational motion produced by the motor into linear motion, a motion controller, and a power source for the motor and motion controller. To learn how many types of motors and actuators operate, see Appendix F and G respectively. The device components used to measure contractile forces include: a system for implementing a Wheatstone Bridge-style strain gauge, a signal conditioner, a data acquisition board, and a power source. To learn how many types of transducers and load cells measure applied forces, see Appendix H. Attachment methods and frame construction were not addressed until further stages of design.

#### ***4.2 Proposed Design #1***

The preliminary design incorporated many of the features of the previous biaxial testing device. The device was entirely mounted onto an 80-20 aluminum slotted frame. This frame would allow the device to be easily configured, as parts could be moved around in a matter of minutes. Stepper motors were placed onto each side of the frame and connected to Kerk rails, which would translate the rotation of the stepper motors into precise linear displacement. On the end of the Kerk rails were two mounted torque transducers, one along each axis. The torque transducers were attached to the gels using lexan L-beams similar to those mounted on the previous biaxial device. The L-beams were equipped with V-jewels, which eliminated frictional forces which could cause shear stresses during cycling. The gels were suspended in a Plexiglass bath and held in place with hooks. To address the poor user interface associated with these hooks, punch mechanisms (seen in Figures 36 and 37 in Appendix H) and multi-hook alignment

devices (seen in Figure 38 and 39 in Appendix H) were evaluated to ensure exact placement of hooks for each sample. Additionally, the attachment of all hooks could be performed in around five minutes, as opposed to the estimated four hours needed for attachment of individual hooks. This design can be seen in Figure 9 below.

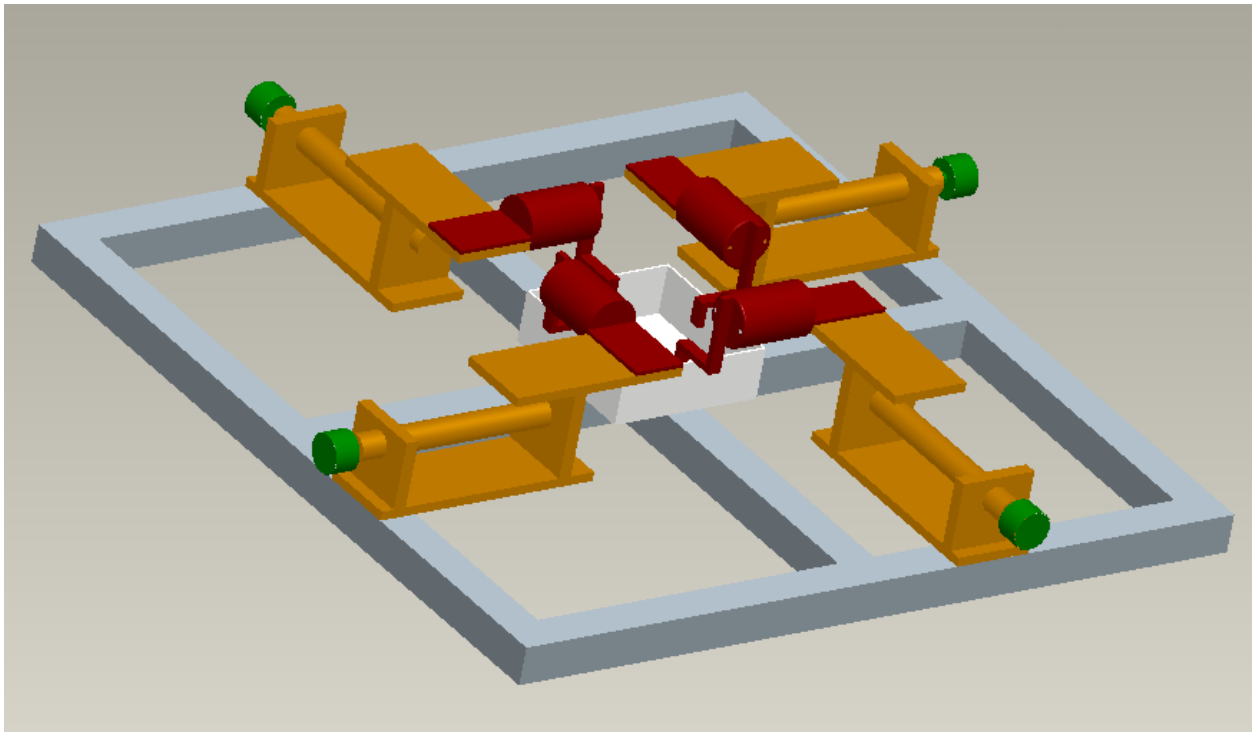


*Figure 9: Proposed Design #1*

**In the first proposed design, the green stepper motors move the Kerk rails in orange forward and backwards. The red torque transducers are attached to the top of the Kerk rails, and reach into the bath to measure contractile forces into the sample by employing an L-beam method.**

The proposed cycling system utilizing Kerk rails required approximately nine square feet of space. Due to the size of the proposed design, the device would be enclosed inside of a bioreactor that modeled incubation conditions. Unfortunately, it was too big for an incubator. Therefore, methods for regulating temperature, carbon dioxide levels and maintaining 100% humidity were evaluated.

The temperature can be regulated by creating computer controlled resistor heating units. Sensors such as thermocouples, resistance temperature detection units (RTD), or thermistors can be placed in a feedback loop to ensure that the gels remain at body temperature.

CO<sub>2</sub> regulation can be achieved by using thermal conductivity sensor, infrared sensor, or heated CO<sub>2</sub> lines. These units come with sensors that provide feedback indicating the amount of CO<sub>2</sub> present in the atmosphere. Complete air saturation can be maintained using the same mechanism.

#### ***4.2.1 Necessary Iterations to Proposed Design #1***

The use of a torque transducer was an ideal set-up for our device, as the attached beams could reach down into the Plexiglass bath without exposing the transducers to fluids which could potentially destroy them. However, the most accurate torque transducer that can be purchased without creating a custom device has a maximum range of one oz-in (~141 N-m). Literature values for previous measurement of contractile forces produced by fibroblast-seeded collagen gels indicated that the maximum expected gel contraction over a 48-hour test is approximately 6mN. These force readings were obtained from a gel with an exceptionally high cell density: roughly 10 million cells per milliliter [19]. In order to measure in the range of 6mN, a 1 oz-in torque transducer would require a beam one meter in length to be suspended from it. The torque transducer must be suspended more than one meter above the Plexiglass bath chamber, which is illogical and difficult to manufacture. Any mechanical disturbance – for example, someone walking past the device – would create a slight vibration in the long beam which would mask the contractile force measurements.

The creation of a bioreactor to house our device is outside the scope of the project. The design becomes much easier when the device is scaled down to fit inside of an incubator. Dr.

Billiar's lab has several unused incubators that have been designated for our device testing. Therefore, the method for cycling the gels – stepper motors attached to Kerk rails – must be scrapped and new electronic components capable of cycling applied gels must be researched.

The hooking mechanisms proved to be too difficult to manufacture. Several assemblies were created that incorporated four hooks that could be placed into the collagen gel simultaneously. Testing of these assemblies to determine the improvements to user interface can be found in the Methodology section. It was found that hooks were still very frustrating to use and other attachment designs were evaluated.

It was decided that in order to reduce noise created by mechanical disturbances, noise cancellation feet should be added to the device. These feet could be screwed directly into the 80-20 frame, and would ensure that the device is not sitting directly onto an incubator shelf or bench-top.

### ***4.3 Proposed Design #2***

The only components of the preliminary design that were incorporated into the second design were the 80-20 aluminum frame and the Plexiglass bath chamber. The 80-20 aluminum frame was mounted onto four anti-vibration feet purchased for Air Incorporated. These feet were leftover from the creation of the biaxial testing device, as the previous MQP group had purchased two sets. The feet consisted of four inch stainless steel legs with a rubber stopper at the base of each leg. The new Plexiglass bath now included resistors running along the base of the chamber. These resistors could be used to heat the fluid inside of the bath chamber, allowing one-hour contractile force tests to be run on a bench-top instead of in an incubator. This addition increased the versatility of the device, as both short and long-term tests could now be run in two separate environments.



Combination actuator/microstepping motors were discovered for minimal cost. Portescap sold a line of microstepping motors with a non-rotating actuator with unit prices under \$100. The maximum stroke length of the actuator was 0.9 inches, which was well within our expected range. The microstepping motor had an accuracy of 0.001 inches, so very precise strains could be placed on the applied tissue. For specs and drawings of the Portescap model 35DBM10B1B-K actuators, see Appendix I. These actuators were placed on each side of the Plexiglass bath and attached to the gels by silk suture.

These sutures were tied to alligator clips that were systematically placed along the porous polyethylene anchors in which the fibroblast-seeded collagen gels were grown. The alligator clamps were simple plastic miniature hair clips provided by one of the project members. These alligator clips proved to be difficult to attach to the collagen gels; however, they proved to be an upgrade over hooks as they could be placed precisely. Extensive testing was not performed on the alligator clamps, so analysis was not completed to the extent of previous attachment testing.

Force measurements were taken using a transducer-class strain gauge. Force transducers are capable of accurately measuring in the range of 1mN – the approximate minimum force reading expected from fibroblast-seeded collagen gels. Using two force transducers positioned along both axes of contraction would allow us to precisely measure cell contractile forces with little expected mechanical noise error. This proposed design can be seen below in Figure 10.

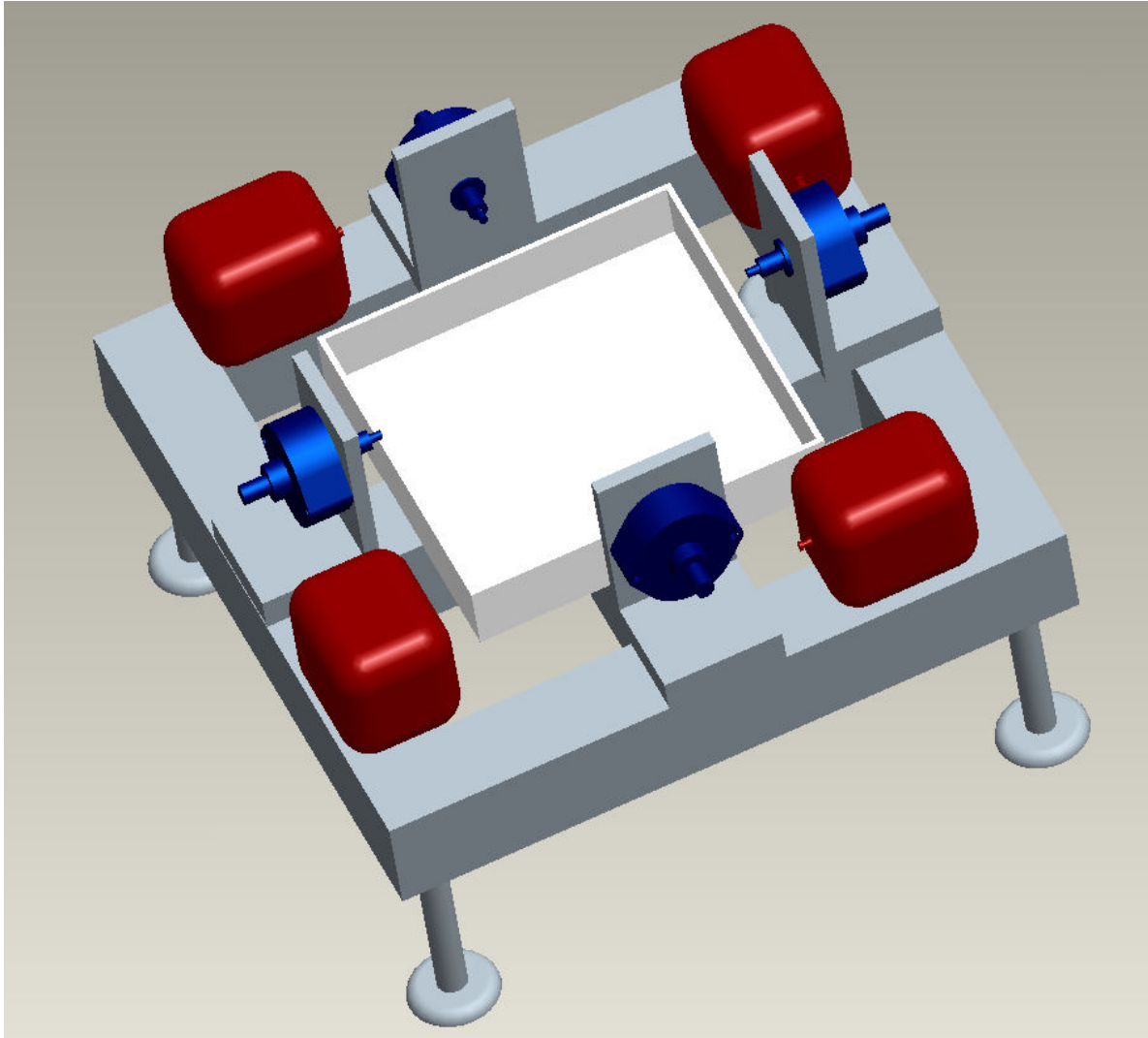


*Figure 10: Proposed Design #2*

**In the second proposed design, the blue digital linear actuators are arranged on all four sides of the bath. They are connected to the sample by a pulley system and sutures (not pictured). The red force transducers are also aligned around the bath and are attached to the sample with separate sutures.**

Force transducers measure similarly to torque transducers. Inside the device are several Wheatstone Bridge strain gauges attached to a rigid beam. For more information about how a transducer-class strain gauge works, refer to Appendix H. Whereas the beam on torque transducers is external to the device, so it can be varied in length, force transducers are equipped with a small beam protruding from one side of the transducer. This beam is typically no more than one-centimeter long; a larger protruding beam would be susceptible to breaking. Therefore,

a force transducer cannot be equipped with a long beam that is lowered into the bath as per previous proposed designs. A pulley system was theorized to translate the contractile forces created by the applied gels to the force transducer. This system kept the force transducer far away from the bath chamber so that it wouldn't come in contact with the bath fluid, which would break the transducer.

#### ***4.3.1 Necessary Iterations to Proposed Design #2***

The principal design flaw discovered in the second proposed design is the requirement of a pulley system to transfer contractile forces to the force transducer. Pulleys increase the likelihood of frictional forces producing inaccurate contractile forces findings, both between the suture and the pulley and between the pulley and the fixed pin that it rotates around. Unlike the torque transducer discussed in proposed design #1, the force transducer could not be affixed to the end of the microstepping motor and actuator. Therefore, whenever the gel was cycled, the sutures leading to the force transducer would become slack, leading to incorrect or absent contractile force readings. A solution to this problem was never devised. It was decided that this system was far too complicated and created too many chances for terrible data readings.

The proposed actuator/microstepping combination motors met all of the criteria designated by our objective to stretch and measure force biaxially. The device specifications were acceptable and the size, stroke length and cost of the devices fit all of our constraints. At this stage, the design team decided to incorporate these motors into the final device. Each proposed design from this point forward will include four Portescap linear actuator motors.

#### ***4.4 Proposed Design #3***

The third proposed force measurement instruments were low capacity load cells. A load cell in the appropriate force range and desired size was discovered. Futek Advanced Sensor

Technology manufactures a load cell with a maximum force capacity of 10g (~100mN). For specs and drawings of the Futek model LSB200 load cells, see Appendix I. Load cells measure compression and tension forces, and therefore could be attached to the end of the Portescap actuators and cycled along with the gels. For more information about how a load cell works, refer to Appendix H.

In order to minimize the size of the device, it was optimal to screw the load cell directly onto the end of the actuator. However, the tip of the actuator was manufactured with a 2-56 threaded screw, which did not match up the 4-40 thread on each side of the actuator. To ensure a tight connection between the actuator and load cell, a ¼” extensor beam was proposed. This extension would have a 2-56 tap on one side that could screw into the actuator and a 4-40 thread on the other side into which the load cell would screw.

Load cells can only measure forces that are applied along the plane of the load cell. Therefore, the load cell had to be positioned so that it was at the same height as the collagen gels floating in the bath chamber. Due to this configuration, beams leading from the load cell to the gel attachments must reach over the bath walls and descend back down to the fluid level in the bath chamber. Lexan beams were designed in the shape of a “U” (hereafter referred to as “U-beams”) that could screw into the load cell, reach over the bath, and attach to the applied gel. The stiffness of the ¼”x¼” Lexan beams would ensure the transfer of cell contractile forces directly back to the load cells. On the end of each Lexan beam, a small hook was attached that could seat a pulley. These pulleys would reduce shear stresses created during gel cycling.

The alligator clips from the last proposed design were discarded in favor of a larger manufactured clamp. These clamps would be stainless steel, consist of three sections that would fold onto themselves, and six hooks that would tightly hold the collagen gels. They could be

precisely placed and would have uniform thickness across the gel. For drawings of this clamp design, see Appendix H. The clamps would be connected around the pulley on the end of the U-beams using silk suture.

There was a concern that the weight of the U-beam would cause it to rest on the edge of the bath chamber. If the U-beam were to rub against the chamber during either mechanical cycling or force measurement, there would be a substantial error in the force readings caused by frictional forces. To offset this prediction, the bath chamber was fitted with tiny Teflon rollers below each of the Lexan beams. For drawings of this roller design, see Appendix H.

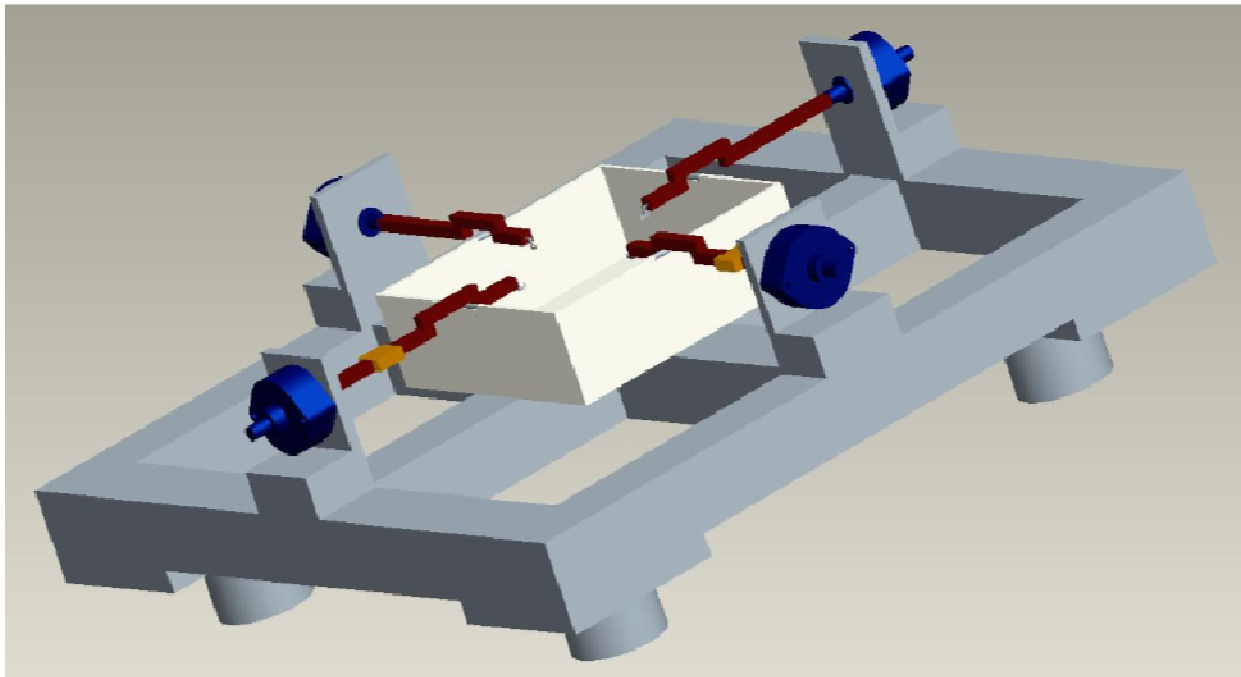


*Figure 11: Proposed Design #3*

**In the third proposed design, the Portescap actuators are placed in series with two load cells (yellow) and red Lexan beams which reach over the walls of the bath chamber. There they attach to the sample using clamps (not pictured).**

The actuators were mounted onto adjustable bases that could be moved towards or away from the bath. They were screwed directly into the frame, which also allowed them to be

disconnected and rotated around the frame quickly. For a CAD drawing of the final appearance and dimensions of each actuator base, refer to Appendix J.

The 80-20 frame maintained its shape and approximate size from the previous design, but was now mounted on top of new feet. Four Isonoe Isolation Feet were added to the frame. For more information on these feet, refer to Appendix I. These top-of-the-line noise cancellation feet decreased our expected error by further minimizing the effect external mechanical disturbances had on contractile force readings. For noise testing results comparing the final isolation feet with previous frame configurations, refer to the Methodology.

#### ***4.4.1 Necessary Iterations to Proposed Design #3***

The primary alteration made to this penultimate design was complete changes to the clamping system. The single clamps proved too difficult to manufacture, and sterilization procedures that would allow reuse of these clamps proved too large of a task to undertake. Instead, Dr. Raymond Dunn of UMass Medical provided our team with sterilized vascular clamps. These vascular clamps, manufactured by S&T Microsurgical Instruments, could be attached to the porous polyethylene anchor surrounding the fibroblast-seeded collagen gels in a matter of seconds. The clamps were equipped with Styrofoam floats to ensure that they didn't sink the gel to the bottom of the bath chamber.

At this stage of design, it was determined that a manufactured Plexiglass bath chamber was not ideal for the device. The chamber would require sterilization following each test, and new chambers would require several days to make. Disposable petri dishes offered a plastic fluid receptacle that was sterilized upon purchase and was disposable. This also reduced the amount of manufacturing required for completion of the device. This design alteration was made after

determining that the U-beams would not rest against the bath chamber and problems with friction did not have to be addressed.

The final U-beams were manufactured out of  $\frac{1}{16}$ " stainless steel rods instead of Lexan. These rods were flexible enough to be manually bent, ensuring that they were manufactured uniformly, but stiff enough to transfer all forces back to the load cell. To view the appearance and dimensions of these U-beams, refer to Appendix J. The pulleys were removed from the end of the beams; it proved challenging to keep them perfectly horizontal without cementing them in place – eliminating the original purpose of the pulleys. The sutures leading to the vascular clamps were hooked directly onto the end of the U-beams.

To attach the stainless steel U-beams to the load cell, collet holders were manufactured which would tighten around the beams when screwed tightly and release the beams when loosened. The collet and chuck used for each holder were manufactured by Dremel for use on their hand-held multi-tools. The design and manufacturing procedures used in the creation of each collet holder is discussed in the Methodology.

## 5.0 Methodology

### 5.0 Construction

#### 5.1.1 Fixed Hooks

Four prototypes were constructed and tested individually with a control clamp on the opposite side of the sample. These were constructed using varying small fish hooks, super glued to rectangular and trapezoidal geometries cut from thin plastic. Control clamps were sections of sandpaper glued to the sample.

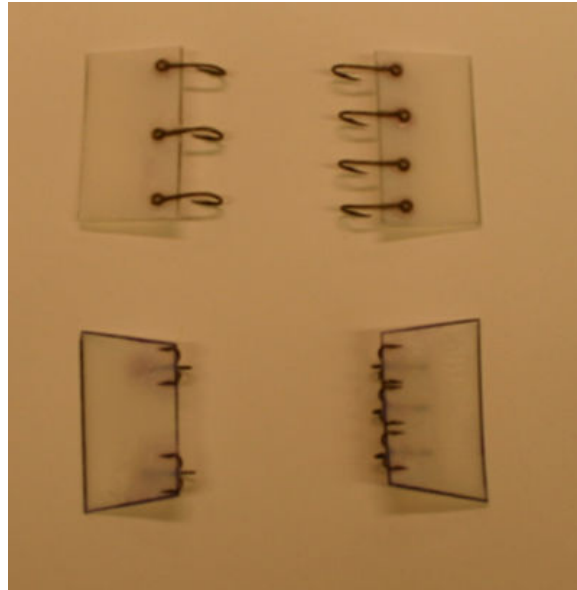


*Figure 12: Fixed Hook Prototypes*

This image shows (from top left, clockwise) 3, 4, 3, and 2 hook prototypes. Also considered was the shape of the holders, either rectangular or trapezoidal.

#### 5.1.2 Vascular Clamps

Micro-vascular clamps were used to clamp onto the samples. These clamps proved to work with gels with and without anchors, were easier to apply, and damaged the sample less frequently than previous methods of attachment. The clamps appeared to close on the sample with negligible slipping of the gel or deformation at the attachment site, indicating a minimal stress concentration at the grips. In addition, Styrofoam beads are easily fixed onto the clamps in



order to float the clamps and sample in the bath chamber. Silk sutures were tied to the clamps to provide a loop to put over the stainless steel u-beams.

### ***5.1.3 U-beams***

Beams were fabricated from 1/8<sup>th</sup> and 1/16<sup>th</sup> inch stainless steel. The 1/8<sup>th</sup> inch was very difficult to bend at sharp angles and seemed to be heavier than needed. The 1/16<sup>th</sup> inch was easier to bend at angles close to 90° and their light weight would minimize off axis force on the load cell-actuator assembly.

### ***5.1.4 Collets***

An apparatus was required to tightly hold the stainless steel U-beams in place during testing, but also to release them between tests to allow free movement of the bath chamber. This objective was achieved by manufacturing collet holders capable of functioning with a Dremel 1/16” collet and chuck. The collets and chucks were purchased at a hardware store, and were not manufactured by the design team. However, the chucks require an odd screw size that cannot be purchased, and therefore the holders had to be created on a lathe. The holders were manufactured from 1/2” aluminum rod stock on a Haas lathe found in the Washburn machine shop. Four units were made with the dimensions found in Appendix J. A 4-40 threaded hole was tapped into the back-end of each collet holder. In this way the collets were attached to the load cells and horizontal extension beams.

### ***5.1.5 Horizontal Actuator Extension Beams***

Proposed Design #3 called for the actuators to be placed in a horizontal line with the load cell, collet, U-beam and clamp. This configuration proved to be quite unwieldy, as each side of the device now required approximately nine inches of space to function. A two foot by two foot

device was not considered compact enough to easily fit into an incubator, so options for shortening the device were explored.

The final design employs a parallel configuration of the load cell and the actuator. A horizontal extension bar connects the actuator, which extends away from the bath chamber, with the load cell and collet. These horizontal beams were manufactured from ¼” thick aluminum stock, and are approximately 2.5” long and ¼” wide. The dimensions of the horizontal extension beams can be found in Appendix J. The beams were tapped with two different threaded holes: one 2-56 thread which was capable of screwing onto the end of the actuator and one 4-40 thread which was capable of interfacing with the load cell. To attach the load cell to the beam, a 4-40 screw was threaded through the horizontal extension beam until a small portion of the threaded rod was visible on the other side of the beam. The load cell was then screwed onto the exposed threaded rod. This configuration saved approximately three inches per side of the actuator, and allowed the final configuration to measure only 11.5” by 11.5”.

#### ***5.1.6 Actuator Mounts***

An adjustable base for each actuator was created from solid angle aluminum stock [for CAD drawings of these bases, see Appendix J]. Two 5/16” wide x 1” long grooves were drilled into one side of the L-bracket, in order to allow the base to move towards and away from the test chamber. Three holes were drilled into the other side of the L-bracket. A 1.4” in diameter hole was drilled into the center of the L-bracket face, into which an actuator was fitted. The actuator was secured by placing by inserting screws through two 4-40 threaded holes on either side of the larger actuator hole.

### ***5.1.7 Frame***

The frame was constructed using extruded 80-20 aluminum. The stock was cut in order to build a frame that was 10x10 inches through the centerline of the pieces. All hardware needed to assembly the frame was included. Simple construction was completed by using a single sized Allen wrench and the hardware components provided.

### ***5.1.8 Isolation Feet***

Cancelling external noise became the biggest challenge faced during the design process. It was estimated from literature reviews that the lowest contractile force that should be expected from collagen gels used in our validation protocols (discussed later in section 5.0) was 0.1g (10mN). This value was 1/100 of the load cell's capacity, which hinted that the load cell may not be accurate at these levels. Additionally, external noises such as footfalls or the natural vibrations of the incubator created readings on the load cell which were higher than the expected measurable results. Reliable noise cancellation feet were researched, so that the device would not simply be measuring external noise instead of contractile forces.

Anti-vibration feet are often purchased to stabilize manufacturing or testing devices. There are many standard options that can be found online. These anti-vibration feet are composed of a steel leg connected to a rubber foot and are screwed into the base of the machine. Typically used to cancel large disturbances that may offset manufacturing production, these feet are rated for heavy machines and do not isolate the device from small vibrations.

Further options for anti-vibration feet were researched, leading to the purchase of the Isonoe Isolation Feet [for specifications, see Appendix I]. These feet are top-of-the-line noise cancellation units manufactured for DJ turntables. The outer shell and legs the isolation feet are made of magnesium instead of steel, as they are not rated for thousand-pound CNC machines,

but rather 20 pound turntables (the device weighs approximately 14 pounds). The interior is cradled by viscoelastic polymer bands specially designed to cancel small vibrations. The effect of the Isonoe isolation feet on the transference of external vibration to the load cells mounted on the device can be seen in results of the noise testing.

### ***5.1.9 Isolation Feet Attachment***

The Isonoe isolation feet were manufactured with threaded rods (metric screw size 5) as legs. They could not be directly attached to the aluminum frame of the device, therefore plates were attached to each corner of the base of the frame [for CAD drawings of these plates, see Appendix J]. The plates were 3"x4"x1/2" and made of aluminum stock. They contained three threaded holes: two 1/4"-20 threaded holes in order to screw each plate into the special nuts received with the frame and a third threaded hole through which the isolation feet were attached.

These plates can be easily manufactured from another material; this would be the easiest way to add weight to the device. The use of stainless steel plates would add a few pounds of excess weight, which could be useful in stabilizing the device against external noise. Aluminum was used only after it was deemed impossible to cut stainless steel and lead stock to size due to a lack of appropriate tools.

## ***5.2 Control System Overview***

The schematic below shows the set up of the data acquisition and motion control. The load cell is connected to a power supply for 5 volt excitation and a SCC-SG24 National Instruments strain gauge module that is a component in the NI SC-2345 Signal Conditioner. This signal conditioning block is connected to the computer, where National Instruments Measurement and Automation, and LabVIEW software is used for data acquisition. The NI PCI-7334 motion controller was used because it could control four axes, and as with the previous components was

readily available for use in the lab. The yellow boxes indicate the placement of two load cells (100mN  $\pm$ 0.05mN; Futek Advanced Sensor Technology, Irvine, CA). The grey colored actuators show the perpendicular arrangement to achieve biaxial stretch (Danaher Motion Portescap; West Chester, PA).

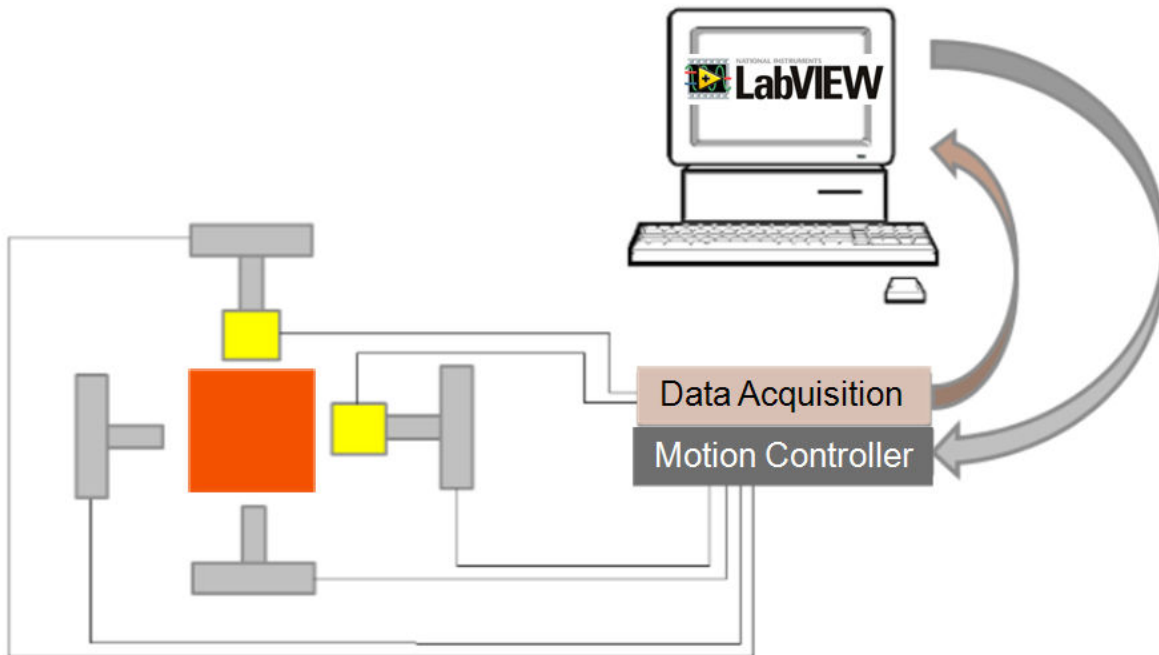


*Figure 13: Schematic of Final Device*

**This schematic shows the data acquisition and motion control capabilities of LabView. The force readings obtained from the load cell were collected in LabView. Additionally, the actuators were moved by the motion controller, also powered by LabView.**

### ***5.3 Verification of Subsystems***

Before complete construction of the device, we needed to verify that each individual component worked as it was intended. This involved testing the actuators, validating the load cells, verifying the noise dampening capability of the isolation feet, performing bench top studies and experiments in the incubator with acellular samples. The following work verified that all systems functioned properly and in unison.

### ***5.3.1 Actuator Motion***

The actuators were reported to have a step size of 0.001”/step. National Instruments Measurement and Automation software was used to verify this. Markers were placed on the actuator and a step size of 600 steps was input into the software. After each movement calipers were used to determine the size of displacement. To compensate for human error thirteen displacements were measured. These values were averaged and the displacement/step was calculated.

### ***5.3.2 Load Cell Calibration***

Load cell calibration was necessary to verify the accuracy of the data sheet provided with the device. To accomplish this, the device was powered by a 5 volt DC power supply. A multi-meter was attached to the load cell and mV output was recorded in the laboratory notebook. A series of various weights were suspended from the load cell, and the mV output was recorded upon each subsequent weight. This procedure was repeated as the weights were removed and the mV/gram ratio was recorded. The load cell was suspended from a rigid beam; therefore its initial weight was zeroed after input the values into Microsoft Excel. From this raw data, a mV/gram chart was developed, the slope of which was compared with the calibration factor reported on the data sheet supplied by the manufacturer. This slope was found to be identical with that reported on the manufacturer’s data sheet.

To verify the mV to gram calibration factor; weights of unknown mass were suspended from the cell. The mV output was recorded and the experimental calibration curve was applied, then the mass of the object was verified by measurement on a laboratory scale.

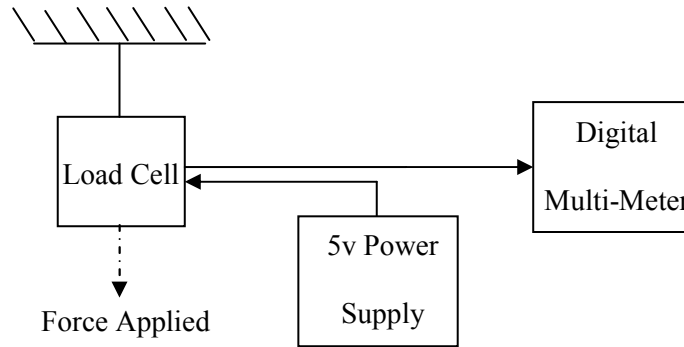


**Figure 14: Load Cell Calibration**

This figure shows the set-up for the load cell calibrations.

## **5.4 Bench-Top Testing of Sub-Systems**

In order to verify the efficacy of the device bench-top studies were performed. This enabled the team to test design possibilities, determine the ability of the various parts of the device to perform their intended function, and make needed iterative changes.

### **5.4.1 Fixed-Hook Testing**

The team tested a fixed-hook system. This test was designed to evaluate the efficacy of a ‘fixed-hook’ attachment method. This design is best described as an array of small hooks that are secured in position along a rigid fixture. In this way it is hypothesized that the user will more easily be able to attach the sample to the device. Specifically this device would alleviate the need to insert individual hooks, while retaining the advantages of the hook system. The objectives were to: apply fixed-hook prototype w/ current biaxial device, investigate the feasibility of a fixed-hook system, evaluate ease of attachment, compare the differences in hook number, evaluate manufacturing methods, and investigate possible manufacturing methods.

The acellular testing sample was made of a latex square, about 1 square inch. This material was chosen due to its higher strength and elasticity than the matrices that will be used on the device. The latex allowed for testing the prototypes at higher forces than are expected during

normal use, which allowed for evaluation of damage to the sample and integrity of the manufacturing methods used.

Uniaxial tensile testing was completed with the current biaxial device. This was done to evaluate the holding force of the manufacturing methods described previously. In addition, these tests allowed for evaluation of the feasibility of a fixed-hook system from initial attachment to tensile testing. Four tests were conducted with one clamp per test, while the control clamp opposite the fixed hook was constructed using sand paper and a quick drying adhesive.

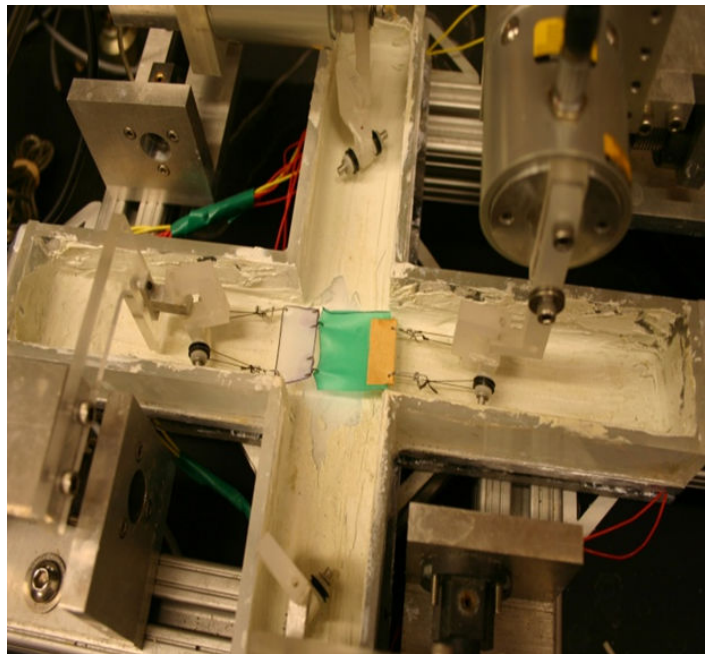


*Figure 15: Fixed-Hook, Two Hook Prototype*

**Uniaxial testing showed feasibility of attachment method. This process revealed mechanical strength of the hook device and revealed additional loading complications**

#### ***5.4.2 Uniaxial Tensile Test with Rice-Craft Paper***

A uniaxial tensile test using rice paper was performed to test the following components: clamps, pulleys, bath, u-beams, collets, actuator, and a load cell. Objectives for this experiment were as follows: evaluate the ability of the clamps to hold the sample, evaluate the effectiveness of the suture method to attach the clamps to the beams, determine the effectiveness of the pulley



wheels at minimizing friction, evaluate the u-beam collet interface, verify load cell output and precision, verify actuator precision and motion

The 25mm sample of rice paper was gripped with vascular clamps. Monofilament nylon sutures were used to attach the clamps to the pulleys. Pulleys were placed onto the U-beams without any securement method; however, pretension was used to keep the suture-pulley interface taught. U-beams were secured to the device by attachment to the customized collets. A 4-40 thread screw was used to attach the collet directly to the load cell.

National Instruments software, Measurement and Automation, as included in LabView package was used to cycle the sample at 6% absolute strain with seven second delay between application of strain and relaxation. A virtual instrument (VI) was created using the LabView software to obtain and calibrate the load cell data acquisition. This data was exported to an excel file for analysis.

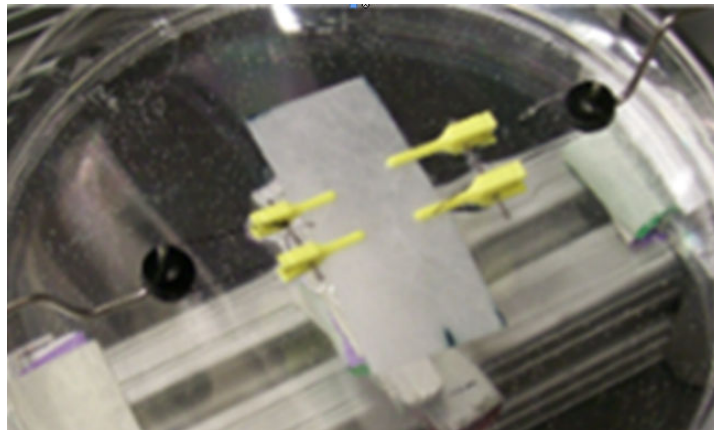


*Figure 16: Proof-of-Concept Testing*

Above is the device loaded with a rice paper sample in a uniaxial static arrangement. Note the initial use of pulleys placed on the u-beams, intended for reduction of friction.

### ***5.5 Incubator Testing of Sub-Systems***

In order for the device to obtain long-term data on cell seeded gels, it must function within an incubator, where temperature and CO<sub>2</sub> levels are kept at physiological conditions.

First it was important to compensate any readings for the effect of temperature change on the device, therefore thermal drift measurements were obtained. Also, an acellular collagen gel was used as a model in order to save time and cells, to show the device could function within the incubator.

### ***5.5.1 Thermal Drift Measurements***

It was important to quantify any thermal drift in force measurement after the load cell is moved from room temperature into the incubator at 37 degrees Celsius. The device was setup as if a test were to be completed in similar fashion to the rice paper test. The setup was then moved into the incubator and data was acquired until a stable force reading was obtained for an extended period of time

### ***5.5.2 Acellular Collagen Gel***

First, a PDMS channel was produced by casting PDMS into the lid of a 60 mm Petri dish. The 25 mm wide channel was then cut from the dish, leaving a hydrophobic trench for which to cast the collagen gel. Poursous polyethylene anchors were placed into the trench for the gel to cast into and to provide a surface to grip with the vascular clamps. The collagen was cast following the protocol in KLB026-004 at a collagen concentration used in Eastwood and Brown, 1994. The gels were allowed to polymerize for three hours to be sure they could withstand transplantation from the dish and into our device. Upon loading into the device, the gels were stretched to the original 25 mm width, including the anchors. Data acquisition was acquired until force equilibrium was obtained.

## ***5.6 Validation***

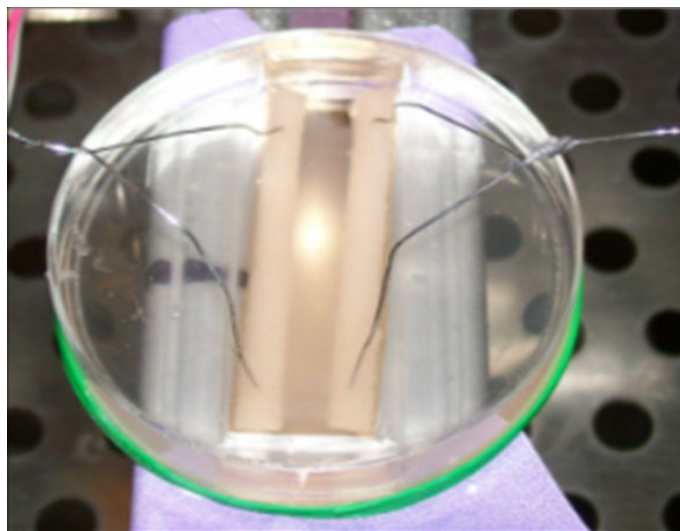
There are a variety of factors that could cause false readings that appear to be cell force. It is important to follow previous methods and show the device is capable of repeating

previously published data. To do this, one of the first culture force monitors was used as a reference. Experimental data was also gathered to validate that the device was capable to working with gels grown in a Flexcell culture plate.

### ***5.6.1 Uniaxial Cell Force Measurement***

In order to validate the efficacy of the force measurement data obtained using this device it was necessary to reference previous literature. Previous culture force monitors used fibroblast seeded collagen gels cast between two porous polyethylene anchors, which were secured to the device via stainless steel suture wire [8]. The cell density, collagen concentration and device setup were replicated using our device. Gels were cast in a PDMS channel and force measurement data was recorded over 24+ hours.

To determine that the force output was gel contraction and not thermal drift, as well as to distinguish active cell force from passive force of the gel Cytochalasin-D was added after 24+ hours. The concentration to volume of application must be optimized to maximize its effect on the cells. Significant changes in volume can change force read by the load cell, however, concentration of Cyto-D must be high enough to take effect.

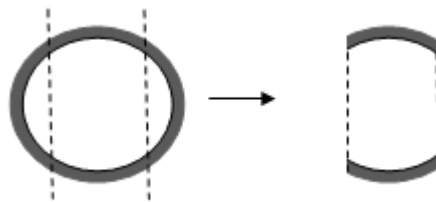


**Figure 17: Validation Testing**

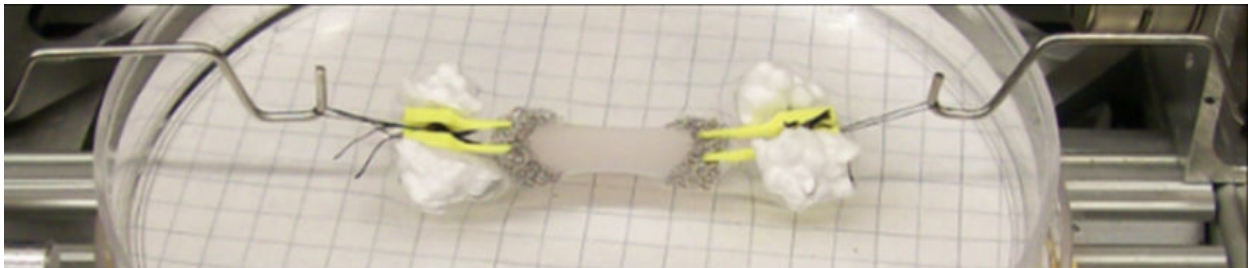
**A fibroblast-seeded collagen gel cast between porous anchors and stainless steel suture wire for the purpose of uniaxial validation.**

**5.6.2 Experimental Data**

Gels grown and preconditioned in Flexcell culture plates were tested using our device. The gels were removed from the silicone membranes and parallel cuts were made to provide a sample that could be tested uniaxially, shown below:

**Figure 18: Preparation of Flexcell Gel**

**This diagram shows the appropriate surgical cuts made to the collagen gels used to perform experimental testing.**

**Figure 19: Uniaxial Testing**

**The samples were cut and then placed into the device. They were stretched back to their original dimensions and then allowed to contract.**

After cutting the sample the gels were gripped with vascular clamps, to which polystyrene beads were attached. The clamps and sample were suspended in a PBS bath (9:1 H<sub>2</sub>O: PBS) that had been warmed in a 32 degree celcius water bath. The sample was then stretched to its original dimensions and force data obtained for 10 minutes in order to minimize cooling of the

PBS bath and sample. In an attempt to see active cell force KCl was then applied and testing continued for 10 minutes.

## **6.0 Results**

This chapter summarizes the data from the verification and validation completed during the design methodology. Data included in this section verifies the proper functionality of the individual components of the device. Additionally, representative data from the bench-top and incubator validation is presented in this section.

### ***6.1 Verification of Sub Systems***

The data below verifies that the actuator and load cells used in our device work properly and as their function requires. It was important to verify the specifications reported by the manufacturer before attempting to construct and test the complete device. In addition it was crucial in this process to ensure that the various other components, (clamps, beams, collets, etc.) would function as intended.

#### ***6.1.1 Actuator Motion***

Using the National Instruments software, Measurement and Automation the velocity of the actuator was set to 200rpm, and acceleration and deceleration to 100rpm, it was found that the stepping rate was not dependant on the target position assigned. When a step distance of 600 steps was input, the device would actuate 0.06 inches; 0.0001 inches per step. Also, it was found that by just changing the target position's sign, the actuators could be moved in either direction. This experiment showed that could actually microstep the actuator to achieve a precision higher than expected. This capability was confirmed by the manufacturer.

#### ***6.1.2 Verification of Load Cell Calibration***

The results of the load cell calibration indicated that the data sheets provided by the manufacturer were accurate. A total of eight data points were recorded per test. The figure below is a representative test. The slope of the curve indicates the calibration factor and was

compared to that which was reported on the manufacturer data sheet. The experimental calibration curve was exactly the same as reported on the data sheet.

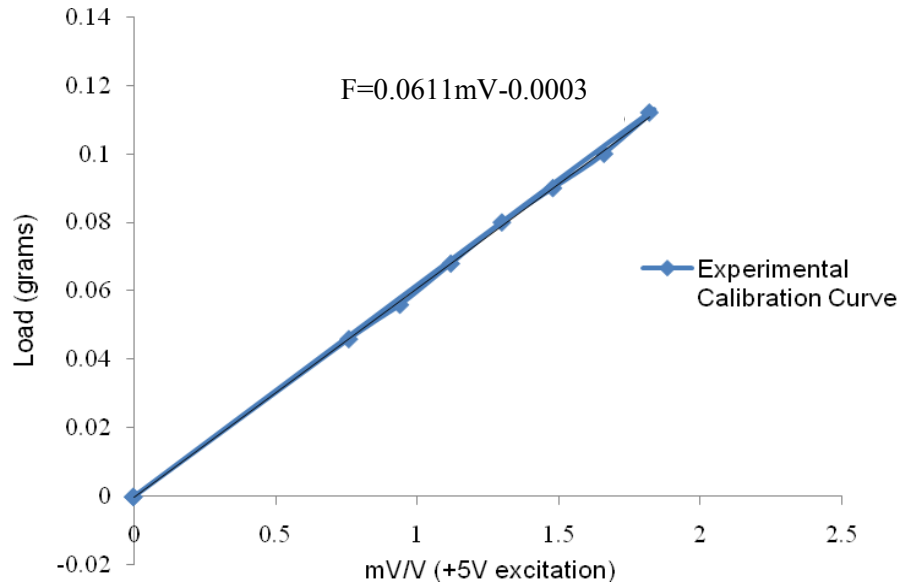


**Figure 20: Load Cell Calibration**

*The experimental calibration curve determined by applying various weights and recording the mV output of the load cell.*

### **6.1.3 Rice Paper Test**

After calibrating the load cells and showing that the actuators are suitable for the measurement of cell contractile forces a simple proof of concept test was performed. This test was a uniaxial tensile test, which required two actuators and one load cell. In order to mimic a cell seeded gel, a sample of rice paper was used, which is a standard for such tests. The sample was dynamically stretched and the force was measured. These results can be seen in Figure 21 below.

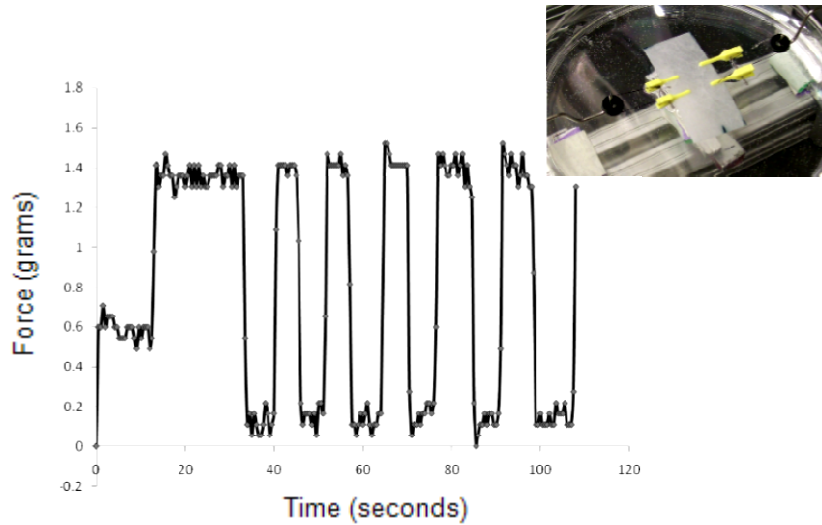


**Figure 21: Proof-of-Concept Testing**

Dynamic stretch of a rice-paper sample. Force data was recorded over six cycles (about 2 minutes).

## 6.2 Validation

The follow data was obtained in order to validate the cell force readings obtained during testing cell seeded gels. As shown in previous research [8], the 37°C temperature in an incubator causes a change in force readings; therefore, thermal drift data was obtained for the device. Also, in order for validation of our device, previous research needed to be repeated in an attempt to achieve similar values, only in this way can we consider the data obtained in the future valid.

The force values obtained from the following data show thermal drift over time, acellular collagen gel and fibroblast seeded collagen data over 20+ hours in an incubator.

### 6.2.1 Thermal Drift

A test of thermal drift was performed to determine how long the components in the incubator needed to “warm up” before the force readout of the load cell was constant. As seen in Figure 22 below, the thermal drift equilibrates over ten hours.



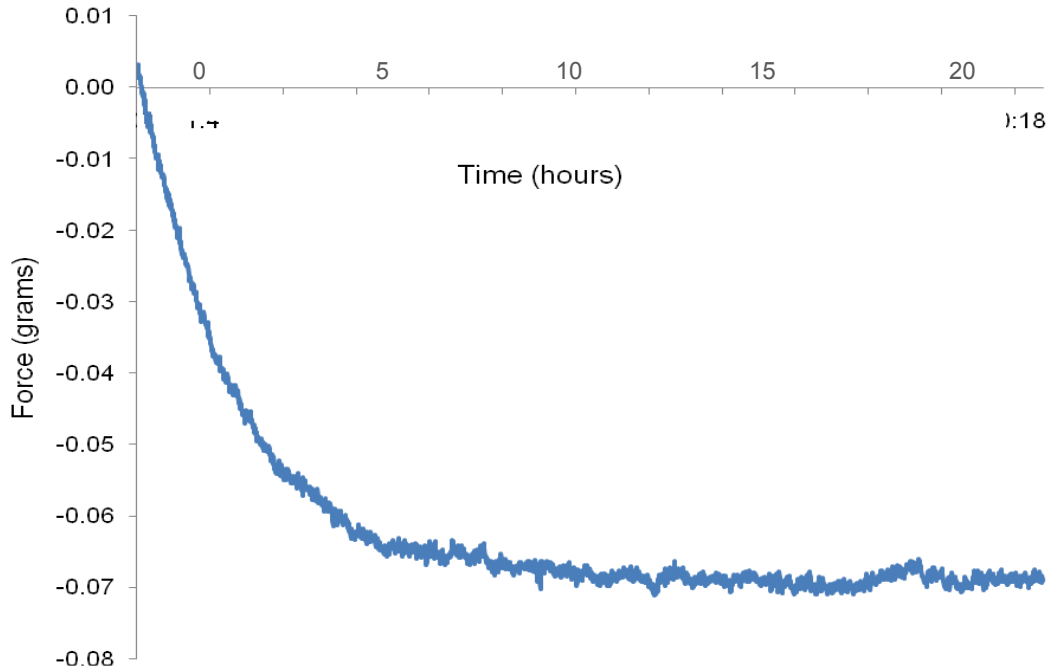
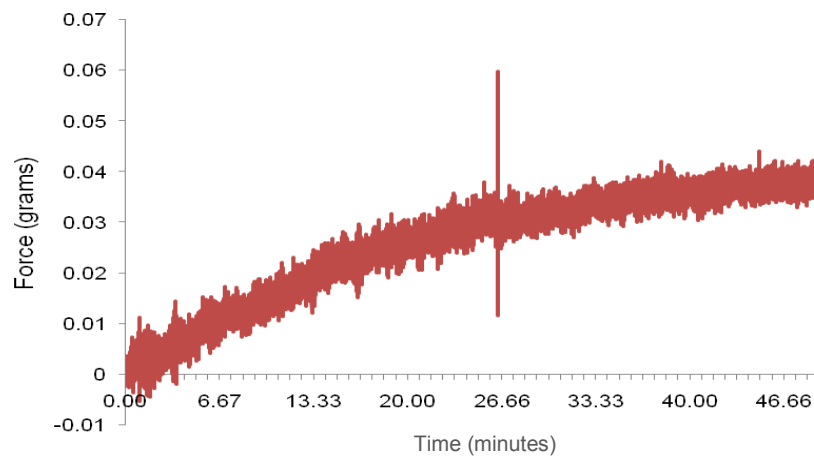


**Figure 22: Thermal Drift**

The thermal drift of the device when placed in an incubator. The test took place over 20 hours, with equilibrium achieved at 10 hours.

### 6.2.2 Acellular Collagen Testing

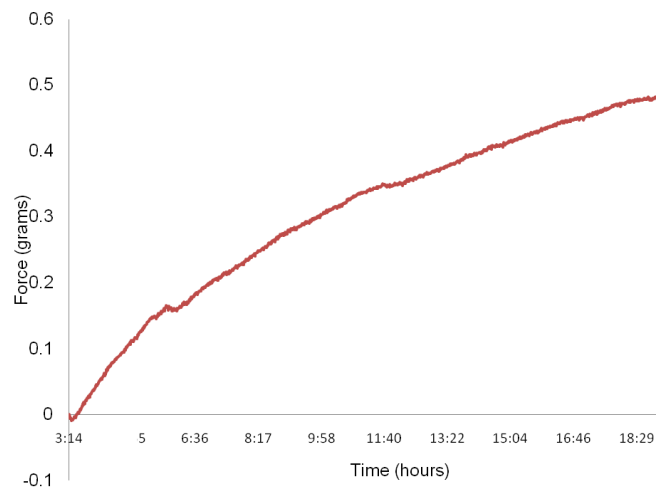
Acellular testing of a collagen gel in the device was performed to determine the exact protocol and timing of steps for testing the cell populated collagen gels. Additionally, this test provided data on how long the collagen gel took to equilibrate to a maximum force.



**Figure 23: Uniaxial Acellular Validation**

**Acellular collagen was cast into the device and allowed to contract. This test was completed inside an incubator.**

As shown in Figure 23, the acellular collagen gels equilibrated to a maximum force of 0.035 grams after 50 minutes. The sharp peak at 26 minutes is attributed to lab interference (i.e. opening and closing of the incubator door).

**6.2.3 Validate Uniaxial Cell Force Measurement in Populated Gels****Figure 24: Uniaxial Cellular Validation**

**A fibroblast-seeded collagen gel was cast into the device and allowed to contract. This test was completed statically inside an incubator.**

Figure 24 shows the force started equilibrating after eighteen hours and the maximum force obtained was approximately 0.48 grams. Data before three hours was excluded due to unacceptable levels of noise caused by adjusting the experimental set up.

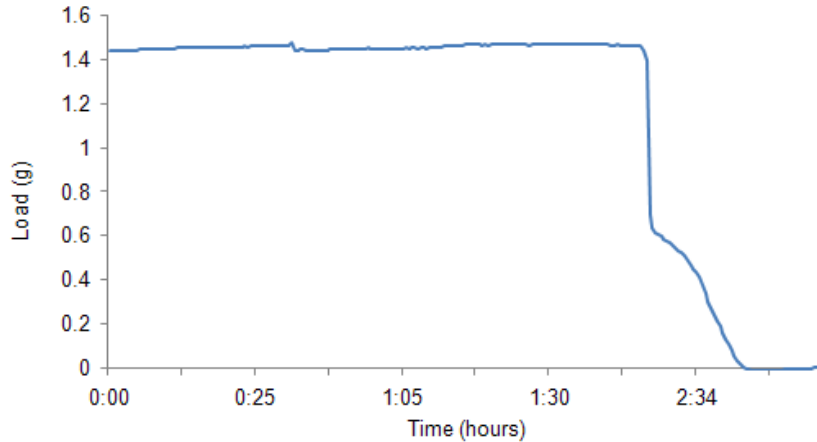


**Figure 25: Cytochalasin-D Application**

After 24-hours of polymerization, the fibroblast-seeded collagen gel was assumed to have reached equilibrium. Cytochalasin-D was applied to disintegrate the cytoskeleton, causing a sharp drop in contractile force.

Figure 25 shows that after the gel polymerized for 24 hours the application of Cytochalasin-D resulted in the force within the gel going to zero. These data would indicate that after 24 hours the cells were actively applying about 1.4 grams of force on their collagen matrix.

#### **6.2.4 Noise Testing**

Minimization of the effect of ambient disturbances on the load cell force readings was important for ensuring accurate contractile force measurements. Any mechanical disturbance, for example: if someone open and closed the incubator door, could jar the sample out of place and ruin a 40-hour test. Even if the sample was not ruined, the amount of force read by the load cell during this disturbance would be at least ten times the size of the contractile force. The final contractile force curve would have an aberrant force reading that would dwarf the remainder of the data points. For an example of literature contractile force curves see Appendix A.

In hopes of reducing this noise, the device was placed onto Isonoe Isolation Feet (see specifications in Appendix I). In order to gauge the noise-reducing effects of these feet, and

ensure that the load cells were not simply reading environmental noise rather than contractile forces, noise validation was completed.

Throughout the following tests, two samples were taken using LabView. A simple fast fourier transform (FFT) VI was created in order to determine the sampling frequency at which the device readings were most affected by noise. A FFT plot compares the sampling frequency (Hz) with the amplitude (V) that the load cell is transmitting to the data acquisition board. A second VI was run simultaneously to acquire the intensity of environmental noise read by the load cell in the same conditions as the FFT plot. This graph is displayed as force as a function of time.

It was first necessary to verify the affects of the noise isolation feet. To complete this experiment, three test groups were chosen: the device with no feet attached, the device equipped with standard metal and rubber feet, and the device with the viscoelastic and magnesium Isonoe feet. These readings were performed on the lab bench top. Each test was completed twice, once with no environmental disturbances and once with a project member jumping up-and-down approximately one foot from the device. The magnitude of these disturbances can be viewed in the Force v. Time graphs which accompany the FFT plots below.

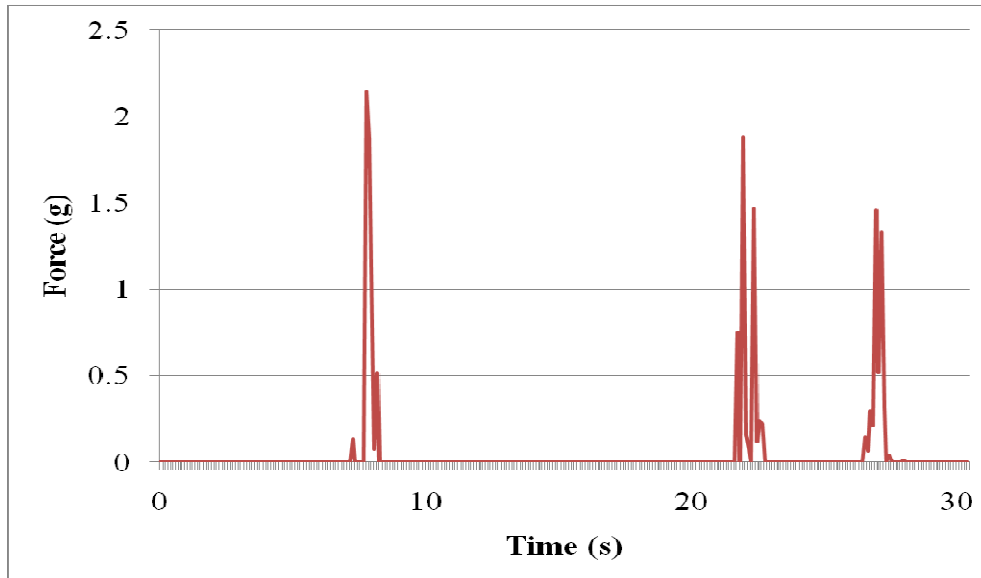


*Figure 26: Force v. Time Noise Reading – No Feet & No Noise*

The graph above shows the load cell force readings during the bench top noise testing when no feet were attached to the base of the device. Note that despite making an attempt to minimize surrounding disturbances, the load cell is still affected by ambient noise.

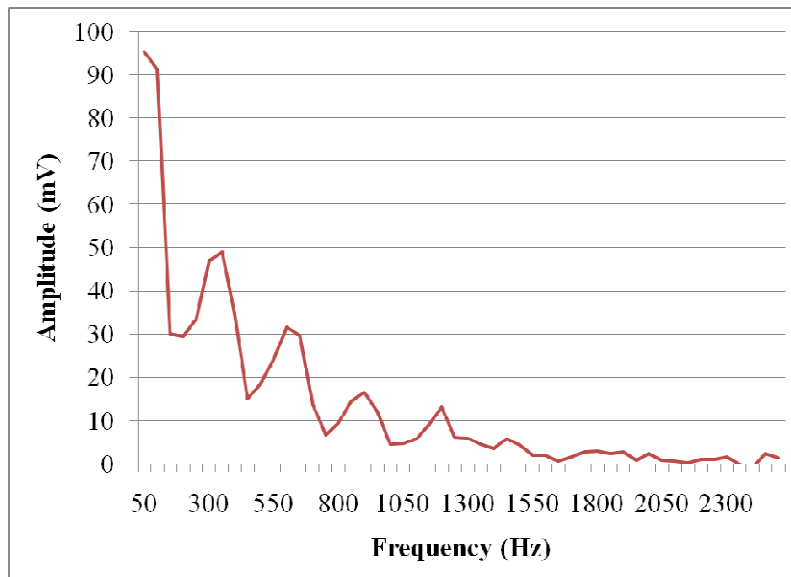


*Figure 27: FFT Plot – No Feet & No Noise*

The plot above shows the FFT plot during bench top noise testing when no feet were attached to the base of the device. At this point, no disturbances were purposely created.

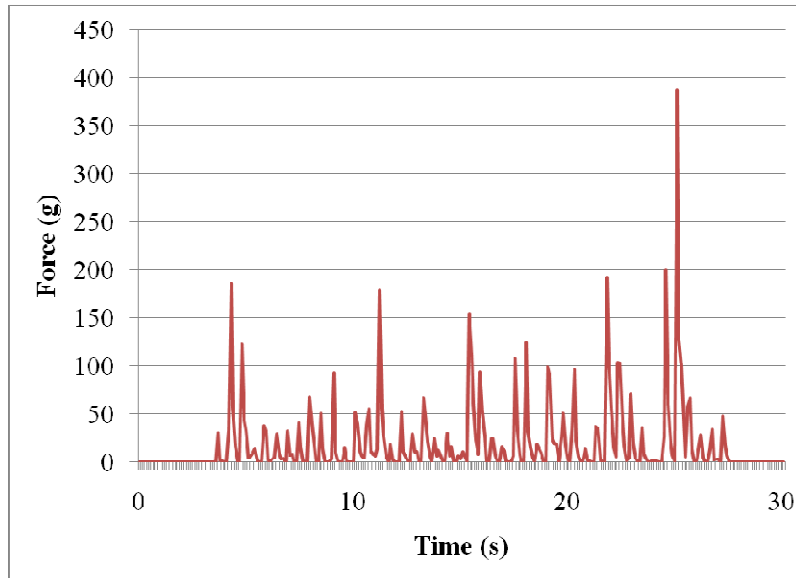


*Figure 28: Force v. Time Noise Reading – No Feet & Noise Created*

The graph above shows the load cell force readings during the bench top noise testing when no feet were attached to the base of the device. A team member jumped near the device twice a second to create the force disturbances.

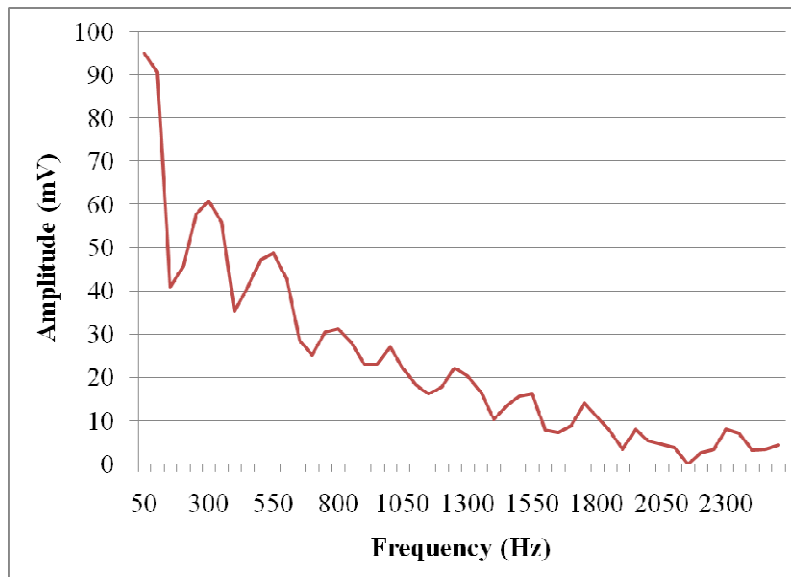


*Figure 29: FFT Plot – No Feet & Noise Created*

The plot above shows the FFT plot during bench top noise testing when no feet were attached to the base of the device. At this point, disturbances were purposely created to gauge the affect of environmental disturbances on the force readings. The amount of noise created by higher frequencies increases.

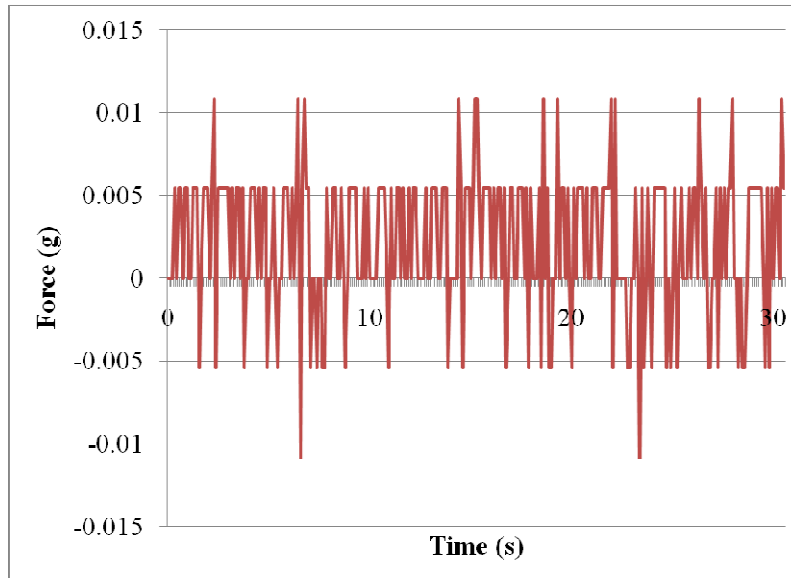


*Figure 30: Force v. Time Noise Reading – Standard Feet & No Noise*

The graph above shows the load cell force readings during the bench top noise testing when the standard feet were attached to the base of the device. At this point, no environmental disturbances were created.

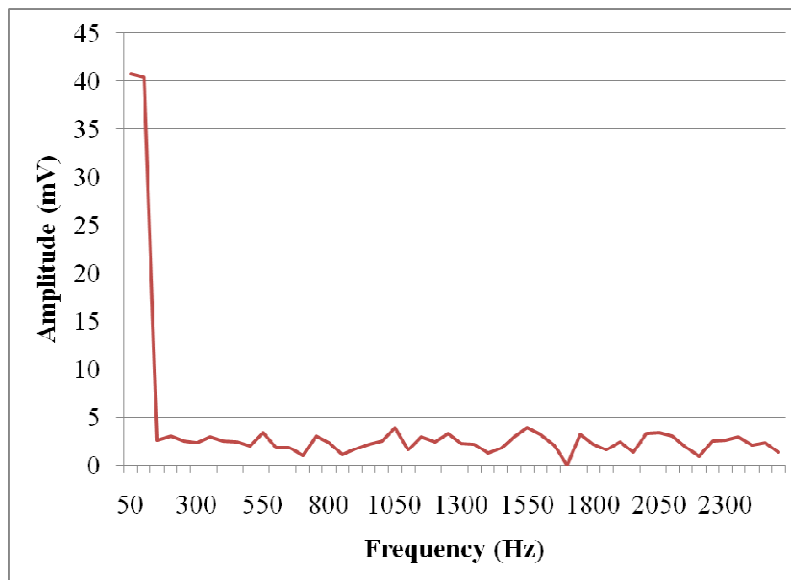


*Figure 31: FFT Plot – Standard Feet & No Noise*

The plot above shows the FFT plot during bench top noise testing when the standard feet were attached to the base of the device. At this point, no disturbances were purposely created.

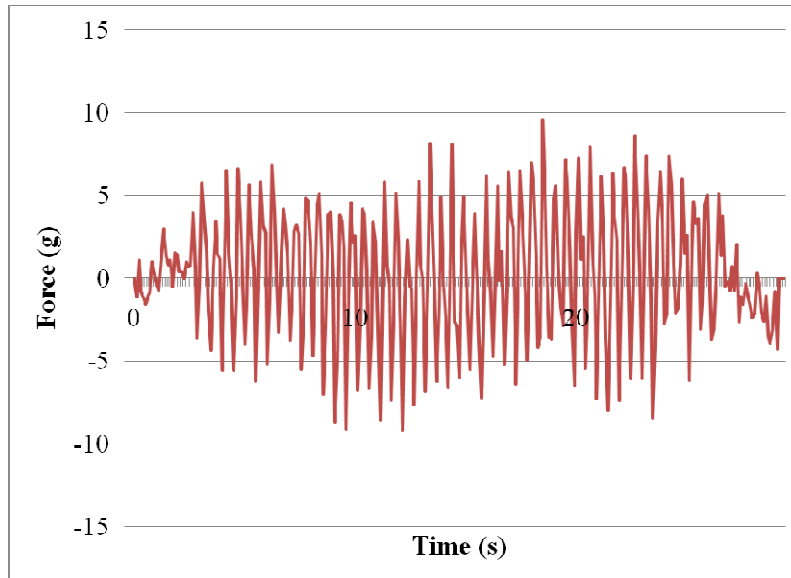


*Figure 32: Force v. Time Noise Reading – Standard Feet & Noise Created*

The graph above shows the load cell force readings during the bench top noise testing when standard feet were attached to the base of the device. A team member jumped near the device twice a second to create the force disturbances. Note that the standard feet are capable of minimizing ambient forces down to an error of 0.01 (see Figure 31) when a small amount of noise must be cancelled, but are no match for the equivalent of an earthquake.

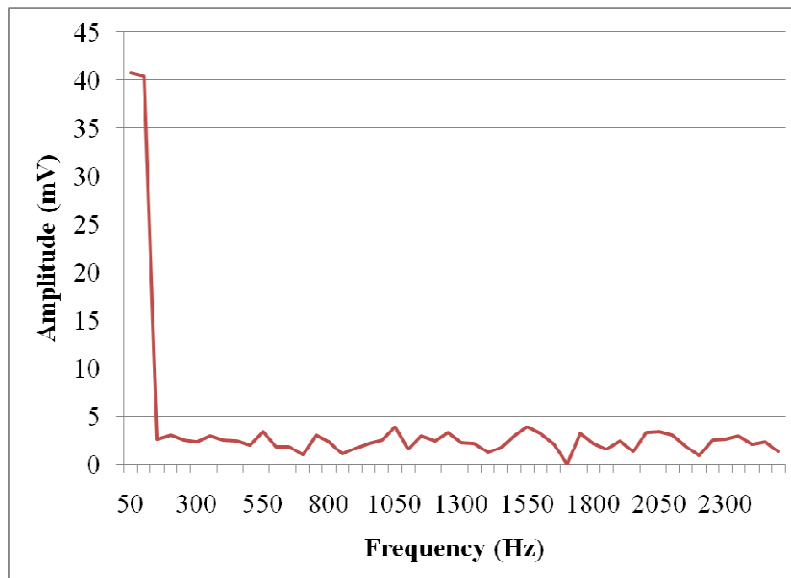


*Figure 33: FFT Plot – Standard Feet & Noise Created*

The plot above shows the FFT plot during bench top noise testing when standard feet were attached to the base of the device. At this point, disturbances were purposely created to gauge the affect of environmental disturbances on the force readings. There were no substantial changes to the FFT plot when noises were created, suggesting that the majority of the noise in the force readings are occurring in the range from 0-100 Hz.



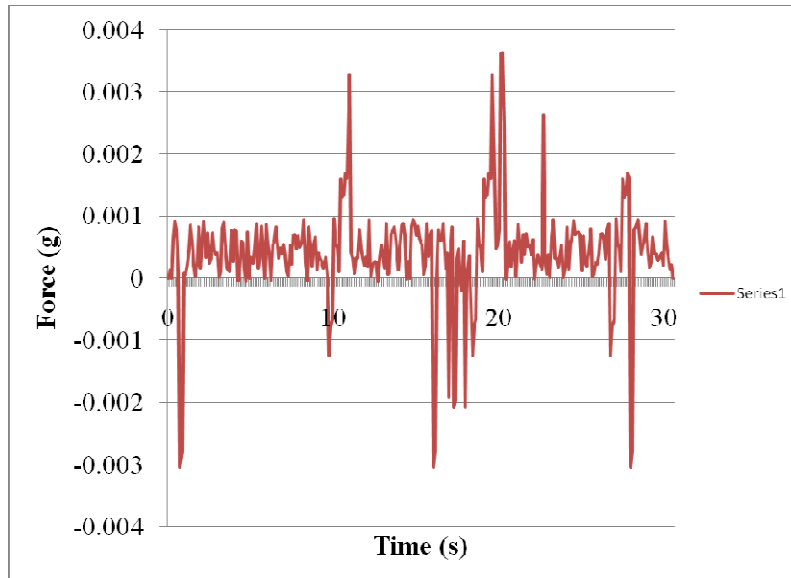


**Figure 34: Force v. Time Noise Reading – Isonoe Isolation Feet & No Noise**

The graph above shows the load cell force readings during the bench top noise testing when the Isonoe feet were attached to the base of the device. At this point, no environmental disturbances were created. It can be seen that the new feet decreased the load cell error by approximately 60%.

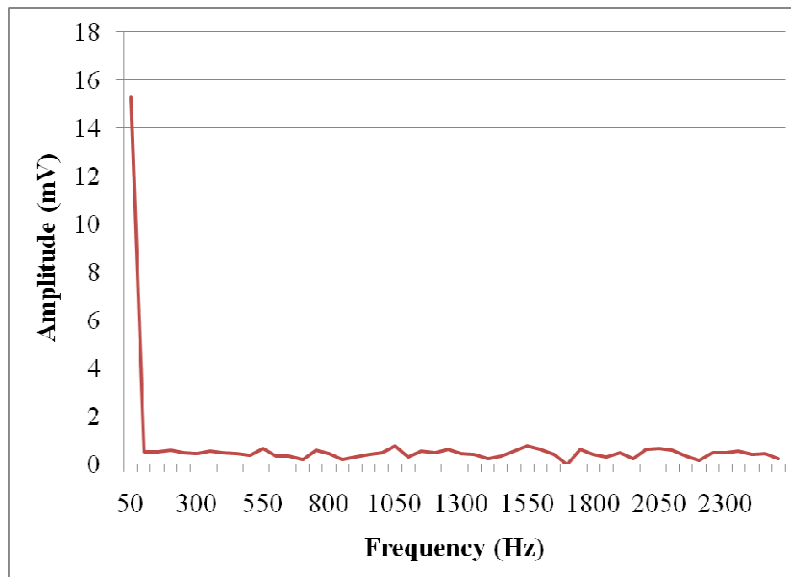


**Figure 35: FFT Plot – Isonoe Isolation Feet & No Noise**

The plot above shows the FFT plot during bench top noise testing when the Isonoe feet were attached to the base of the device. At this point, no disturbances were purposely created.

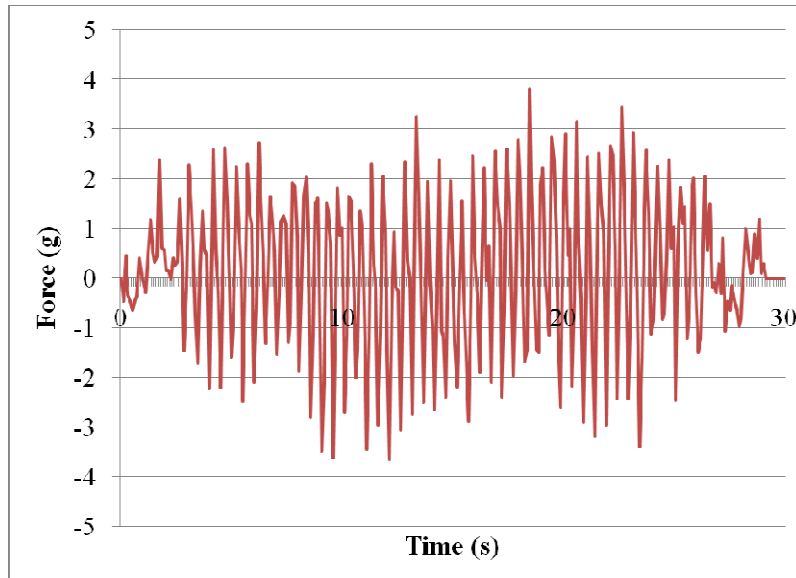


*Figure 36: Force v. Time Noise Reading – Isonoe Isolation Feet & Noise Created*

The graph above shows the load cell force readings during the bench top noise testing when Isonoe Isolation feet were attached to the base of the device. A team member jumped near the device twice a second to create the force disturbances. The Isonoe feet were capable of dampening this extreme case of environmental disturbance by approximately 60%.

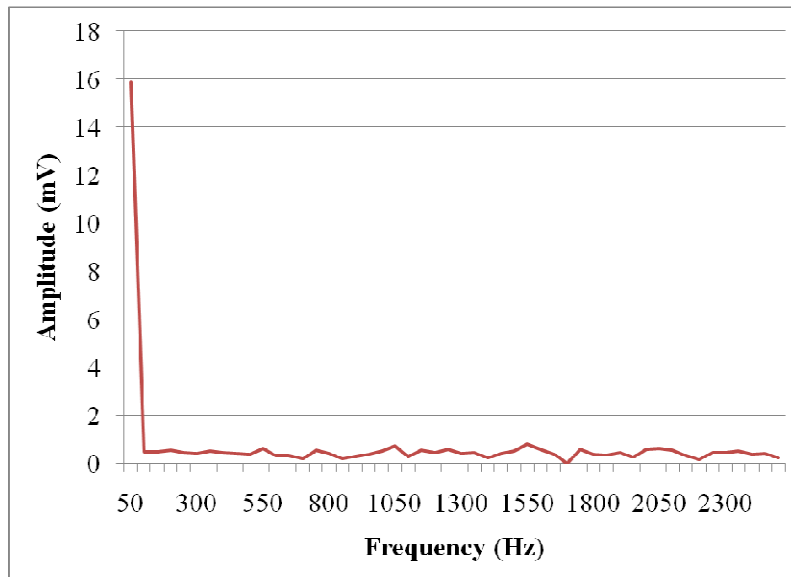


*Figure 37: FFT Plot – Isonoe Isolation Feet & Noise Created*

The plot above shows the FFT plot during bench top noise testing when Isonoe Isolation feet were attached to the base of the device. At this point, disturbances were purposely created to gauge the affect of environmental disturbances on the force readings. There were no substantial changes to the FFT plot when noises were created, suggesting that the majority of the noise in the force readings are occurring in the range from 0-100 Hz.

Once the Isonoe Isolation feet were proven to be the most effective method of reducing the effect of environmental disturbances on the device's force output, noise analysis was completed in the incubator under testing conditions. FFT plots were taken when the device was unloaded, when the device was loaded with an acellular collagen gel, and finally when the actuators were moving. Samples were taken at every frequency to determine an appropriate frequency to noise filter for further testing. The resulting plots can be seen below.

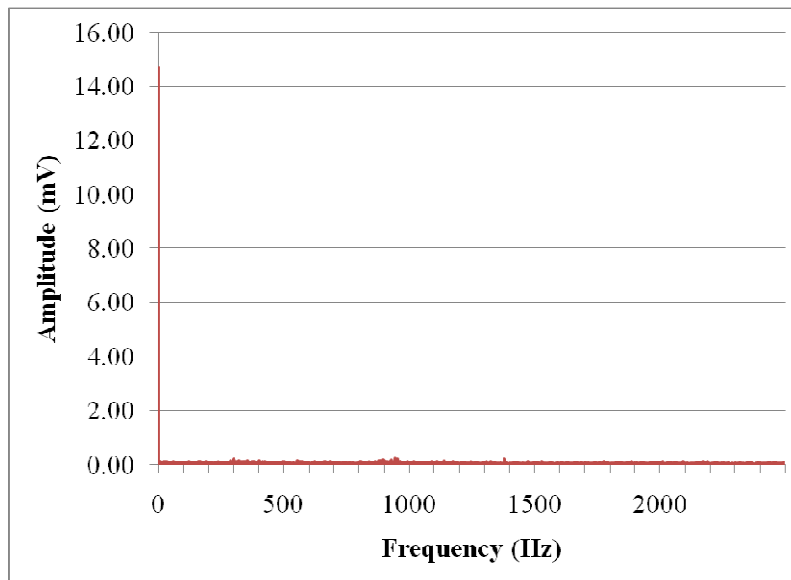


*Figure 38: FFT Plot – Incubator with No Load*

**This FFT plot was taken with the device inside of an incubator and attached to the Isonoe Isolation feet. It was not loaded with a sample. There is an obvious peak at 0-1Hz; otherwise there are no relevant disturbances.**

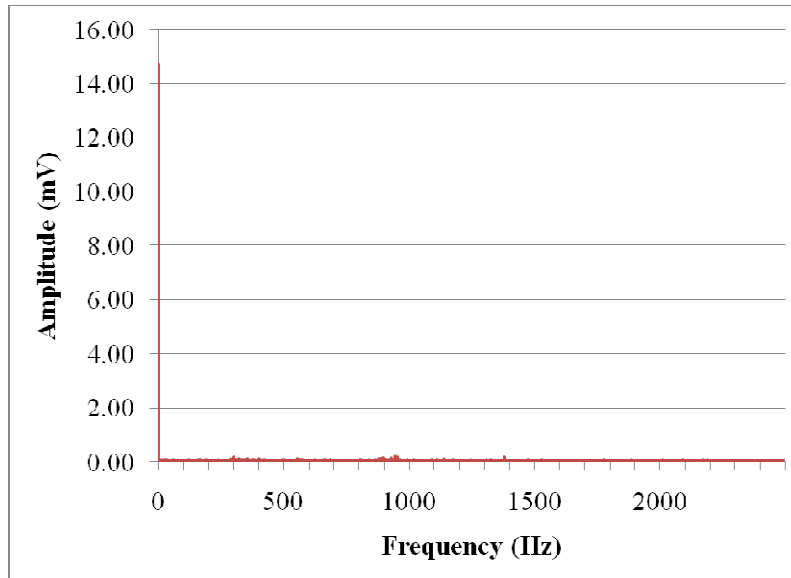


**Figure 39: FFT Plot – Incubator with Acellular Collagen Gel Loaded**

This FFT plot was taken with the device inside of an incubator and attached to the Isonoe Isolation feet. It was loaded with an acellular collagen gel. It appears identical to the non-loaded FFT Plot above. There is an obvious peak at 0-1Hz; otherwise there are no relevant disturbances.

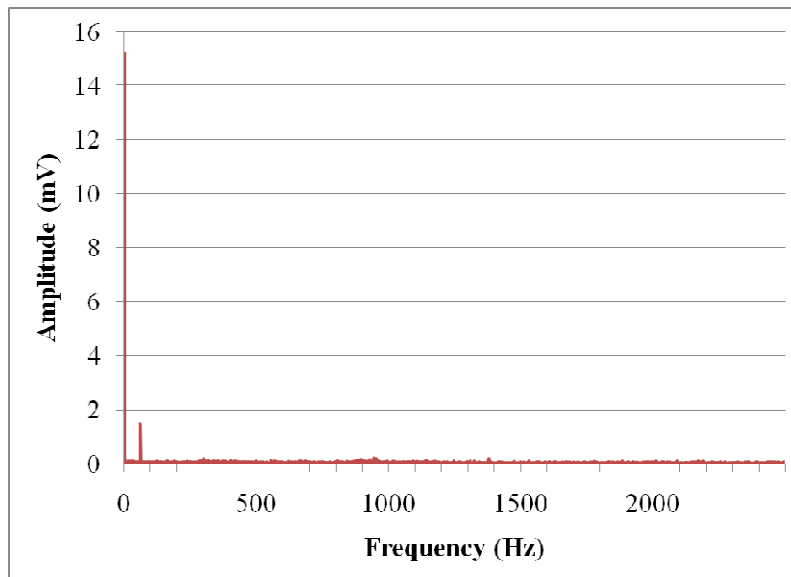


**Figure 40: FFT Plot – Incubator with Acellular Collagen Gel Loaded and Actuating**

This FFT Plot was taken with the device inside of an incubator and attached to the Isonoe Isolation feet. It was loaded with an acellular collagen gel, which was then actuated several times. There is a second peak at 60Hz. This data will be used to create a filter of the recordings that are acquired from the load cell.

### 6.3 Experimental Testing

Experimental data was obtained for the purpose of obtaining previously unattainable data. These experiments show the potential application of this device for testing matrices grown in Bioflex plates and to perform biaxial force measurement.

#### 6.3.1 Fetal Fibroblast and IPF

For the purpose of comparison two graphs were created, force per area and force per cell. Also, previous literature has used force/cell and force/mm<sup>2</sup> as standard metrics.

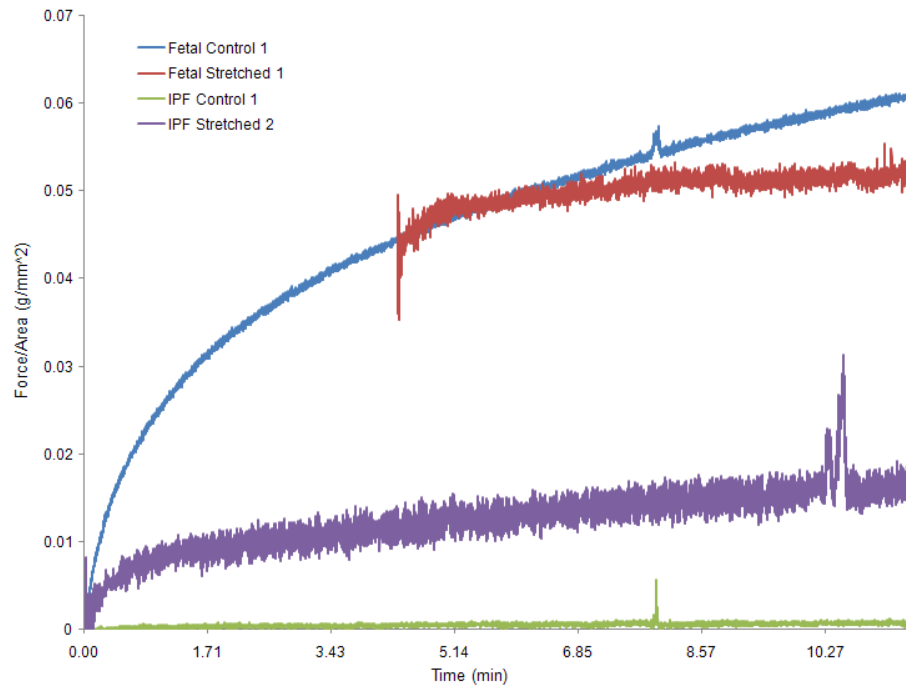


**Figure 41: Force per Area**

The fetal fibroblast and IPF test groups were placed into the device to determine their contractile forces. The force readings were divided by the cross-sectional area of the gel, which differed in each sample.

It can be seen from Figure 26 that the fetal cells contracted the most, and the fetal control contracted more than the fetal stretched. By contrast, the IPF cells control cells contracted less than the IPF stretched cells.

Cell Type	Maximum Force Per Area (mN/mm <sup>2</sup> )
Fetal Control	0.658
Fetal Stretched	0.532
IPF Control	0.071
IPF Stretched	0.198

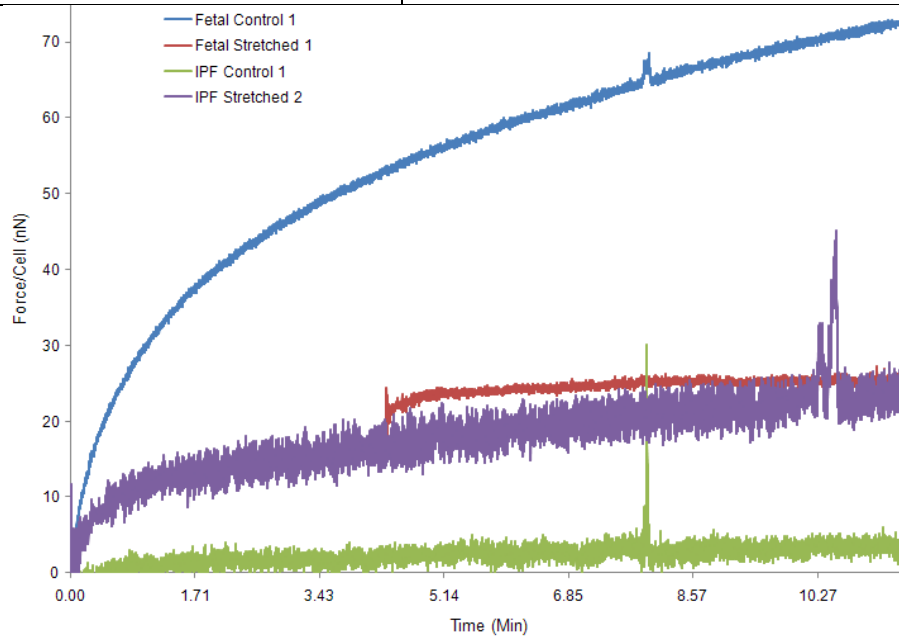


**Figure 42: Force per Cell**

The fetal fibroblast and IPF test groups were placed into the device to determine their contractile forces. The force readings were divided by the number of cells present in each gel, which differed in each sample.

Figure 27 shows the force obtained per cell. The fetal control has the highest maximum force, and the IPF control has the lowest maximum force per cell; however, it can be noted that the fetal stretched and the IPF stretched have approximately the same magnitude of the maximum force per cell.

Cell Type	Maximum Force Per Cell (mN)
Fetal Control	0.0784
Fetal Stretched	0.0261
IPF Control	0.0042
IPF Stretched	0.0285

## **7.0 Analysis and Discussion**

The results reported were designed to validate each axis of the device independently. The data indicated that the device is capable of obtaining cell force measurements with acceptable range and precision. In addition, the device is capable of operating within an incubator while requiring minimal space.

### ***7.1 Verification of Sub Systems***

The results of the sub system verification were optimal. The 0.001"/step precision reported for the actuators would have been sufficient. However, the results indicated that it was possible to obtain a precision of 0.0001"/step. This indicates that it might be possible to apply strains with extremely high precision. Additionally, the small step size would allow the device to be used with cell seeded gels on an extremely small size, where small, precise strains are needed. By controlling these actuators with the National Instruments software, the user has great control over the stretch applied to the sample. Dynamic tests are also a possibility using these actuators, as shown in the dynamic rice paper test. Future research may require dynamic force measurement testing, in which these actuators may still be used. It should be noted that the linear position of the actuator is not rigidly fixed. In other words, there appears to be some movement in the linear hold position of the actuator. This was not an issue during static testing; however, should be addressed before performing future testing where dynamic stretch is required.

The experimental load cell calibration verified that the data sheets obtained from the manufacturer were accurate. The 5mV output of the load cell was a concern, because the strain gauges were rated at 100mV. Initially the concern is that the small 5mV output processed through 100mV would reduce the resolution of the data output. However, it was found that using LabVIEW software the input window could be minimized to 5mV. In this way the 5mV

output would be encoded across the entire bit size and the output would remain at a high resolution. This discovery enabled work to continue without the purchase of an amplifier for the system. These findings may prove useful should force measurements systems with mV outputs be used in the future.

Both acellular tests provided insight on important iterative design changes. The vascular clamps worked exceptionally well; however, there should be a permanent method to attach polystyrene beads to be sure the clamps float in the bath. Next, the suture used to loop the clamps over the u-beams must be a flexible suture. The monofilament polymer suture was too rigid, while the silk suture worked very well. During the rice paper test, pulleys were placed over the end of the u-beams. These proved to be cumbersome and made it very difficult to attach the clamps to the beams. After attempting, unsuccessfully, to secure the pulleys in a way that would allow for easier suture attachment, the pulleys were abandoned all together. Because the device is made to measure contractile force and does not incorporate strain analysis, the friction of the silk suture on the u-beams was deemed acceptable.

The u-beam-collet-load cell assembly worked well and allowed for easy set-up and break down of the device. In addition, these components allowed for easy customization for sample size, bath size and uniaxial versus biaxial testing. The actuator mounts and adjustable frame also allowed for configuration of the device depending on the needs of the user and the experiment test set-up needed.

Data obtained during the acellular testing verified that the device was operational and testing could be performed using cell seeded gels. The device could apply a precise amount of stretch and the load cell could measure force in acellular collagen gels. After a few iterative changes as discussed above, testing of cell seeded gels was the next step.



## 7.2 Validation

The data (shown in results) was compared to the uniaxial testing performed by Eastwood and Brown, 1994, shown Figure 28 below.

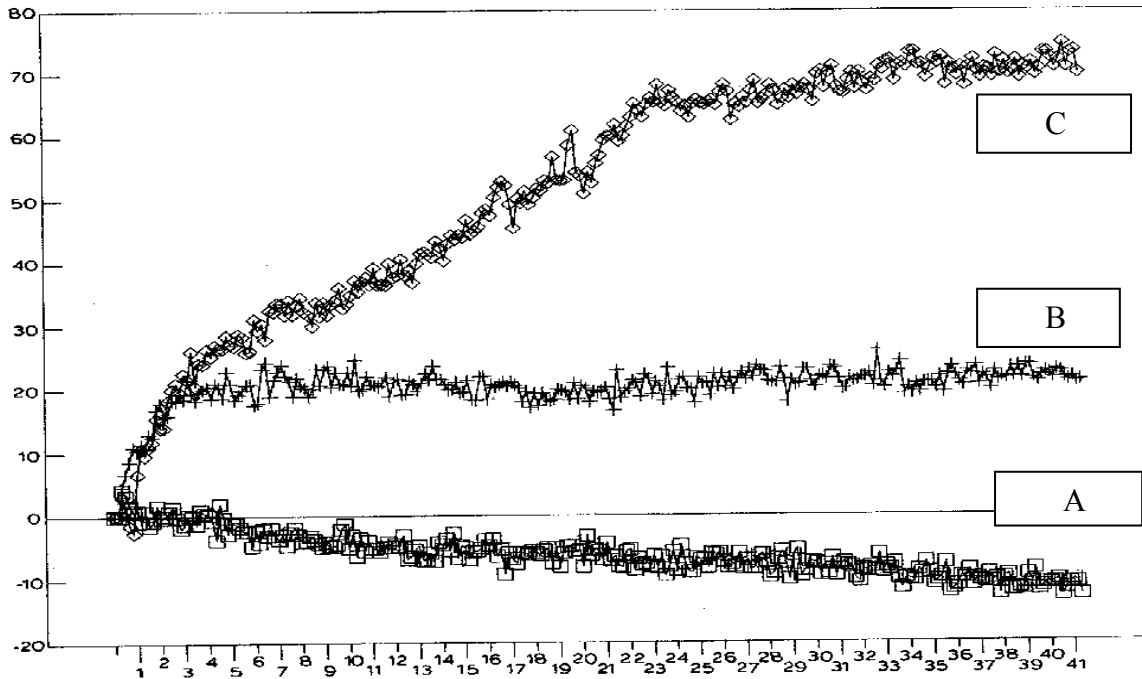


**Figure 43:** Previously published results of uniaxial testing over a period of 41 hours. Point A represents the thermal drift data, point B is the acellular collagen gel data, and point C is the fibroblast populated collagen gel data (Eastwood and Brown, 1994).

The results obtained experimentally show strong similarities to the data reported by Eastwood and Brown. Extended studies of 40+ hours are required and multiple sample sizes are necessary to validate that the device is capable of obtaining data that was previously reported. However, the initial results appear very promising, obtaining values within ranges that are expected for experiments of this kind. For example, the testing of the fibroblast seeded collagen

gel. The force for this matrices obtained by Eastwood and Brown at 20 hours was about 0.052g and the validation force obtained over the same period of time was found to be about 0.048g.

To discern passive collagen force from active cellular force, and complete the validation testing, the last test that was performed was with cytoclasin-D as in previous literature (Kolodney, Wysolmerski, 1992). That data obtained experimentally, as described in the uniaxial validation section of the results, produced similar data as the Wysolmerski paper. In both cases when cyto-D was added the force dropped to zero, which indicates that the cytoskeleton of the cells was disabled and active forces were measured. There is a need to repeat these trials in order to have a large enough sample size for statistical analysis and comparison with previous literature. This was not possible during our research due to time restrictions and deadlines. Additionally, the previous experiments within the field have utilized devices when the gel is cast into the device. In order to validate our results, our device, which was designed with a different set of objectives and goals, specifically the ability to measure gels cast outside the device, needed to be altered. This resulted in testing using the device in a way which it was not primarily intended. Although this process is needed, the methods must be optimized.

### ***7.3 Experimental Testing***

This data shows that our device is capable of obtaining force measurements from gels grown and preconditioned in a BioFlex culture plate. From the results obtained it can be seen that our device was able to measure distinctly different force curves for each cell type and could be a valuable tool in measuring the effect of cyclic stretch on cell contractility.

## **8.0 Future Recommendations**

### ***8.1 Biaxial Force Trials***

The capacity of the device to measure static uniaxial contractile force in fibroblast-seeded collagen gels was validated using previous materials and methods from culture force monitors found in literature (Eastwood, Brown 1994 & Kolodney, Wysolmerski 1992). Further testing was completed to prove that our device was capable of differentiating contractile forces in gels seeded with disease state and normal fibroblasts using our devised attachment methods. Force readings from these tests can be viewed in the Results section. Through these tests, it was proven that the device was capable of accurately measuring contractile forces along one plane.

Time constraints prevented the project team from thoroughly validating the device for biaxial static and dynamic stretch tests. Future work should first prove that the device is capable of measuring active contraction along two axes. The academic value of this device is in its ability to determine contractile forces in multiple tissues for the purpose of comparing the forces present in disease states to normal tissue. The ability to clamp a cruciate sample into the device, cycle it to align the extracellular matrix similarly to native tissue, and produce accurate force readouts of active contraction of the seeded cells is the final step for this device. One biaxial validation

using fibroblast-seeded collagen gels in a cruciate-shaped sample is the only requirement to complete this recommendation.

The Flexcell collagen gels that will constitute most of the samples measured by the device are difficult to cut into cruciate samples. The gels begin to contract immediately following their release from the polyethylene anchors into which they are grown. In order to produce a uniform strain field near the center of the gel, which is optimal when collecting force measurements, the corners of the gels must be cut away. This cruciate sample will immediately start to contract, so an efficient method is needed in order to cut all four corners quickly and precisely. A biaxial punch was devised, but never constructed. A cylindrical punch that would fit around the gel and hold it in place would allow the application of a constructed razor apparatus. The razors would quickly cut all four corners, and prepare the sample for loading. This punch was never machined due to time constraints.

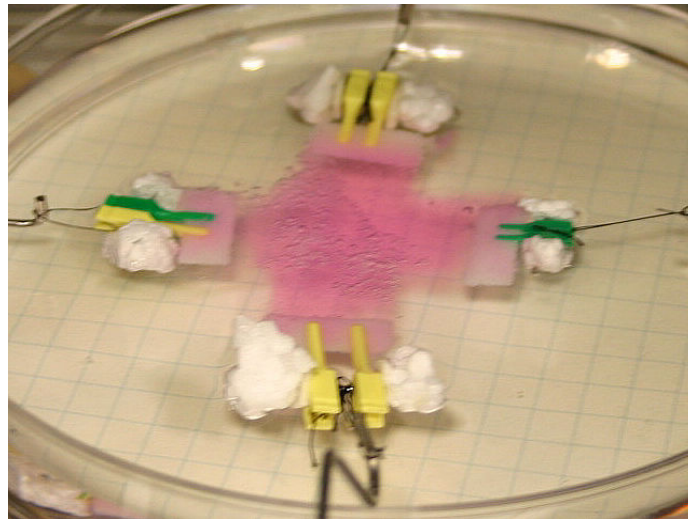


*Figure 44: Cruciate-Shaped Acellular Test*

**The image shows an example of a biaxial cruciate sample that should be used for validating the device biaxially. The gel used in this sample was acellular collagen.**

## ***8.2 Visual Strain Analysis***

Currently, the device is not equipped with any method for determining the distance that the

applied gels have contracted. The attachment methods include rigid stainless steel beams and sutures which are pulled tight, so it is assumed that the gels are not contracting inward. However, it is possible that the gel is slowly contracting into itself despite the applied tension. Additionally, the method for pulling the gel back to its original dimensions is approximate, and requires visual guessing while holding a ruler to the gel. For these reasons, the ability to visually analyze the gel with a CCD video camera module would be optimal. Markers should be placed onto the gel immediately after the gel is seeded; upon removal, it would then be possible to stretch the markers back to their original dimensions and monitor the gel during contraction.

CCD cameras are very bulky, and the inclusion of the camera onto the device frame would increase its height by approximately 0.3 meters. Other potential difficulties when considering mounting a CCD camera to the device include the expected expense (in the range of \$1000) and the addition of another two cables snaking out of the incubator door.

### ***8.3 Sterile System for the Purpose of Prolonged Testing***

In its current form, the device is neither sealed from the surrounding environment nor stationed inside of a laminar flow hood. Therefore, the contractile force tests that can be completed with the device are not sterile. This places a constraint on the length of time that contractile forces in cellular gel can be measured before the gel becomes compromised due to bacterial exposure. Data may be confidently collected for up to several days; however, week-long testing cannot be performed. If prolonged contractile testing is desired, the device must be enclosed inside of an airtight box and placed in a flow hood. This system must regulate temperature and CO<sub>2</sub> levels to maintain *in vivo* conditions inside of the sterile environment. A miniature incubator could be purchased for this purpose, or a bioreactor could be constructed.

## 9.0 References

- [1] Ahlfors, J-E. W., and K. Billiar. "Biomechanical and Biochemical Characteristics of a Human Fibroblast-Produced and Remodeled Matrix." Biomaterials 28 (2007): 2183-91.
- [2] Arold, Stephen, Joyce Wong, and Bela Suki. "Design of a New Stretching Apparatus and the Effects of Cyclic Strain and Substratum on Mouse Lung Epithelial-12 Cells." Annals of Biomedical Engineering 35.7 (2007): 1156-64.
- [3] Brown, R.A., et al. "Tensional Homeostasis in Dermal Fibroblasts: Mechanical Responses to Mechanical Loading in Three-Dimensional Substrates." Journal of Cellular Physiology 175.323-332 (1998).
- [4] Campbell, B.H., W.W. Clark, and J. H-C. Wang. "A Multi-Station Culture Force Monitor System to Study Cellular Contractility." Journal of Biomechanics 36 (2003): 137-40.
- [5] Chong, C., et al. "Design of a Biaxial Test Device for Compliant Tissue." Major Qualifying Project for Worcester Polytechnic Institute, 2005. 1-168.
- [6] Di Lullo, Gloria A., et al. "Mapping the Ligand-Binding Sites and Disease-Associated Mutations on the Most Abundant Protein in the Human, Type I Collagen." J. Biol. Chem. 277.6 (2002): 4223-31.
- [7] Eastwood, M., and et.al. "Quantitative Analysis of Collagen Gel Contractile Forces Generated by Dermal Fibroblasts and the Relationship to Cell Morphology." Journal of Cellular Physiology 166.33-42 (1996).
- [8] Eastwood, M, D.A. McGrouther, and R.A. Brown. "A Culture Force Monitor for Measurement of Contraction Forces Generated in Human Dermal Fibroblast Cultures: Evidence for Cell-Matrix Mechanical Signalling." Biochimica et Biophysica Acta 1201 (1994): 186-92.

- [9] Eastwood, M., et al. "Effect of Precise Mechanical Loading on Fibroblast Populated Collagen Lattices: Morphological Changes." Cell motility and the cytoskeleton 40 (1998): 13-21.
- [10] Farahani, Ramin Mostofi Zadeh, Naser Asl Aminabadi, and Luther C. Kloth. "Superficial Topography of Wound: A Determinant of Underlying Biological Events?" Medical Hypotheses In Press, Corrected Proof.
- [11] Freyman, T.C., et al. "Fibroblast Contraction of a Collagen-Gag Matrix." Biomaterials 22 (2001): 2883-91.
- [12] Freyman, T.M., et al. "Micromechanics of Fibroblast Contraction of a Collagen-Gag Matrix." Experimental Cell Research 269 (2001): 140-53.
- [13] Freyman, T.M., et al. "Fibroblast Contraction Is Independent of the Stiffness Which Resists the Contraction." Experimental cell research 272 (2002): 153-62.
- [14] Greve, H, et al. "Influence of Collagen Lattice on the Metabolism of Small Proteoglycan Ii by Cultured Fibroblasts." Biochem J 269.1 (1990): 149-55 pp.
- [15] Harley, Brendan A., et al. "A New Technique for Calculating Individual Dermal Fibroblast Contractile Forces Generated within Collagen-Gag Scaffolds." Biophysical Journal 93.8 (2007): 2911-22.
- [16] Horwitz, A.R., and J.T. Parsons. "Cell Migration - Movin' On." Science 286.5442 (1999): 1102-03.
- [17] Hultgardh-Nilsson, Anna, et al. "Expression of Phenotype- and Proliferation-Related Genes in Rat Aortic Smooth Muscle Cells in Primary Culture." Cardiovascular Research 34.2 (1997): 418-30.

- [18] Knezevik, V., T.K. Borg, and J.W. Holmes. "Isotonic Biaxial Loading of Fibroblast-Populated Collagen Gels: A Versatile, Low-Cost System for the Study of Mechanobiology." Biomechanics and Modeling in Mechanobiology 1 (2002): 59-67.
- [19] Kolodney, M.S., and R.B. Wysolmerski. "Isometric Contraction by Fibroblasts and Endothelial Cells in Tissue Culture: A Quantitative Study." The Journal of Cell Biology 117.1 (1992).
- [20] Kopecki, Z., and A. J. Cowin. "Flightless I: An Actin-Remodelling Protein and an Important Negative Regulator of Wound Repair." The International Journal of Biochemistry & Cell Biology In Press, Corrected Proof.
- [21] Kubo, H., et al. "Creation of Myocardial Tubes Using Cardiomyocyte Sheets and an in Vitro Cell Sheet-Wrapping Device." Biomaterials 28 (2007): 3508-16.
- [22] Liu, Yang, et al. "Promotion by Fibronectin of Collagen Gel Contraction Mediated by Human Corneal Fibroblasts." Experimental Eye Research 83.5 (2006): 1196-204.
- [23] Lysaght, M.J, and A.L. Hazlehurst. "Tissue Engineering: The End of the Beginning." Tissue Engineering 10.1/2 (2004): 309-20.
- [24] Marenzana, M., et al. "The Origins and Regulation of Tissue Tension: Identification of Collagen Tension-Fixation Process in Vitro." Experimental Cell Research 312 (2006): 423-33.
- [25] Mohr, D., and M. Doyoyo. "A New Method for the Biaxial Testing of Cellular Solids." Experimental Mechanics 43.2 (2003): 173-82.
- [26] Mudera, V.C., and et.al. "Molecular Responses of Human Dermal Fibroblasts to Dual Cues: Contact Guidance and Mechanical Load." Cell Motility and the Cytoskeleton 45 (2000): 1-9.



- [27] Peperzak, K.A., T.W. Gilbert, and J. H-C. Wang. "A Multi-Station Dynamic-Culture Force Monitor System to Study Cell Mechanobiology." Medical Engineering & Physics 26 (2004): 355-58.
- [28] Poliseno, Laura, et al. "Resting Smooth Muscle Cells as a Model for Studying Vascular Cell Activation." Tissue and Cell 38.2 (2006): 111-20.
- [29] Prajapati, R.T., M. Eastwood, and R.A. Brown. "Duration and Orientation of Mechanical Loads Determine Fibroblast Cyto-Mechanical Activation: Monitored by Protease Release." Wound Repair and Regeneration 8.3 (2000): 238-46.
- [30] Ramtani, S. "Mechanical Modelling of Cell/Ecm and Cell/Cell Interactions during the Contraction of a Fibroblast-Populated Collagen Microsphere: Theory and Model Simulation." Journal of Biomechanics 37.11 (2004): 1709-18.
- [31] Roy, P., et al. "Effect of Cell Migration on the Maintenance of Tension on a Collagen Matrix." Annals of Biomedical Engineering 27 (1999): 721-30.
- [32] Sotoudeh, Mohammad, et al. "A Strain Device Imposing Dynamic and Uniform Equi-Biaxial Strain to Cultured Cells." Annals of Biomedical Engineering 26.2 (1998): 181-89.
- [33] Takakuda, K., and H. Miyairi. "Tensile Behaviour of Fibroblasts Cultured in Collagen Gel." Biomaterials 17 (1996): 1393-97.
- [34] Wagenseil, Jessica E., Elliot L. Elson, and Ruth J. Okamoto. "Cell Orientation Influences the Biaxial Mechanical Properties of Fibroblast Populated Collagen Vessels." Annals of Biomedical Engineering 32.5 (2004): 720-31.
- [35] Zaleskas, J.M., and et.al. "Contractile Forces Generated by Articular Chondrocytes in Collagen-Glycosaminoglycan Matrices." Biomaterials 25 (2004): 1299-308.

## 10.0 Appendices

### *Appendix A: Typical Literature Contraction Graphs*

The following graphs are taken from Eastwood & Brown, 1994 and Kolodney & Wysolmerski, 1992. These are typical contractile force curves expected for uniaxial testing of fibroblast-seeded collagen gels over 40 hours. During uniaxial validation of the device, these graphs were referenced.

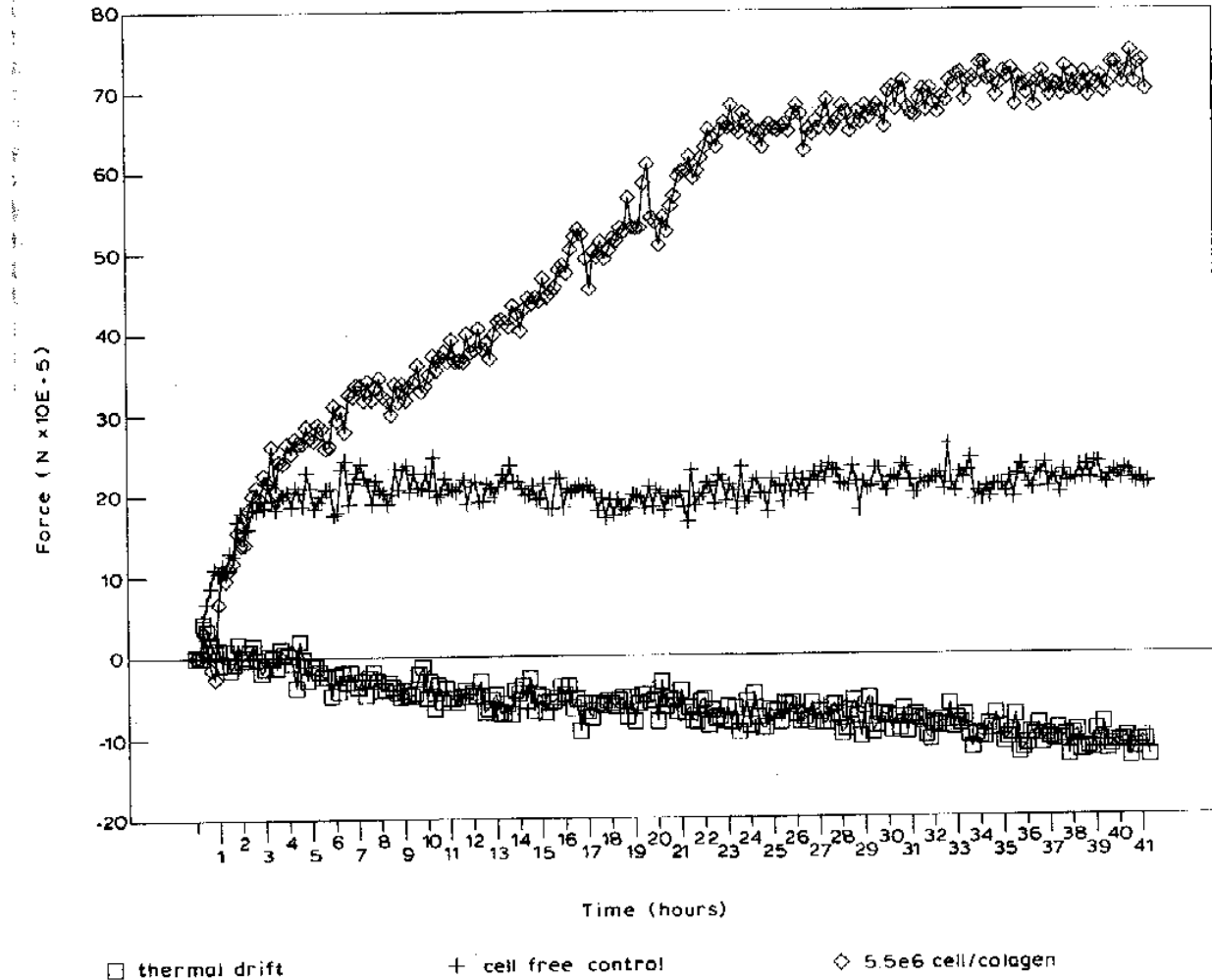


**Figure 45: Eastwood/Brown Contractile Curve**

Contractile force curves comparing long-term remodeling of fibroblast-seeded gels, acellular collagen and the force transducer's thermal. Comparing the fibroblast-seeded curve to the acellular curve allows for the approximation of active cell contraction. [8]

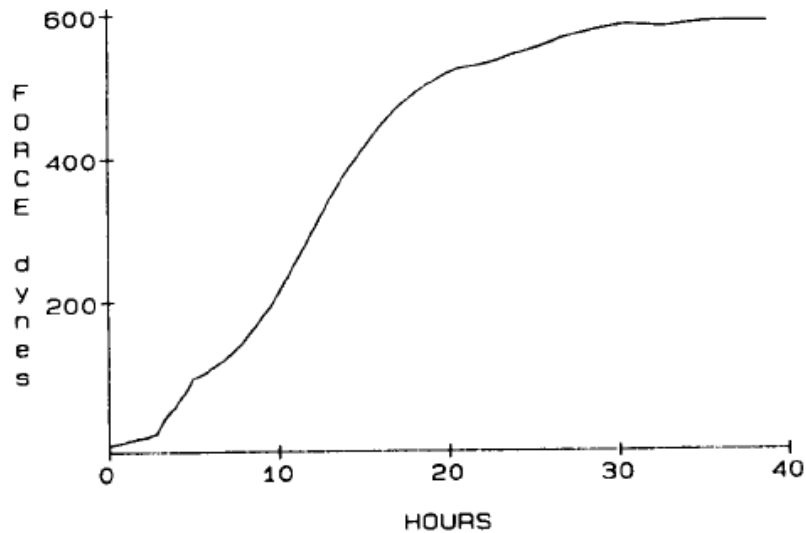


*Figure 46: Kolodney Contractile Curve*

Contraction of a fibroblast-seeded collagen gel over forty hours. Cellular remodeling of the extracellular matrix appears to subside after 35 hours. This curve, along with the cytochalasin-D testing represented in Figure 30 are compared to determine active contraction of fibroblast cells. [19]

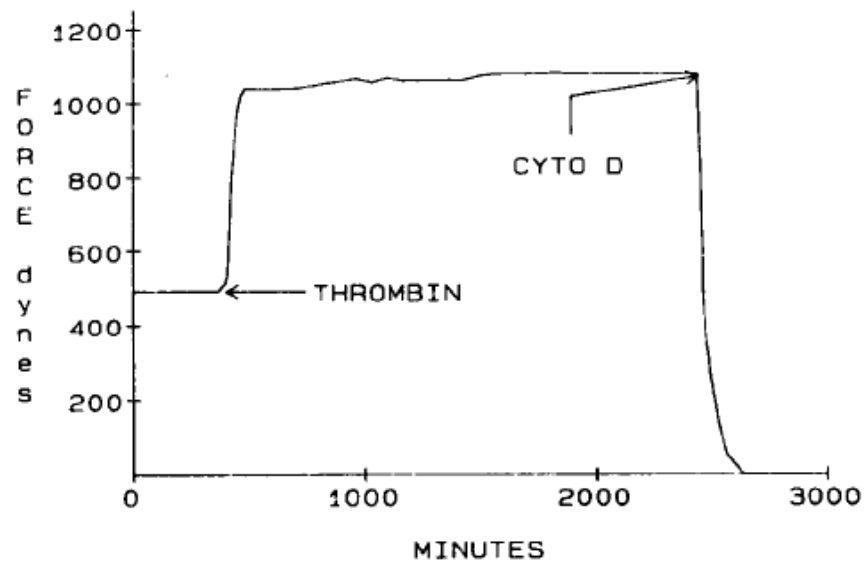
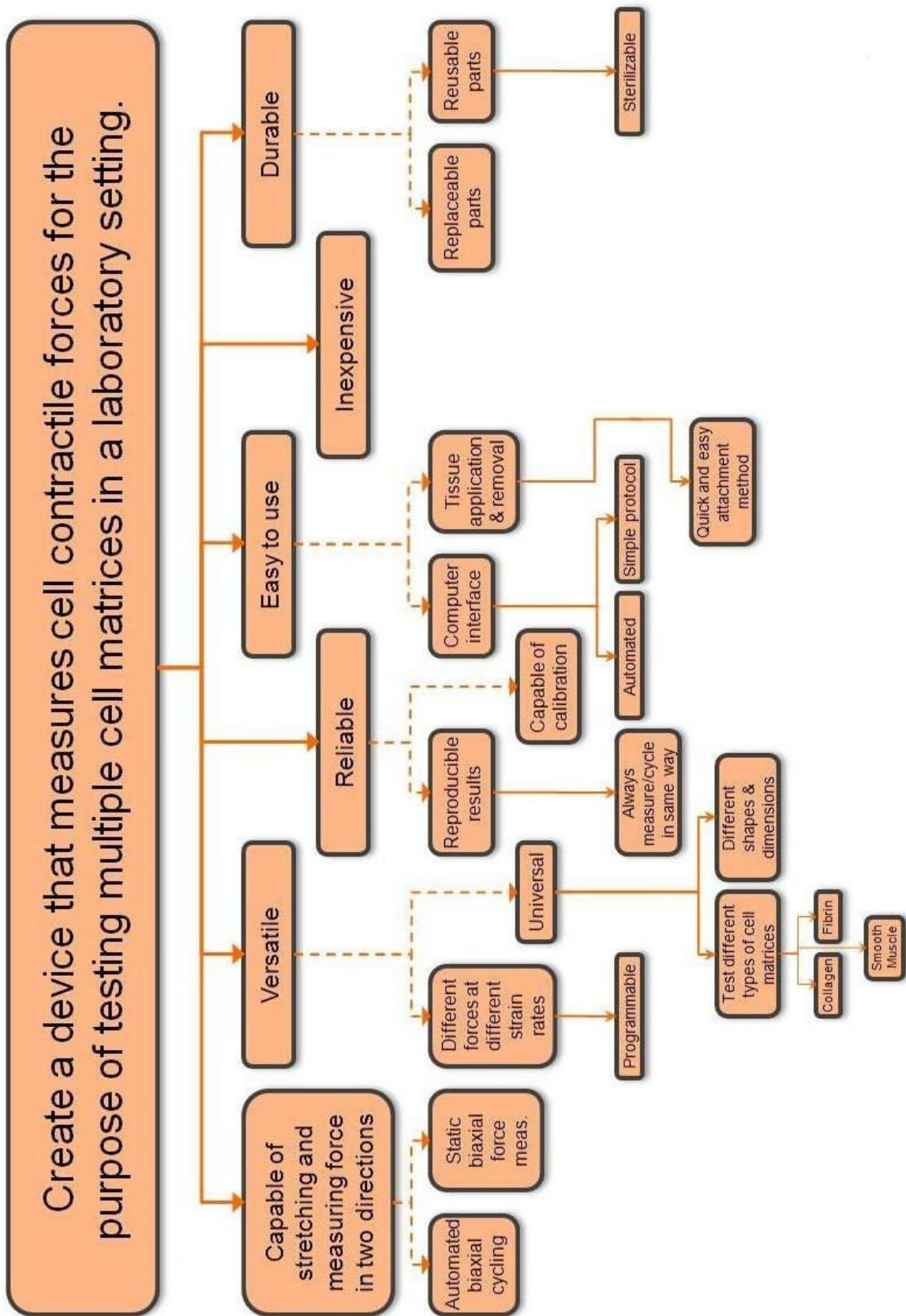


*Figure 47: Kolodney Cyto-D Findings*

Following the forty-hour equilibration of the contraction forces in fibroblast-seeded collagen gels, the cells were subjected to thrombin, which stimulates cell contraction, and cytochalasin-D (Cyto D), which disintegrates the cytoskeleton of the cells, eliminating contraction. This curve, along with the cell contractile curve represented in Figure 29 are compared to determine active contraction of fibroblast cells. [19]

Appendix B: Objective Tree



### *Appendix C: Pairwise Comparison Charts*

These charts were used to order the objectives by importance. When two objectives are compared the more important one gets a one and the less important one a zero, and in the end they are summarized and the ones that have higher values are more important.

S+M = Stretching and Measuring of the Tissue

Ver. = Versatility of the Device with Concerns to Multi-Matrix Testing

Rel. = Reliable

ETU = Easy to Use

Dur. = Durable

Inexp. = Inexpensive

Table 1: Pairwise Comparison Chart filled out by Professor Kristen Billiar

	<b>S + M</b>	<b>Ver.</b>	<b>Rel.</b>	<b>ETU</b>	<b>Dur.</b>	<b>Inexp</b>	<b>Total</b>
<b>S + M</b>	X	1	0	0	0	0	<b>1</b>
<b>Ver.</b>	0	X	0	1	1	1	<b>3</b>
<b>Rel.</b>	1	1	X	1	1	1	<b>5</b>
<b>ETU</b>	1	0	0	X	0	1	<b>2</b>
<b>Dur.</b>	1	0	0	1	X	1	<b>3</b>
<b>Inexp</b>	1	0	0	0	0	X	<b>1</b>

Reliable > Versatile = Durable > Easy to Use > Stretching & Measuring = Inexpensive

Table 2: Pairwise Comparison Chart filled out by Professor Marsha Rolle

	<b>S + M</b>	<b>Ver.</b>	<b>Rel.</b>	<b>ETU</b>	<b>Dur.</b>	<b>Inexp</b>	<b>Total</b>
<b>S + M</b>	X	1	0	1	1	1	<b>4</b>
<b>Ver.</b>	0	X	0	1	1	1	<b>3</b>
<b>Rel.</b>	1	1	X	1	1	1	<b>5</b>
<b>ETU</b>	0	0	0	X	0	1	<b>1</b>
<b>Dur.</b>	0	0	0	1	X	1	<b>2</b>
<b>Inexp</b>	0	0	0	0	0	X	<b>0</b>

Reliable > Stretching & Measuring > Versatile > Durable > Easy to Use > Inexpensive

Table 3: Pairwise Comparison Chart filled out by MQP0702 team

	<b>S + M</b>	<b>Ver.</b>	<b>Rel.</b>	<b>ETU</b>	<b>Dur.</b>	<b>Inexp</b>	<b>Total</b>
<b>S + M</b>	X	1	1	1	1	1	<b>5</b>
<b>Ver.</b>	0	X	0	1	1	1	<b>3</b>
<b>Rel.</b>	0	1	X	0	1	1	<b>3</b>
<b>ETU</b>	0	0	1	X	0	1	<b>2</b>
<b>Dur.</b>	0	0	0	1	X	0	<b>1</b>
<b>Inexp</b>	0	0	0	0	1	X	<b>1</b>

Stretching & Measuring > Versatile = Reliable > Easy to Use > Durable = Inexpensive



**Appendix D: Morphological Chart**

<b>Functions</b>	<b>Possible Means</b>						
Stretch tissue uniaxially using computer control, and if possible, biaxially as well	Pulley: -2 actuators -4actuators	Vacuum	Stainless steel ball	Actuators: -hydraulic - pneumatic	Fishing line	Spinning disk	
Measure forces uniaxially and biaxially	Force transducers	Bending beams	Force transducers and bending beams				
Keep cells at physiological conditions for 48 hours	Incubator	Buffers	Resistors	CO <sub>2</sub> heating lines			
Stabilize itself from internal and external interference	Symmetric	Even base	Screwed into the surface which is standing on	Clamps	Weight on outer edges	Wires	Airtables
Data output: record for 48 hours	Serial ports	Labview					
Attach tissue without harming matrix and cells	Hooks	Clamps	Adhesives	Bio membranes	Sliding Rings	Sutures	Magnetic fluids

## ***Appendix E: Further Importance of Cell Contraction***

### ***Wound Healing***

The process of wound healing relies on lamellipodial crawling of keratinocytes during wound reepithelialization, infiltration of inflammatory cells and migration of fibroblasts required for deposition and remodelling of the extracellular matrix and dermal contraction at the wound site. The healing is mediated by the activation of quiescent fibroblasts, migration of the activated fibroblasts to the site of injury, synthesis of new extracellular matrices (ECM), wound contraction, and ECM remodeling.

Fibronectin, which is an adhesive glycoprotein, plays a great role in cell adhesion, migration, growth, and differentiation. By studying how this protein regulates the wound healing in the stroma of the cornea in the eye, much can be understood about wound healing in general. The fibronectin acts as an attachment mean for the migration of the fibroblasts. This protein has also been found to provide collagen contraction, which was mediated by the formation of stress fibers and focal adhesions. Other proteins that have been used in ECMs are paxillin, phosphorylated paxillin, integrins  $\alpha 5$ ,  $\beta 1$ , and  $\alpha 2$ , and  $\alpha$ -smooth muscle actin ( $\alpha$ -SMA). The stress fibers and focals are important for performing cell contractility. The ability of cells to exert force on a collagen matrix depends on the actin cytoskeleton.

The transformation of the fibroblasts into myofibroblasts, which is a phenotypic transformation, was determined by recognizing the expression of  $\alpha$ -SMA. The expression of  $\alpha$ -SMA was found to be up-regulated by transforming growth factor- $\beta 1$  which induces the transformation of fibroblasts into myofibroblasts. What is interesting is that this transforming growth factor- $\beta 1$  was found only in a stressed collagen lattice but not in cells seeded in a floating collagen gel.

The wound contraction of the derma cells can be explained by proposing two combined mechanisms. The suggestion is that both ECM-cell and cell-cell interactions operate together to cause contraction. For such mechanisms there are two theories that explain the process of contraction. The first suggests that fibroblast locomotion within the connective tissue induces wound contraction, while the second suggests that forces generated by myofibroblasts are transmitted to other cells and surrounding connective tissue through their gap junctions and basement membranes [30]. It is known that fibroblasts are interconnected by extensive cell-cell contact, which suggests that the reorganizing of the matrix requires the presence of stationary contractile fibroblasts. These fibroblasts get interconnected before the onset of wound contraction. This is the point that shows the interaction of both mechanisms suggested above. The initial stress is assumed to come from the cell/ECM interaction, while the additional stress is assumed to come from the cell/cell interaction. What is well known is that the contraction's mechanism is influenced by cell number, cell types, and culture conditions such as the presence of cytokines and growth factors in the culture medium [30]. Force mapping studies of single cells show that cells can generate about  $10^{-8}$  N [31]. When the cells are contracting, their vectors are pointing towards the center of the contracting plane. The way that these cells communicate is by sending signals through gap junctions. It is important that connexins, the proteins responsible for this communication, have not been altered. This may result in diseased states. Ramtani found that fibroblasts are able to produce growth factors that they need themselves. The inhibitors of wound contraction are chitosan and Oleamide. The mechanical forces generated by fibroblastic cells that lead to wound contraction are large enough not only to cause cosmetic scarring, but also to cause major body deformation and loss of joint motion in cases where contraction persists after wound closure [30]. This mechanism of contraction causes stress relaxation and stress

concentration areas throughout the wound. Fibroblasts migrate to these areas due to galvanotaxis, which is the attraction of positively- or negatively-charged cells toward an electric field of opposite polarity. It has been found that stress concentration areas exhibit higher stiffness whereas the stress relaxation regions exhibit lower elastic modulus and therefore lower stiffness. Piezoelectricity and electrical current have been found useful in signaling TGF- $\beta$  which also helps in galvanotaxis for the fibroblasts. If a TGF receptor is seeded into the ECM, it might attract fibroblasts into the stress relaxation areas.

### ***Phenotypic Shifts***

When there is damage done to the wall of an artery the smooth muscle cells (SMCs) change from a contractile phenotype to a synthetic phenotype. This change causes cell differentiation and excreting of cells into the ECM. This has also been performed *in vitro*. After seeding the cells the first thing noticed is the loss in microfilaments and a formation of endoplasmic reticulum and Golgi apparatus. This makes it easy for production of new cells to start.

The shifts are performed when there is gene regulation, which is usually done by manipulating mRNA. In order to shift from synthetic to contractile phenotypes, cells are seeded with substrates of fibronectin or laminin and collagen IV. The shifts can be controlled by adding fetal bovine serum. By controlling the concentrations of it, the cells can switch from contractile to synthetic phenotype and vice versa. This causes the cells to create smooth muscle  $\alpha$ -actin, which is necessary for smooth muscle contraction. The phenotypic modulation of arterial SMCs in primary culture includes an integrated series of changes in the expression of genes for transcription factors, extracellular matrix components, matrix receptors, matrix-degrading enzymes, growth factors, and growth factor receptors. Such a complicated process enables the SMCs to migrate, proliferate, and deposit ECM. This type of wound healing is important for

keeping the homeostasis of the body.

## ***Appendix F: Motor Systems***

Four motors will be used to cycle the applied tissue ten to twenty times. Cycling the tissue or gel removes any preliminary tension in the matrix that would potentially skew the contractile force measurements. These motors should have a minute step, which will increase the accuracy of the cycling speed and applied strain rate. An appropriate step would be approximately 0.01 inch per step. The motors should be small, like the rest of the device, so that it can be placed inside an incubator.

### ***DC Motor***

A “brushed” direct current (DC) motor is the simplest and cheapest way to convert electrical energy into rotational motion. The mechanical energy produced by the motor is created by electrical current running through a rectangular coil. The current creates a magnetic field around the coil, causing the coil to rotate in an effort to align along the poles of the magnetic field. To prevent the magnetic field from reaching an equilibrium in turn maintaining rotation, the current must be alternated. An alternating current reverses the polarity of the magnetic field, forcing the coil to rotate 180° to maintain equilibrium. The component used to alternate current in a DC motor is called a commutator. Current from the main power supply is fed directly into the commutator where it is routed into the base of the rotating coil. A schematic of a common brushed DC motor can be seen in Figure 48.

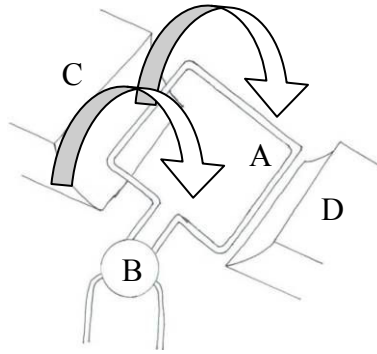


**Figure 48: DC Motor**

**In the schematic above, a rectangular coil (A) is attached to a commutator (B). Electrical current flows through the commutator and into the coil, creating a magnetic field. Letters C and D are the negative and positive magnets that are needed to create an opposing magnetic field to the coil's produced magnetic field.**

The controls of a brushed DC motor are limited to “On” and “Off”. By altering the amount of current entering the motor by way of added resistance to the circuit, it is also possible to vary the output speed of the motor. These limited controls provide very little precision. Although a brushed DC motor is cost effective and has simple functions, strain rates applied to the tissue during cycling would be incredibly inaccurate.

### ***Servo Motor***

A servo motor consists of a simple DC motor in circuit with a potentiometer. Potentiometers are used to vary the resistance in a circuit to produce a desired electrical current. They require a feedback loop to the controlling mechanism. The potentiometer receives a pulse-width modulation signal from the controlling mechanism, which conveys the number of rotations that the DC motor necessary for the desired function. The DC motor is allowed to run until it reaches this predetermined number of rotations, at which point the potentiometer reroutes electrical current away from the DC motor.

Servo motors are either incredibly accurate devices or very inexpensive devices. The small, inexpensive servo motors often used in simple robotics have very little accuracy and are used to

move components of a robot an approximate distance. These motors would be incapable of accurately operating on a small enough scale for the application of this project. Servo motors can also be purchased as all-in-one units where the motion control, input and motor come as one. These systems are very accurate, but also very expensive. They should only be considered when designing an automated assembly line device.

### ***Hydraulic Motor***

Hydraulic linear motors consist of two chambers. The first chamber is referred to as the “generator”. In this chamber, hydraulic fluid, typically some form of oil, is pumped in and out at varying rates. This displacement of fluid creates pressure on the second chamber, the “cylinder”. The hydraulic cylinder moves in a linear fashion in and out of the motor system based on the amount of fluid being forced into the generator. High fluid velocity will cause high pressures and the cylinder will be forced outwards. Low fluid velocity will create a low pressure inside of the generator, and the cylinder will be pulled back into the device. There are many ways that hydraulic motors can then be used to generate mechanical energy. A simplified schematic of this device can be seen below in Figure 49.

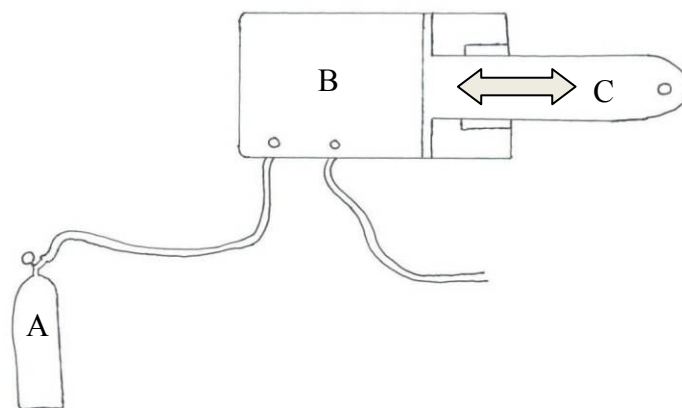


***Figure 49: Hydraulic Motor***

**Hydraulic fluid (A) is forced into the generator chamber (B) which creates a high pressure on the cylinder (C). The cylinder is then forced outwards.**



This system is far less compact than any of the previously described DC motor options. It requires two tubes to be run from the machine to a pressurized fluid tank. For this reason, the device cannot be placed in an incubator. However, hydraulic motors are very accurate as long as the applied pressure is precisely controlled. These motors also produce linear motion, as opposed to the rotational torque produced by the aforementioned DC motors, so there would be no need for a device to translate rotational strain into linear strain.

### ***Pneumatic Motor***

A pneumatic motor operates in the same manner as a hydraulic motor, but uses compressed air instead of hydraulic fluid to create the pressure difference in the generator. The advantages and disadvantages of using a pneumatic motor are the same as a hydraulic motor. Theoretically, it is much easier to attain rotational torque from a pneumatic motor than a hydraulic motor, but this function has no relevance to the device design.

### ***Stepping Motor***

A stepper motor operates similarly to a brushed DC motor. A magnetic field is alternated in order to rotate an internal shaft. However, stepper motors have more than one positive and negative pole, which means the internal shaft does not have to complete half a rotation ( $180^\circ$ ) each time an electrical pulse is applied. This process is best described in the diagram seen in Figure 50.

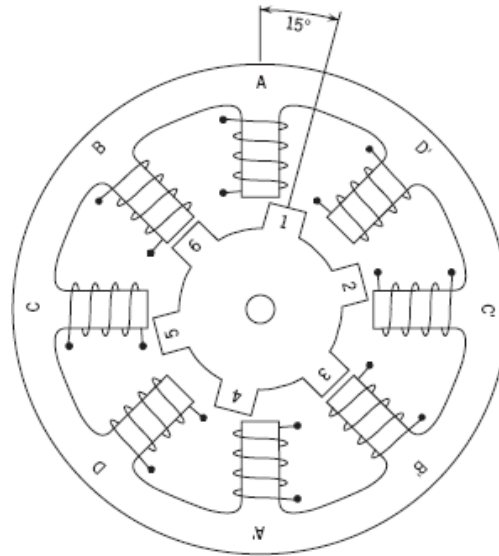


**Figure 50: Stepping Motor**

**In the diagram above, the B and B' nodes are magnetized by an electric current. Therefore, the closest “teeth” that are protruding from the shaft, in this case tooth 6 and tooth 3 align along this magnetic field. When a pulse is applied to another set of nodes, the shaft will rotate. [Retrieved from “Stepper Motor Basics”]**

The number of poles that can be created around the shaft correlates to the accuracy the stepper motor provides. A very high number of poles, such as 180, would allow the device to rotate in increments as small as  $2^\circ$ . Also, the device maintains a high torque even when rotation has been halted, as the internal shaft is constantly under stress from the surrounding magnetic field. A stepper motor with very small pulse increments is optimal for accuracy of the device; however, as the accuracy of the stepper motor increases so does the cost.

A stepper motor fit all of the constraints identified for the motor system. A micro-stepping unit manufactured by Portescap [model: 35DBM10B1B-K; see Appendix I] was discovered that contained a stepping accuracy of 0.001 inches, which would allow precise changes in cycling strain rates. These small steps also provided the positioning control needed when stretching the tissues back to their original sizes. The operating temperature was estimated at between  $-20^\circ\text{C}$  and  $70^\circ\text{C}$ , well within the range of incubation. All Portescap motors are compatible with

National Instrument motion controllers and Labview software, both of which are used extensively in Worcester Polytechnic Institute labs. The motors were both small and inexpensive.

## ***Appendix G: Methods for Achieving Linear Motion***

For the purpose of this project, it is imperative that stretching of the tissue is precise, accurate and cost effective. The overall design of the device dictates that the stretching applied to the tissue should occur in a uniplanar fashion. Several of the motor options described in the previous section produce rotational torque, and require means to translate this force. Secondly, the device should not introduce additional mechanical noise/vibrations into the system. The contractile forces that the device will measure are in the range of five to twenty micronewtons. Any additional friction or mechanical noise would dwarf the forces being measured. Finally, the device should be minimal in size, in order to keep the device compact.

### ***Pulley System***

A simple option for producing linear motion from a DC motor is by attaching a polymeric fiber onto the motor's rotating armature. The fiber will become wrapped around the DC motor as it rotates, retracting the other end along a straight line. This fiber, generally nylon, can be attached to the tissue using a series of pulleys meant to redirect the nylon fiber to the correct angle of tension. This system is inexpensive and simple to construct, but is difficult to control and therefore inaccurate. Additionally, each pulley introduces the potential for frictional forces, which could skew the contractile force data output.

### ***Mechanical Sliders***

Slide rails consist of a drive mechanism, called a rail, which is rotated at the motors output velocity. As the rail spins, it moves a platform suspended above it. There are four types of drives: the screw drive, the ball-screw drive, the belt drive, and the chain drive. These mechanical sliders can tolerate a high amount of torque created by the attached motor. For this

reason, they are often used in conjunction with cheap, inaccurate DC motors in order to increase their stepping accuracy. A schematic of a typical screw drive can be seen in Figure 51.

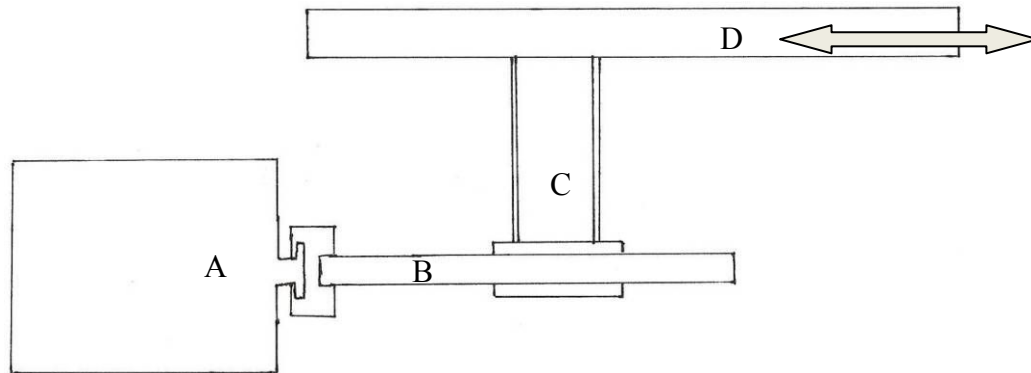


**Figure 51: Mechanical Sliders**

**The rail system is attached to a motor (A) by a crude block fastened around the motor's armature and the screw drive (B). As the screw drive rotates, moves a threaded cylinder (C) linearly up and down the screw. This cylinder is attached to a platform (D).**

Mechanical sliders stabilize the DC motor and reduce noise created by the motor system.

However, they are often six to twelve inches in length. This addition of length could potentially make the device too large to fit inside of a standard incubator. If the device could not fit inside of an incubator, a bioreactor would have to be created so that it could reside on a tabletop or air table. Mechanical sliders fit all of the design criteria for the creation of linear motion except for size, so it was deemed acceptable as a last resort.

### **Actuators**

An actuator is a machine that converts one form of energy (centripetal, magnetic, or pressure) into linear motion. There are many types of actuators, but the four most common designs are the pneumatic actuator, the hydraulic actuator, the electromagnetic actuator, and the motor-controlled actuator.

Pneumatic and hydraulic actuators are continuations of their respective motor systems. In Figure 32, which illustrates the design of both a pneumatic and hydraulic motor, the actuator is

the cylinder which is being forced in and out of the chamber. For this reason, pneumatic and hydraulic actuators are normally not separate systems from their motors and are a two-for-one design commitment.

Electromagnetic actuators consist of a coiled wire (or solenoid) which creates a magnetic field around a cylinder. The electrical current across the solenoid is alternated in order to periodically reverse its magnetic field, and consequently the linear motion of the cylinder. When this magnetic field is reversed, the cylinder is propelled at high velocity either in or out of the chamber. Electromagnetic actuators are fairly inexpensive; however, they tend to create a lot of unwanted mechanical noise due to their quick starts and stops.

A cylinder can also be used to translate rotational energy produced by a motor into linear motion. A typical motor/actuator assembly consists of a running motor set up beside a cylindrical shaft. The motor is connected by a chain or belt to a threaded screw. The screw rotates at the same velocity as the motor, and begins to turn a cylindrical shaft, which is also threaded. This shaft is moved in and out of the chamber depending on the directional rotation of the screw. This design can be seen in Figure 52.

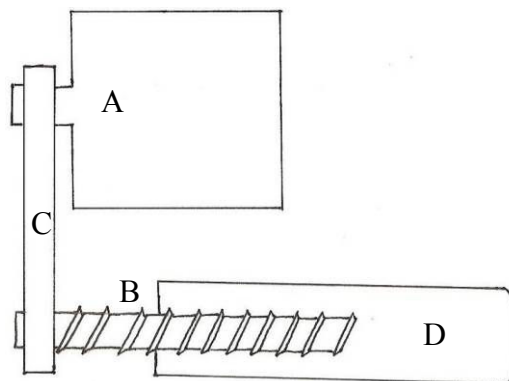


**Figure 52: Motor/Actuator**

**In the motor/actuator assembly above, a DC motor (A) is creating rotational work, which is transferred to a screw (B) by a belt (C). This screw moves a threaded cylinder (D) linearly.**

Recent advances in micro-stepping actuators have produced a combination of a DC motor and an actuator cylinder in one compact device. A DC micro-stepping motor is run around a screw which is threaded into and out of the device based on the motor's direction of rotation. This screw is actuating in a rotating fashion, so to make the actuating shaft non-rotating it is encased in a hollow shaft which is loosely connected to the screw.

The micro-stepping non-rotating actuator was chosen because of its compactness. An actuator with a one inch step - the maximum value of cycling deformation expected to be needed for tests run on the device – is only two and a half inches long. The stepping accuracy of the motor ensures minimal noise, as the motor is capable of actuating slowly in minute steps.

## ***Appendix H: Measure Forces Uniaxially and Biaxially***

The device must measure cell matrix contractile forces within the attached tissue matrix. Following mechanical cycling, the tissue matrix will begin to realign and remodel the ECM. At this point, the matrix will contract inwards. In order to model naturally occurring cell contractile forces, it is necessary to measure these forces in two axes.

The device will have to be able to measure contractile forces in the range of 2-10mN per matrix. This range is substantially smaller than commercial devices, so the components will likely need to be customized. The following are devices which could potentially measure forces in this range.

### ***Strain Gauge***

Strain gauges are the simplest and least expensive method for measuring forces. They perform this function by measuring the deformation of an object, which is directly proportional to strain. The most common form of strain gauge is the foil gauge. A foil strain gauge is a thin wafer made of a metallic foil with a very low bending strength. This gauge is adhered to a material, which is then loaded and deformed. This deformation must be less than 10% of the reference distance, as strain over 10% cannot be measured. As the object's properties change, the foil inside of the strain gauge is compressed or expanded, altering the foil's resistance. The electrical current passing through the strain gauge changes inversely to the foil's resistance. This current can be measured, which determines the gauge factor and applied strain rate. Using these values, the force applied to a beam can be calculated.

Strain gauges are incredibly cheap, costing no more than fifteen dollars each. Additionally, their accuracy can be altered by their placement on the cantilever beam. If a strain gauge were placed close to where the sample was attached to the cantilever beam, it would measure large



forces - in the range of several newtons. If a strain gauge were placed on the cantilever beam several inches further away from the sample it would register forces in the millinewton range. Despite this customizability, strain gauges are difficult to install, as they must be individually adhered to a beam. If a strain gauge had to be replaced, it would be difficult to adhere a new strain gauge in the same position. The device would require recalibration. Strain gauges are very difficult to use for precise measurements because of the human error involved in their placement.

### ***Torque Transducer***

Torque transducers determine the rotational strain applied to an affixed beam. Within the device are multiple foil strain gauges that are already installed and calibrated. Strain is applied to the base of the beam by an external force, which creates a moment about the torque transducer. This measurement can be converted into force by dividing by the distance from the torque transducer to the applied force. Torque transducers are very accurate, but are prone to mechanical noise depending on the length of the affixed beam. A long beam will provide a more precise measurement of the applied strain, but any unexpected force applied externally to the device (for example, if the device is bumped) is likely to create a force on the beam.

It was determined that torque transducers were the optimal measurement tool for the device. The transducers could be suspended above the tissue sample, which was resting in a media bath. Non-bending cantilever beams would transfer the contractile forces produced by the tissue to the torque transducer, which would remain a safe distance from the media. However, commercial torque transducers are only capable of measuring one ounce per inch (1 oz-in). In order to measure contract forces of 10mN, the most accurate torque transducer on the market would require a cantilever beam of approximately 50cm. The length of this beam would make the device impractical for two reasons: it could not fit inside of an incubator, requiring the creation

of a bioreactor and the extreme length of the beam would produce much mechanical noise. For these reasons, alternative methods of force measurement were explored.

### ***Transducer Class Strain Gauge***

Force transducers equipped with strain gauges function similarly to both the foil strain gauges and the torque transducer. A typical force transducer is in the shape of a small rectangular box with a nodule sticking out of one of the sides. This nodule is a cantilever beam with foil strain gauges attached. The purpose of the transducer is to further convert the output signal. Once the strain rate is determined by the foil strain gauges encased inside of the transducer, the output is converted into a force measurement. Force transducers are much easier to use than strain gauges alone as they eliminate excess calculations and do not need to be calibrated.

Force transducers capable of registering a 10mN force can be purchased commercially. These transducers are expensive, ranging in price from four hundred to one thousand dollars per unit. Complications arose when attachment methods from the transducer to the applied tissue were discussed. A cantilever beam could not be used to keep the transducer safely away from the media bath, so a system of pulleys would be utilized. The pulley attachment method was determined to be unusable for this application due to the potential for extra friction force that would skew the contractile force measurements. Secondly, it would be difficult to fix a force transducer onto the actuating arm of the micro-stepping motor. Therefore, the tissue would have to be cycled using one attachment method, and a second attachment method would be needed to attach the force transducer. The engineering of the device proved to be too complicated using a force transducer.

### ***Load Cell***

A form of transducer class strain gauge that measures only tension and compression along the main axis of the device is called a load cell. Whereas force transducers normally measure force as an applied torque about a small protrusion, load cells require the force to be transferred along the plane of the load cell. In this way, it can provide exact measurements for both tension (if the force is pulling away from the load cell) and compression (if the force is pushing on the load cell). A typical application for a load cell is on a guidewire of a suspension bridge; however, much smaller load cells are available for use with smaller loads.

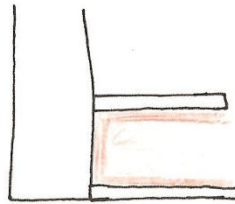
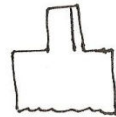
Load cells capable of measuring 10 gram loads (roughly 0.1 Newton) were commercially available through Futek. The cost of this load cell was \$1200. Although it is one of the more costly options, the load cell proved to be small, accurate, and capable of withstanding up to one thousand pounds of load without breaking. Additionally, a load cell could be attached onto the end of the actuating shaft of the micro-stepping motor. An elaborate beam attachment would be necessary to attach the load cell to the tissue along the same plane, but the actuator and force measurement device could be kept a safe distance from the media bath and still accurately measure cell contractile forces.

## Appendix H: Brainstorming Sketches

### Versatility Options

overhanging bars:

locking mechanism for interchangeable bars:



change to:

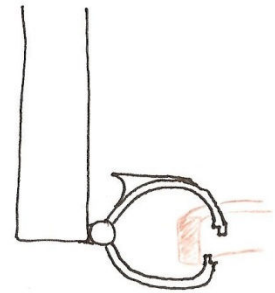
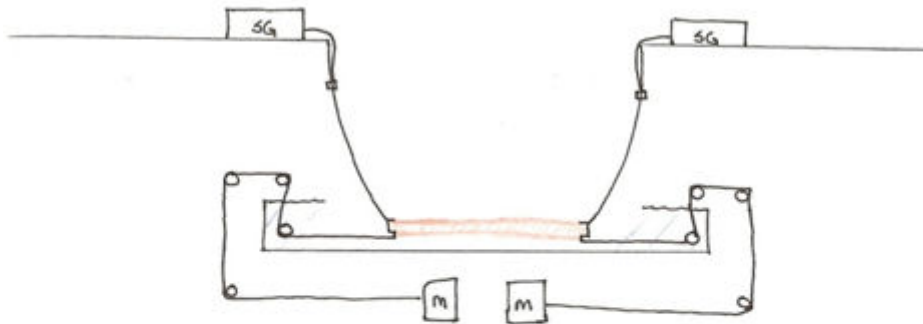


Figure 53: Versatile Beams

Preliminary option for providing versatility to the device. The perpendicular beams have a locking system so that it is possible to easily switch out attachment methods for different types of tissues.

Side View:



Overhead View:

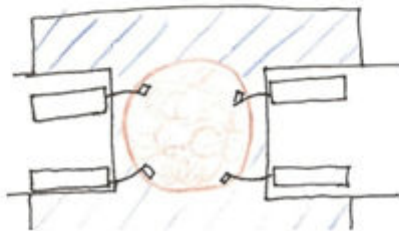


Figure 54: Bending Beams

Functionality of a bending beam system.

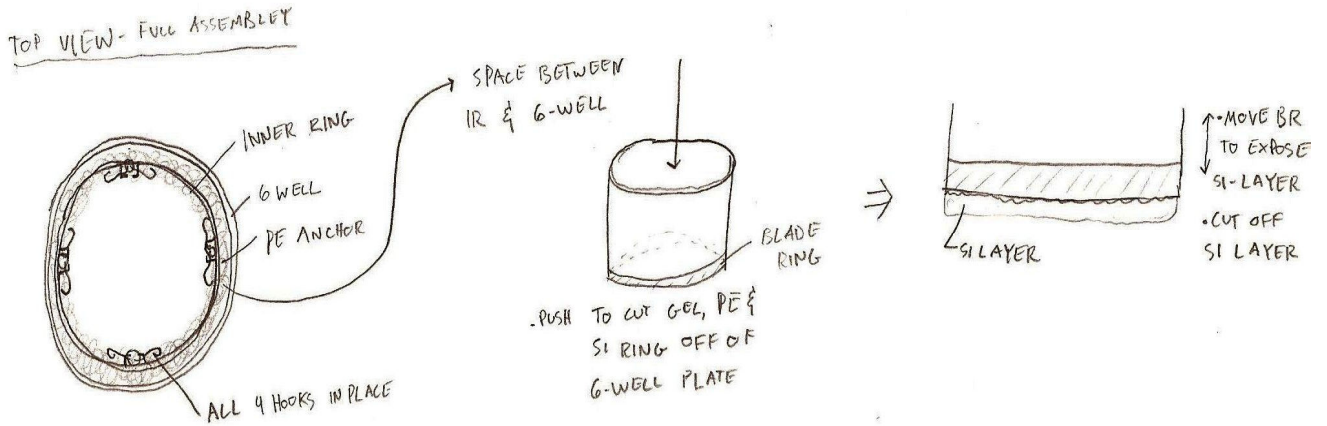


Figure 55: Punch

One option for quick detachment from the six-well plates in which fibrin gels are grown. A series of blades are used to separate the gel from the plates and also the semi-permeable membrane affixed to the bottom of the gel.

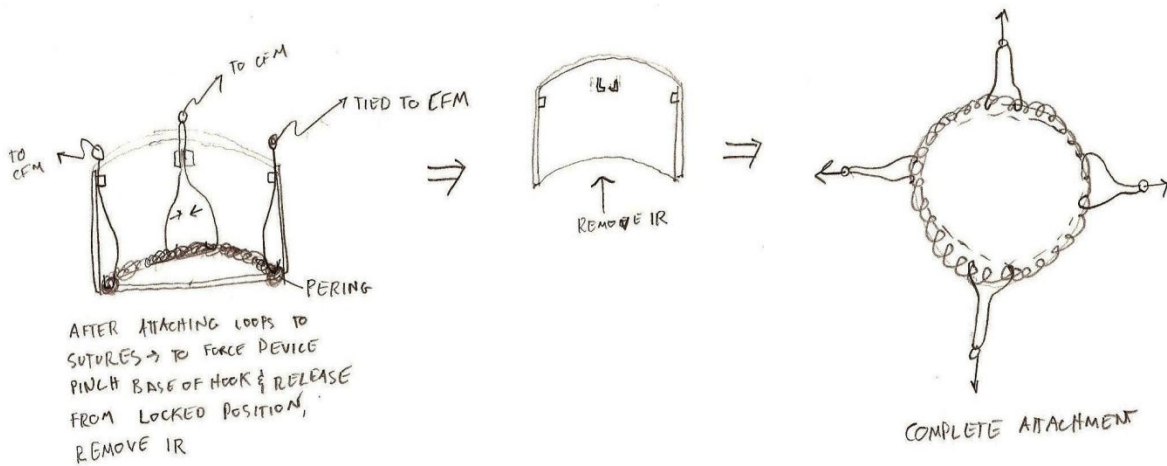
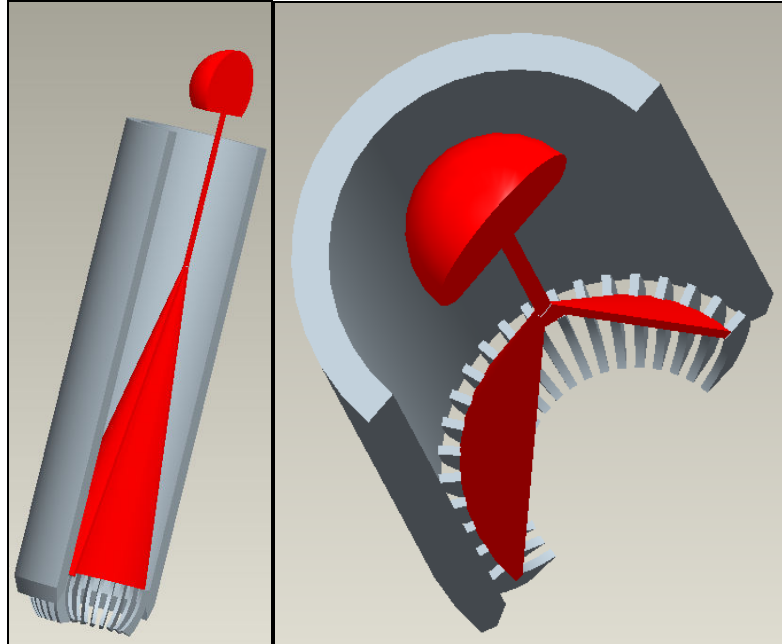


Figure 56: "Cookie Cutter"

A second option for quick detachment from the six-well plates. This method was referred to as the "cookie cutter" system. Hooks are attached to the fibrin gel in a uniform manner before the gel is removed from the six-well plates.



*Figure 57: Punch with Hooks*

Combining the idea of a punch (Figure 36) with the “cookie cutter” (Figure 37) produced this image. The red plunger is depressed into the gel, which angles all of the attached hooks into the surrounding polyethylene anchor.

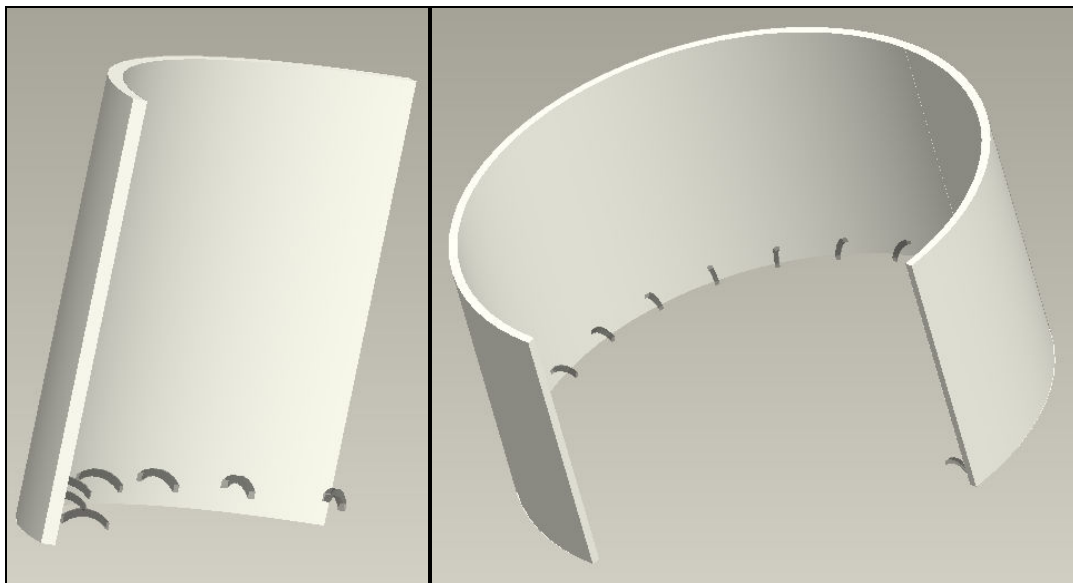


*Figure 58: Spiked Wall*

This four section structure would be used to attach hooks into the Flexcell collagen gels, and then each section would be actuated while still grasping the gel. This was yet another attachment method idea.

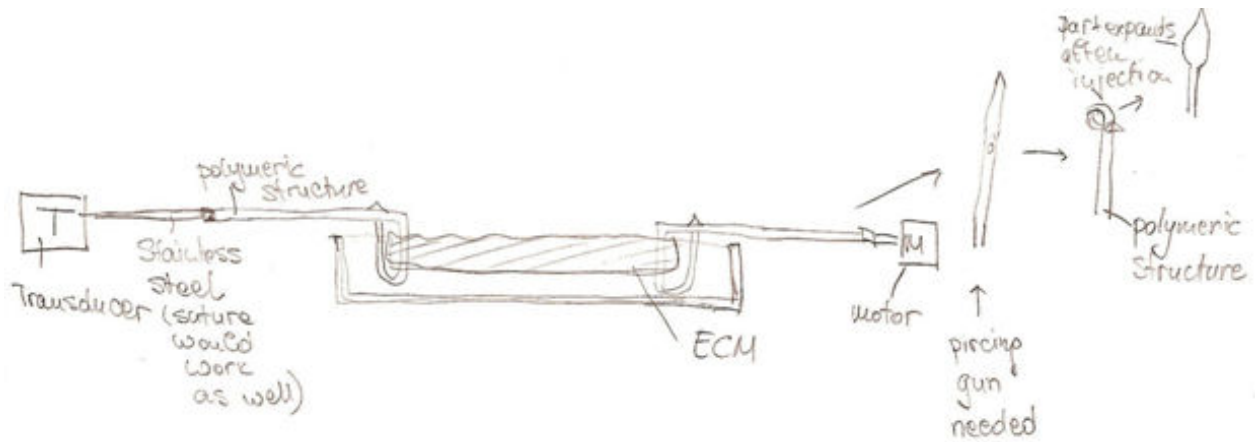


**Figure 59: Stud Gun Attachment Method**

An overall schematic of how linear motor cycling functions along with a punch attachment method. This punch method featured a stud gun to wrap stainless steel suture wire around the gel.

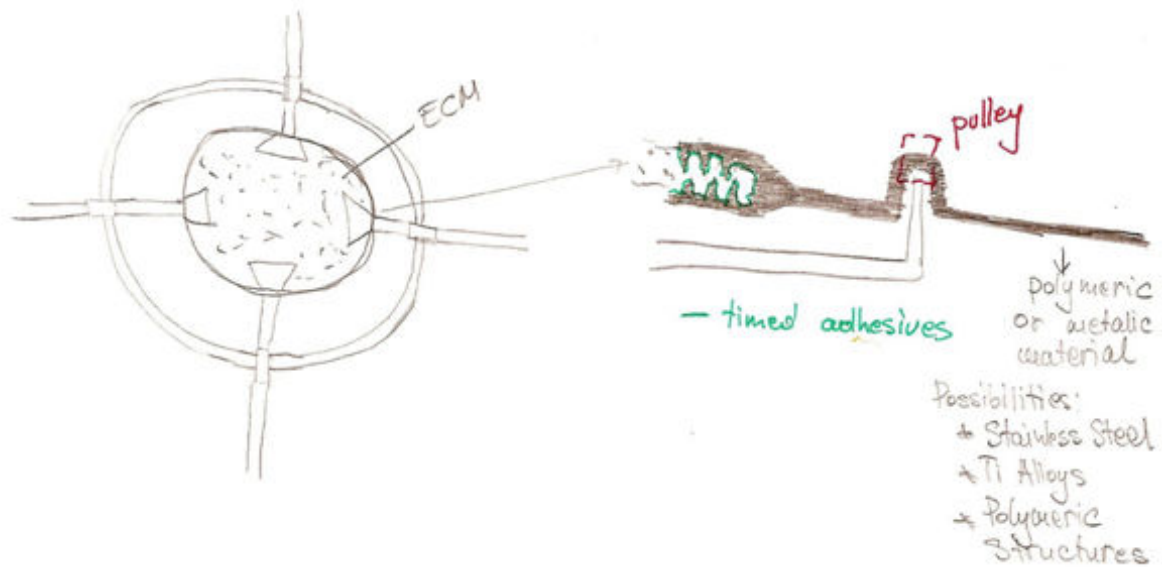


**Figure 60: Preliminary Clamping Sketch**

Preliminary designs of clamps and adhesives used for tissue attachment.

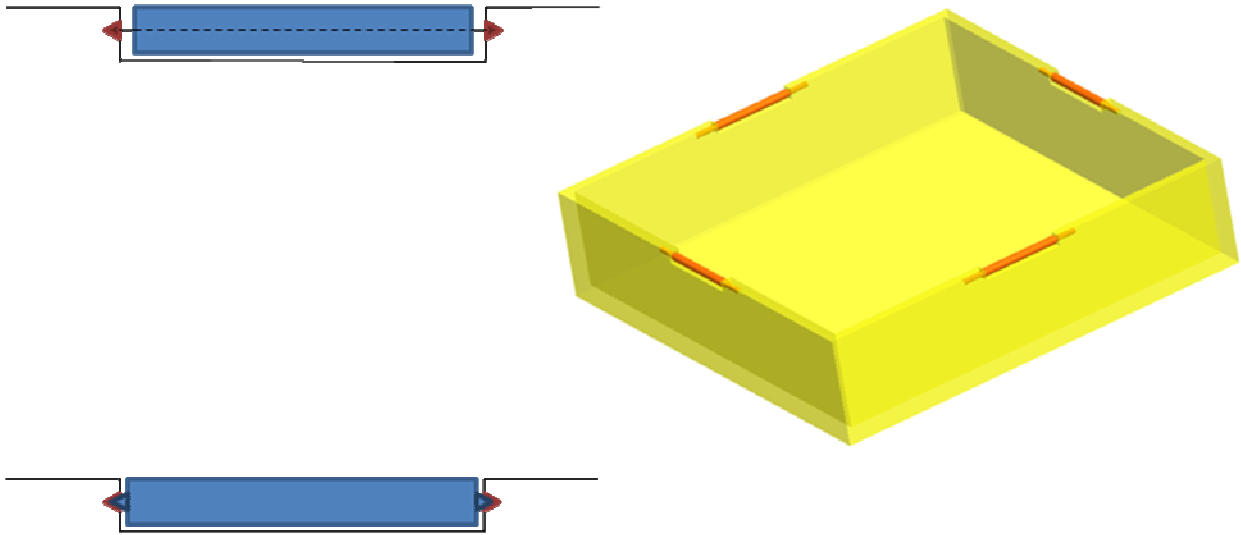


*Figure 61: Teflon Rollers*

In an attempt to offset frictional forces caused by the Lexan or stainless steel beams resting on the walls of the Plexiglass bath, Teflon rollers were added. Two attachment methods were considered.

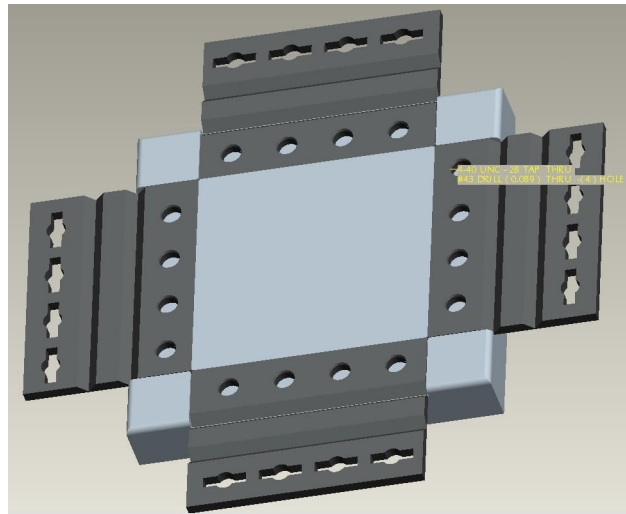


*Figure 62: Manufactured Clamp*

These clamps would be manufactured out of stainless steel and fit all of the objectives of the attachment methods. They were never produced.



## Appendix I: Parts List and Specifications

## Parts List

Part Number	Description	Company	Number	Price
	<b>Bath</b>			
*	6" Sterilized Petri Dish	Corning	x1	
	<b>Frame</b>			
1515-Lite	Aluminum Extruded Framework, 97", 1.5 lb per foot	Air Incorporated	x1	\$43.65
4332	2-Hole Inside Gusset Corner Bracket	Air Incorporated	x12	\$51.60
4307	2 Hole Joining Strip	Air Incorporated	x4	\$13.80
3320	Stainless 5/16 Fasteners	Air Incorporated	x30	\$18.00
----	Isonog Isolation Feet x4	Origin Live	x1	\$121.00
	<b>Motion</b>			
778417-01*	PCI 7334 Low cost stepper motion controller	National Instruments	x1	\$850.50
777936-01*	MID 7604, 4-axis integrated stepper driver power (115V)	National Instruments	x1	\$1,975.50
35DBM10B2B-K	35 mm Digital Linear Actuator	Portescap	x4	\$83.80
	<b>Force Measurement</b>			
FSH02319	10g Capacity Miniature S Beam Load Cell	Futek	x2	\$1,200.00
777459-37*	Signal conditioning module, SCC-SG24, 2-channel, full bridge, 10V excitation	National Instruments	x1	\$265.50
777458-02*	Signal conditioning carrier, SC-2345, hinged lid, universal AC)	National Instruments	x1	\$220.50
779066-01*	PCI 6221 M series multifunction DAQ, two 16 bit analog outputs	National Instruments	x1	\$427.50
	<b>Attachment Methods</b>			
*	Vascular Clamps	Biover	x2	
4485	Quick Change Collet Nut Set	Dremel	x4	\$8.50

\* were acquired free of cost

*Portescap Digital Linear Actuator*

DIGITAL LINEAR ACTUATORS | 35DBM-K SERIES

**35DBM-K** (Captive) SERIES

HIGHEST FORCE PER FRAME SIZE



**GENERAL SPECIFICATIONS**

Max Pull-in Rate* (Steps/Sec)	425
Power Consumption	5 Watts
Insulation Resistance	20MΩ
Bearings	Radial Ball
Weight	3 oz (85.2gm)
Operating Temperature Range	-20°C ~ 70°C
Storage Temperature Range	-40°C ~ 85°C

\* Measured with 2 phases energized

Formerly  
**K922-S SERIES**

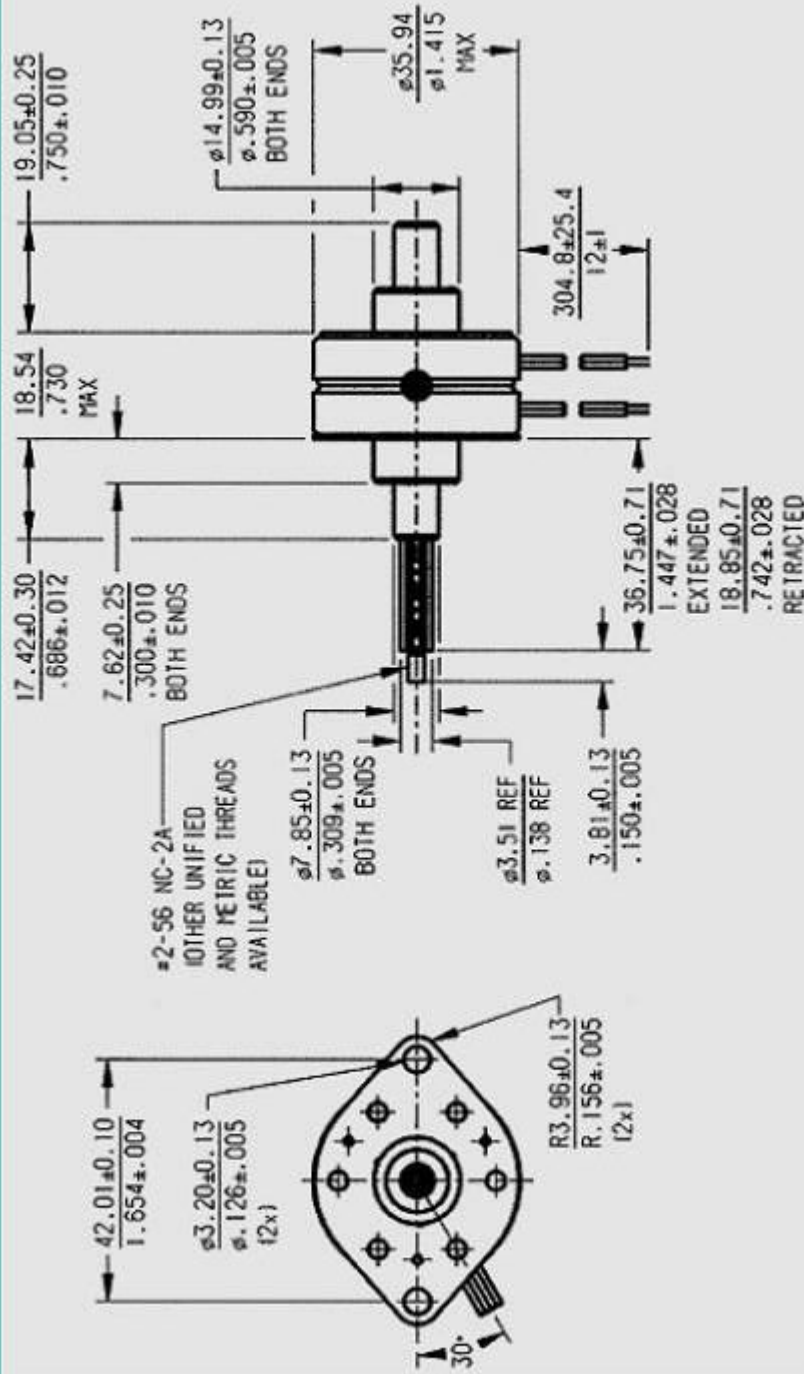


The specifications in this publication are believed to be accurate and reliable. However, it is the responsibility of the product user to determine the suitability of Portescap products for a specific application. While defective products will be replaced without charge if promptly returned, no liability is assumed beyond such replacement.

Portescap Danaher Motion motors will not be CE marked where the Low Voltage Directive, the Electro-Magnetic Compatibility or other appropriate EU directives are not applicable - this is an EU legal requirement.

MECHANICAL DIMENSIONS

UNITS = MM / INCHES



- Notes:
1. Not recommended to use at the fully retracted and extended positions.
  2. Shaft axial backlash: 0.15/0.006 MAX

DIGITAL LINEAR ACTUATORS | 35DBM-K SERIES

TECHNICAL SPECIFICATIONS

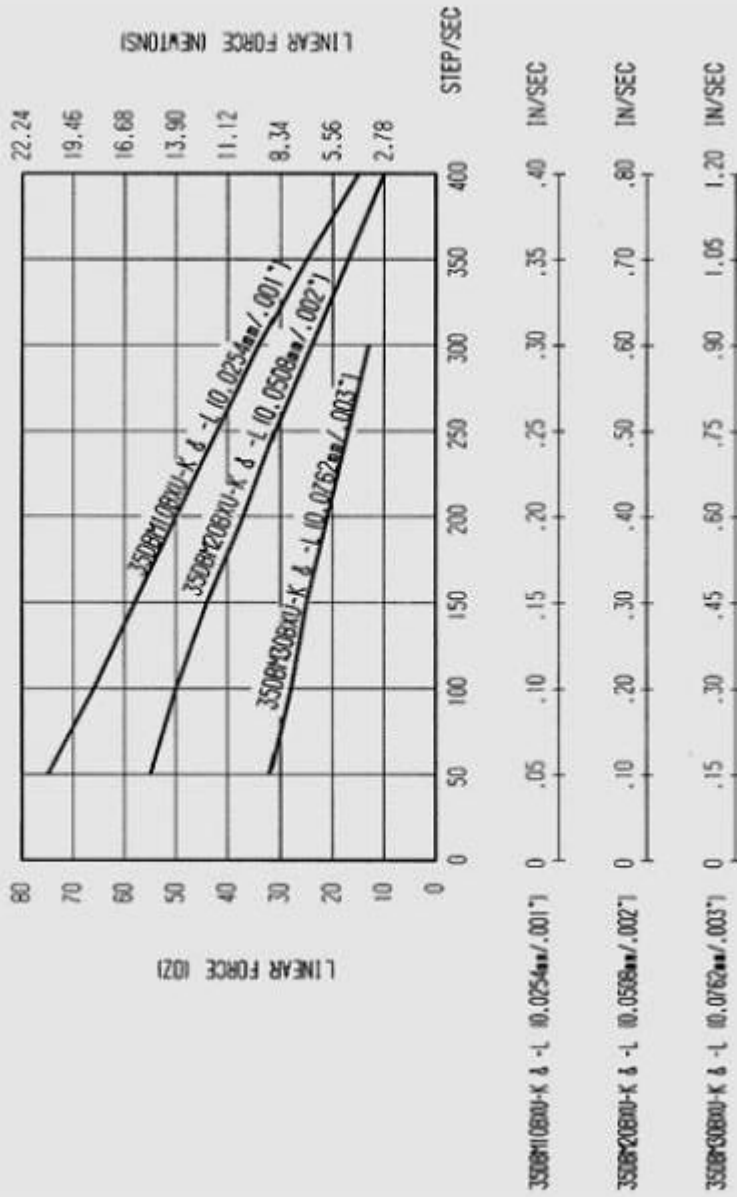
Part Number	DC Operating Voltage	Linear Travel Per Step*	Maximum Travel	Maximum Force*	Minimum Holding Force (Unenergized)
35DBM10B1U-K	5	.001" (0.0254mm)	.875" (22.2mm)	75 oz (20.9N)	40 oz (11.1N)
35DBM10B2U-K	12	.001" (0.0254mm)	.875" (22.2mm)	75 oz (20.9N)	40 oz (11.1N)
35DBM20B1U-K	5	.002" (0.0508mm)	.875" (22.2mm)	55 oz (15.3N)	10 oz (2.8N)
35DBM20B2U-K	12	.002" (0.0508mm)	.875" (22.2mm)	55 oz (15.3N)	10 oz (2.8N)
35DBM30B1U-K	5	.003" (0.0762mm)	.875" (22.2mm)	30 oz (8.3N)	5 oz (1.4N)
35DBM30B2U-K	12	.003" (0.0762mm)	.875" (22.2mm)	30 oz (8.3N)	5 oz (1.4N)

\* Measured with 2 phases energized

Coil Type	Unipolar
Coil Data	1U (5vdc) 2U (12vdc)
Resistance Per Phase	10Ω 58Ω
Inductance Per Phase	5.2mH Ref 30mH Ref



TYPICAL LINEAR PULL-IN FORCE vs LINEAR RATE AT 20°C



Note: Linear force is against opposite end of axial thrust spring

**Futek Miniature S Beam Load Cell**

**FUTEK MODEL LSB200 (L2357)**

**Drawing Number: FI1041-C**

**INCH [mm] R.O.= Rated Output**

WIRING CODE (WC1)

+Excitation	-Excitation	+Signal	-Signal
RED	BLACK	GREEN	WHITE
Shield			
FLOATING			

**S-BEAM JUNIOR LOAD CELL**

*DESIGNED FOR INLINE LOADING IN TENSION & COMPRESSION*

*AVAILABLE IN #4-40 AND M3x0.5 METRIC THREADS*

Stock #	Capacity lb (N)	Thread Size	R.O. (nom.)	BRIDGE RESISTANCE	SHUNT CAL. VALUE
FSH02534	10g	#4-40	0.5 mV/V	1000 Ω nom.	301K Ω
FSH02319	(0.1)	M3x0.5			
FSH02666	20g	#4-40			
FSH02667	(0.2)	M3x0.5			
FSH02535	50g	#4-40			
FSH02663	(0.5)	M3x0.5			
FSH02536	100g	#4-40	1 mV/V		150K Ω
FSH02664	(1.0)	M3x0.5			
FSH02602	250g	#4-40			
FSH02665	(2.5)	M3x0.5			
FSH00091	1	#4-40	2 mV/V	350 Ω nom.	
FSH00101	(4.5)	M3x0.5			
FSH00092	2	#4-40			
FSH00102	(8.9)	M3x0.5			
FSH00093	5	#4-40			
FSH00103	(22.2)	M3x0.5			
FSH00095	10	#4-40			
FSH00104	(44.5)	M3x0.5			
FSH00096	25	#4-40			
FSH00105	(111)	M3x0.5			
FSH00097	50	#4-40	60.4K Ω		
FSH00106	(222)	M3x0.5			
FSH00098	100	#4-40			
FSH00107	(445)	M3x0.5			

**SPECIFICATIONS:**

<p><b>RATED OUTPUT</b> SAFE OVERLOAD</p> <p><b>ZERO BALANCE**</b></p> <p><b>EXCITATION (VDC OR VAC)</b></p> <p><b>BRIDGE RESISTANCE</b></p> <p><b>NONLINEARITY</b></p> <p><b>HYSTERESIS</b></p> <p><b>NONREPEATABILITY</b></p> <p><b>TEMP. SHIFT ZERO</b></p> <p><b>TEMP. SHIFT SPAN</b></p> <p><b>COMPENSATED TEMP.</b></p> <p><b>OPERATING TEMP.</b></p> <p><b>MATERIAL</b></p> <p><b>WEIGHT</b></p> <p><b>DEFLECTION</b></p> <p><b>CABLE: #29 AWG, 4 Conductor, Spiral Shielded Silicone Cable, 5 ft [1.5 m] Long</b></p> <p><b>ACCESSORIES AND RELATED INSTRUMENTS AVAILABLE</b></p> <p><b>CALIBRATION (STD)</b></p> <p><b>CALIBRATION (AVAILABLE)</b></p> <p><b>CALIBRATION TEST EXCITATION</b></p> <p><b>*SENSOR STRUCTURE CAN HANDLE HIGH OVERLOADS BUT #4-40 and M3x0.5 THREADS MAY LIMIT OVERLOAD AT HIGHER CAPACITY</b></p> <p><b>** ZERO BALANCE IS BASED ON LAYING SENSOR ON ITS SIDE (THREADS HORIZONTAL)</b></p>	<p><b>SEE CHART</b> 1000% of R.O.</p> <p>200% of R.O. Tension Only (50-100 lb)*</p> <p>±3% of R.O., ±5% of R.O. (10-20g)</p> <p>10 Max</p> <p><b>SEE CHART</b></p> <p>±0.1% of R.O.</p> <p>±0.1% of R.O.</p> <p>±0.05% of R.O.</p> <p>±0.01% of R.O./°F [0.018% of R.O./°C]</p> <p>±0.02% of LOAD/°F [0.036% of LOAD/°C]</p> <p>60 to 160°F [15 to 72°C]</p> <p>-60 to 200°F [-50 to 93°C]</p> <p>ALUMINUM (10g-10lb), STAINLESS STEEL (25-100lb)</p> <p>0.3 oz [9 g]</p> <p>0.003-0.005 [0.07-0.13]</p>
--	--

10 THOMAS  
IRVINE, CA 92618 USA  
1-800-23-FUTEK (38835)

INTERNET:  
<http://www.futek.com>

*Air Incorporated Aluminum Extruded Framework*

Extruded Profiles

**1515-Lite**



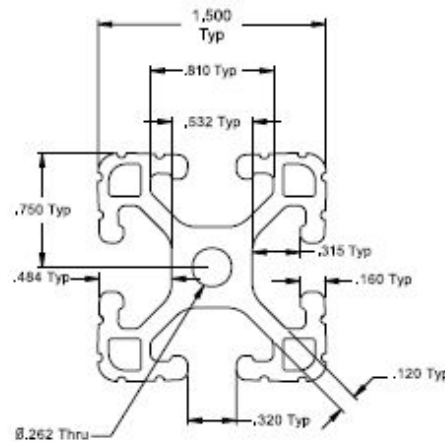
**VIBRATION  
PROOF**

Material	6105-T5
Finish	Clear Anodized
Weight Per Foot	1.5408 Lbs.
Stock Length *	97" +/- .125"
	145" +/- .125"
	242" +/- .125"
Moment Of Inertia	IX= .0789" <sup>4</sup>
	IY= 1.0672" <sup>4</sup>
Estimated Area	1.3237 Sq. In.

\* Request other lengths to match your specs with our Cut to Length Service (PIN 7010) on page 356.

1515-Lite was developed for applications with lighter weight and strength requirements than our heavier wall extrusions.

The 1515-Lite version is ideal for lighter load bearing structures, guarding, and light weight frames.



Office Furniture



**1515-Lite Machining Service Quick Reference**

Cut to Length Service Number .....	7010
Drill .295" Access Hole .....	7050
Anchor Fastener Counterbore .....	7040
Tap Extrusion End (5/16-18) .....	7060

Additional machining services can be found on pages 356-360.

Phone: 260-248-8030 • Fax: 260-248-8029  
www.8020.net

## Stepper and Servo Motor Drives

### NI MID-7604, NI MID-7602

- High-efficiency, bipolar chopper stepper drives
- User-selectable microstepping and peak current
- Integrated power supply
- CE approved and UL recognized

### NI MID-7654, NI MID-7652

- High-efficiency servo amplifiers
- User-selectable peak current and continuous current
- Integrated power supply
- CE approved and UL recognized



### Overview and Applications

The National Instruments MID-760x integrated stepper motor power drives and MID-765x integrated DC-brush servo motor power drives offer reliable, easy-to-connect drive solutions for National Instruments motion controllers. The NI MID-760x provides stepper motor control from the NI 7330, 7340, and 7350 controllers. The MID-7650 provides DC-brush servo motor control from NI 7340 and 7350 controllers. Because the MID-760x and the MID-7650 have all the required motion drive and motion I/O signals, they offer all the features of a universal motion interface wiring module with the enhancements of a powered motor drive in a single product. The NI MID power drives connect to motion controller boards through a single-shielded cable that transfers all motor commands, as well as motion I/O control and feedback signals.

The MID-7604 and MID-7602 are 4-axis and 2-axis stepper motor drive units, respectively. The MID-7654 and MID-7652 are 4-axis and 2-axis DC-brush servo motor drive units, respectively.

These compact, well integrated drives incorporate per-axis amplifiers, motor-power DC bus supplies, low-voltage motion I/O supplies, and pluggable screw terminal connectivity in a single rugged metal enclosure. This optimized system wiring design simplifies motion component selection.

### High-Efficiency Architecture

The MID-760x power drives incorporate an efficient bipolar chopper architecture that converts step and direction control signals into winding currents for 2-phase stepper motors. The MID-765x power drives incorporate an efficient servo amplifier architecture that converts analog control signals into winding currents for DC-brush motors. The pulse width modulation driver technology in the MID-765x accurately controls motor winding current, while reducing motor heating, lowering ripple current, and improving overall motor performance. Active fan cooling provides optimal motion power drive operation.

Model	Stepper	Servo	NI 7330	NI 7350 NI 7340	(V)	Motor Drive (A)	Compact Current/Axis Diagnostic LEDs	Front Panel Enclosure and Microstepping	Front Panel Selectable Peak Current	Selectable Axes
MID-7604	✓	-	✓	✓	24	0.2 to 1.4	✓	✓	✓	4
MID-7602	✓	-	✓	✓	24	0.2 to 1.4	✓	✓	✓	2
MID-7654	-	✓	-	✓	48	0.8 to 5 continuous 10 peak	✓	-	✓	4
MID-7652	-	✓	-	✓	48	0.8 to 5 continuous 10 peak	✓	-	✓	2

Figure 1. Stepper and Servo Motor Drive Features



## Portable, Shielded SCC Module Carriers

SCC Carriers

### NI SC-2345 Series

- Shielded carriers for up to 20 SCC modules
- Portable, low-profile packaging
- Cables directly to an E Series or Basic multifunction DAQ device
- Powered by DAQ device (additional power options available)

#### SC-2345 Connector Block

- Strain relief for signal wiring
- Hinged lid for easy access

#### SC-2345 Carrier with Configurable Connectors

- Panelettes for sensor connectivity
- Panelettes for control and display
- Blank panelettes for filler

#### Operating Systems

- Windows 2000/NT/XP

#### Recommended Software

- LabVIEW
- LabWindows/CVI
- Measurement Studio
- Lookout
- VI Logger

#### Other Compatible Software

- Visual Basic

- C/C++, C#

#### Driver Software (included)

- NI-DAQ 7



### Overview

The National Instruments SC-2345 Series consists of two types of carriers, the SC-2345 connector block and the SC-2345 with configurable connectors. These enclosures for SCC signal conditioning modules connect directly to 68-pin DAQ devices. They include sockets for SCC modules, along with screw terminals for convenient connection to digital I/O and counter/timer (GPCTR) signals from the DAQ device. These carriers offer three power options to increase the flexibility of deployment.

Data Acquisition and Signal Conditioning

### SC-2345 Connector Block

The SC-2345 includes 20 SCC sockets, labeled J1 through J20 (see Figure 1). Sockets J1 through J8 accommodate SCC modules for conditioning signals on the analog input channels of the DAQ device. For example, an SCC module plugged into socket J1 conditions signals for channels 0 and 8 of the device.

You can use sockets J9 through J16 for either digital I/O modules or dual-stage analog input conditioning. When using dual-stage conditioning of analog inputs (for applicable modules), wire your input signal to the first-stage module (in sockets J9 through J16). The SC-2345 routes the output signal of the first-stage SCC module to the input of the second stage SCC module internally (see Figure 2). When using sockets J9 through J16 for digital I/O, simply plug in a digital SCC module or the SCC-FT01 for custom digital applications. You can use any combination of SCC digital input or digital output modules. The digital I/O lines of E Series or Basic multifunction DAQ devices are configurable for input and output on a line-by-line basis. You can also access the DIO lines of the DAQ device using the screw terminal block.

Sockets J17 through J20 access the two analog output channels and the GPCTR channels 0 and 1.

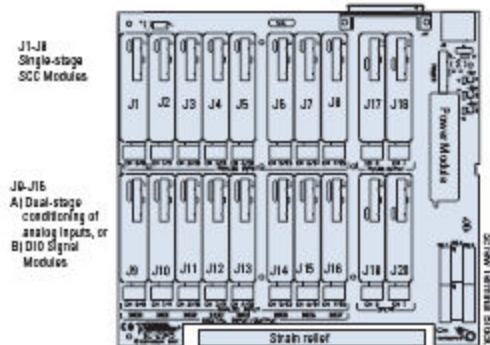


Figure 1. Diagram of Socket Layouts on SC-2345 Connector Block

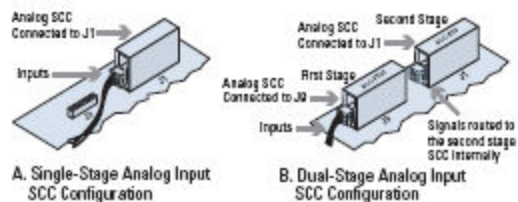


Figure 2. Single-Stage and Dual-Stage Analog Input SCC Configuration for the SC-2345 Connector Block

## *Isonoe Isolation Feet*



The Isonoe Isolation System is sold in packs of 4 isolators.

Each isolator has a 6mm thread, making the system compatible as a retrofit with many industry-standard turntables and CD players.

The Isolation Feet are equally effective at blocking the ingress of vibration from the mechanical assemblies of both turntables and CD players; the more isolation from vibration afforded to the optical tracking mechanism within a CD player, the less work needs to be performed by the error-correction software, preserving detail and spatial integrity.

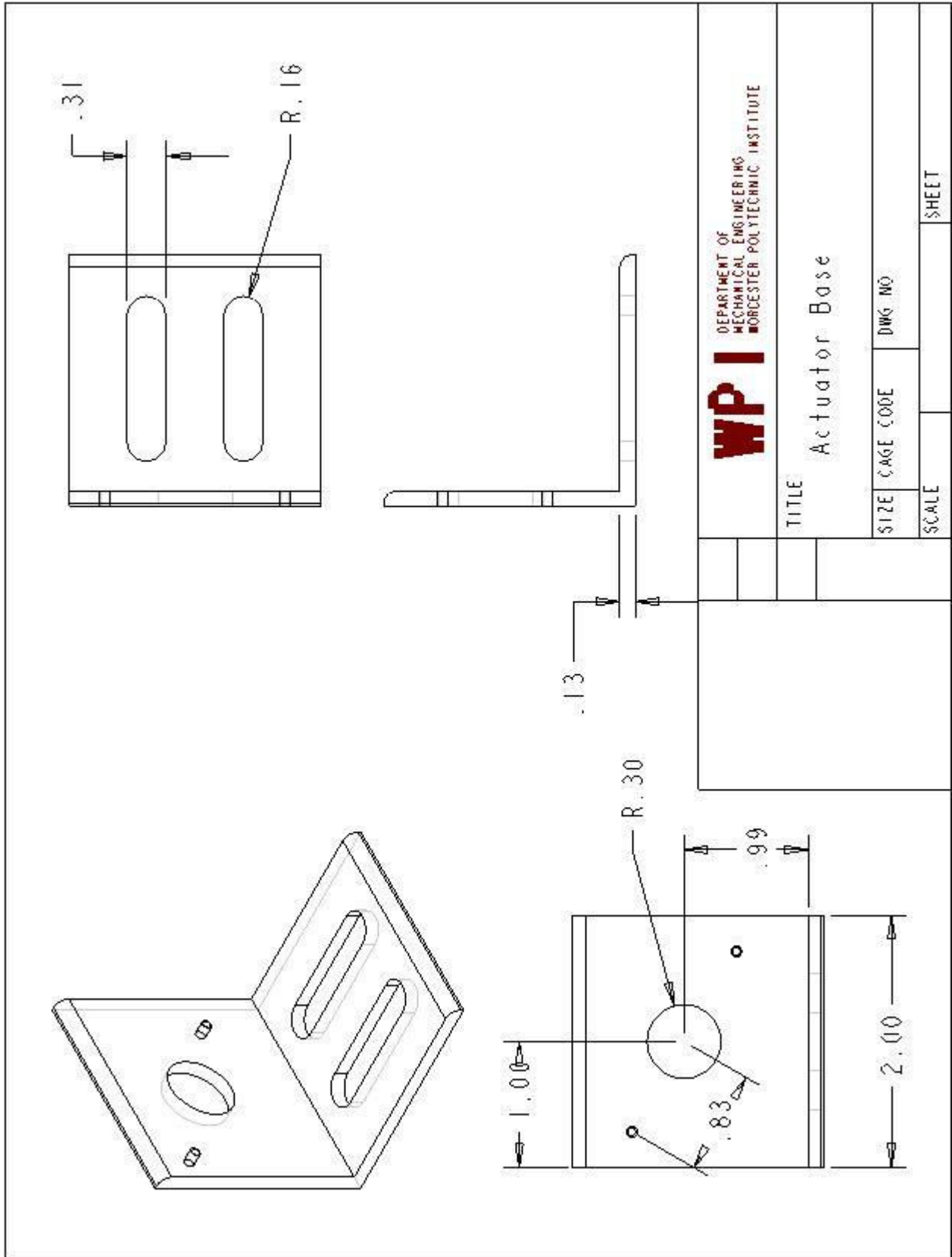
Accompanying Sorbothane Boots are also available to seat the bearings and maximise isolation (Sorbothane is a renowned polymer within the medical, aerospace and hi-fi industries, originally designed to mimic the vibration absorbing properties of human flesh).

A standalone isolation platform is due for imminent release.

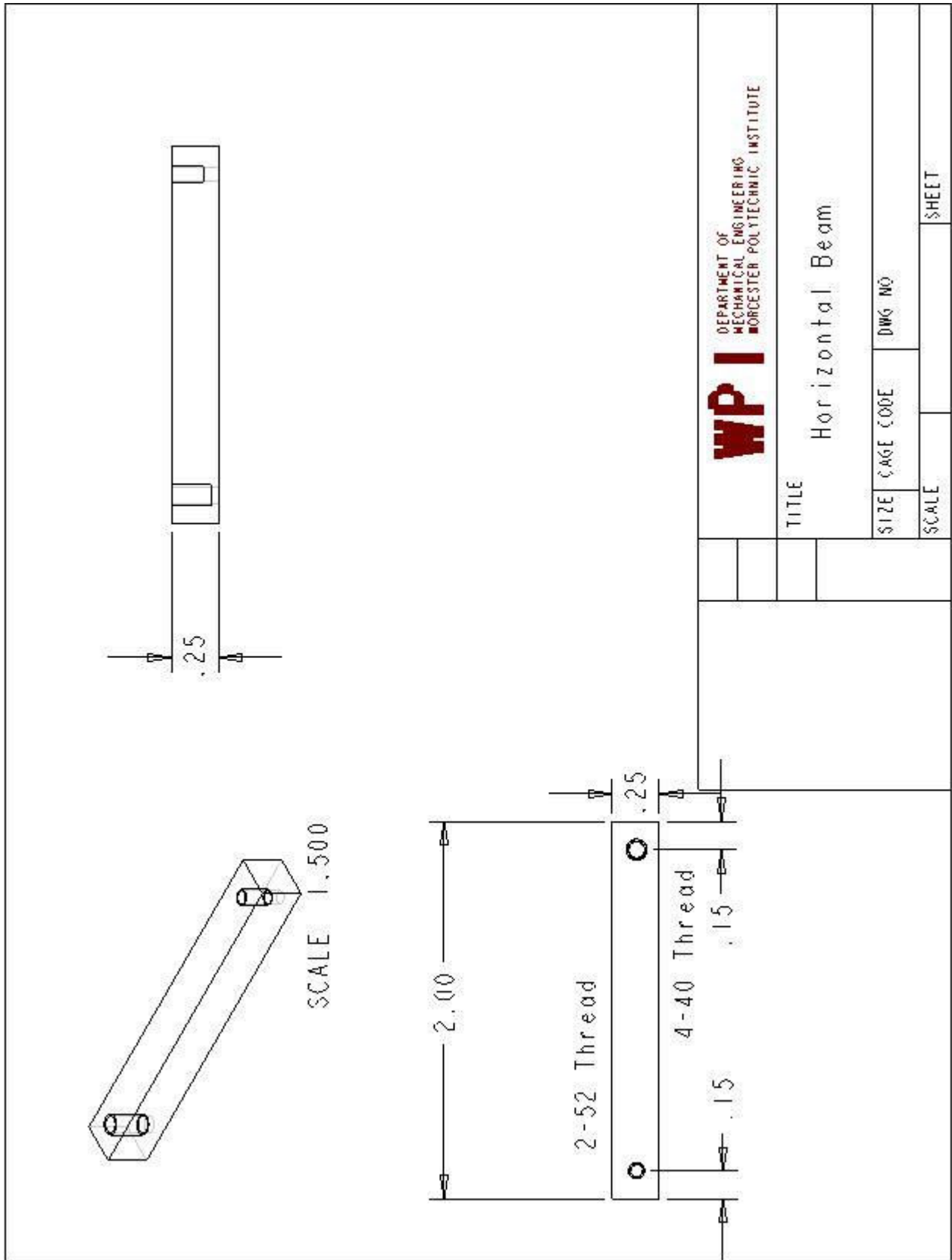
The Isonoe Isolation System is machined in the UK at a specialist engineering facility on multi-axis CNC equipment typically costing upwards of a quarter of a million pounds per machine

**Appendix J: Manufactured Parts**

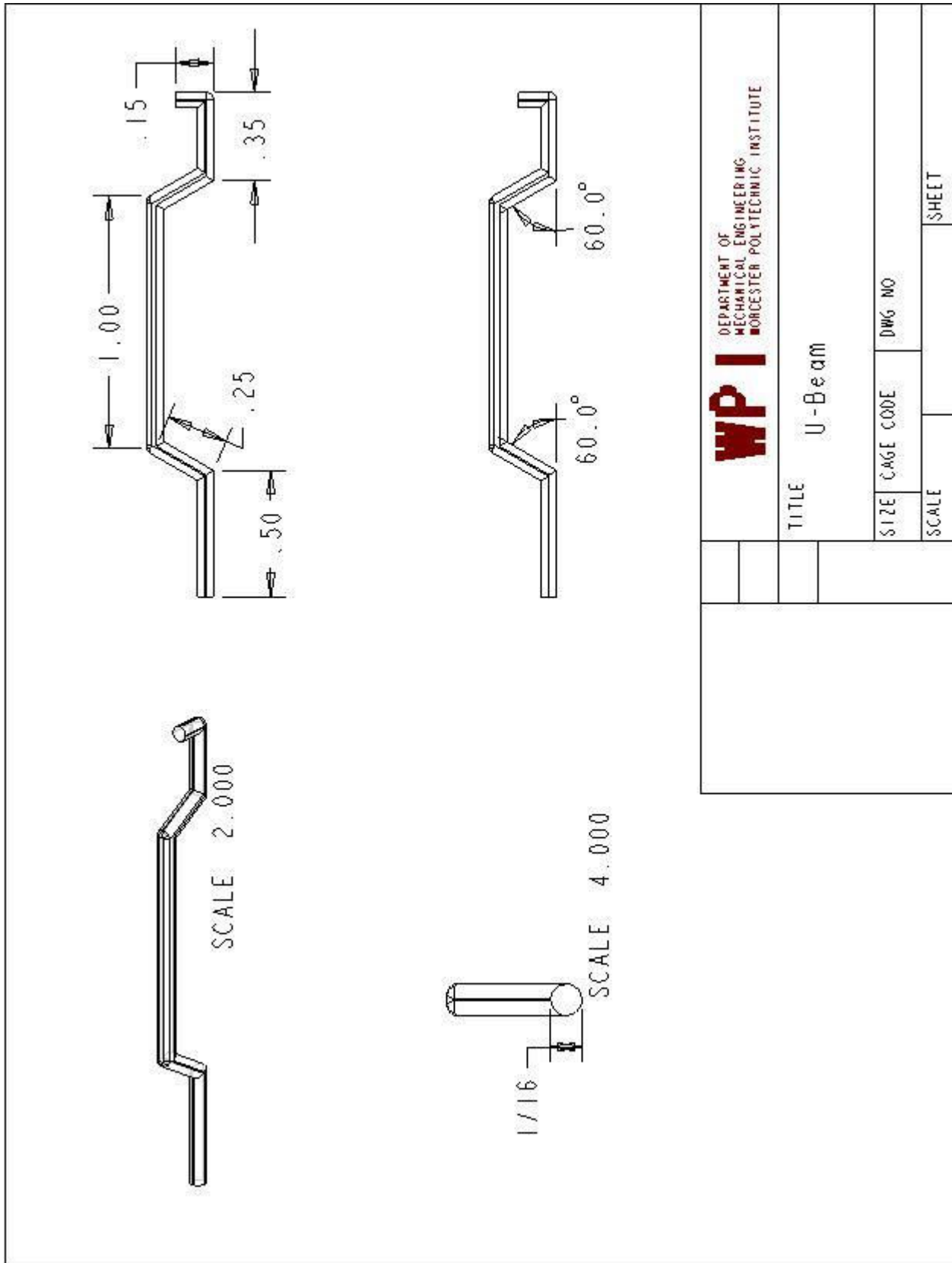
**Actuator Base**




*Horizontal Extension Beam*

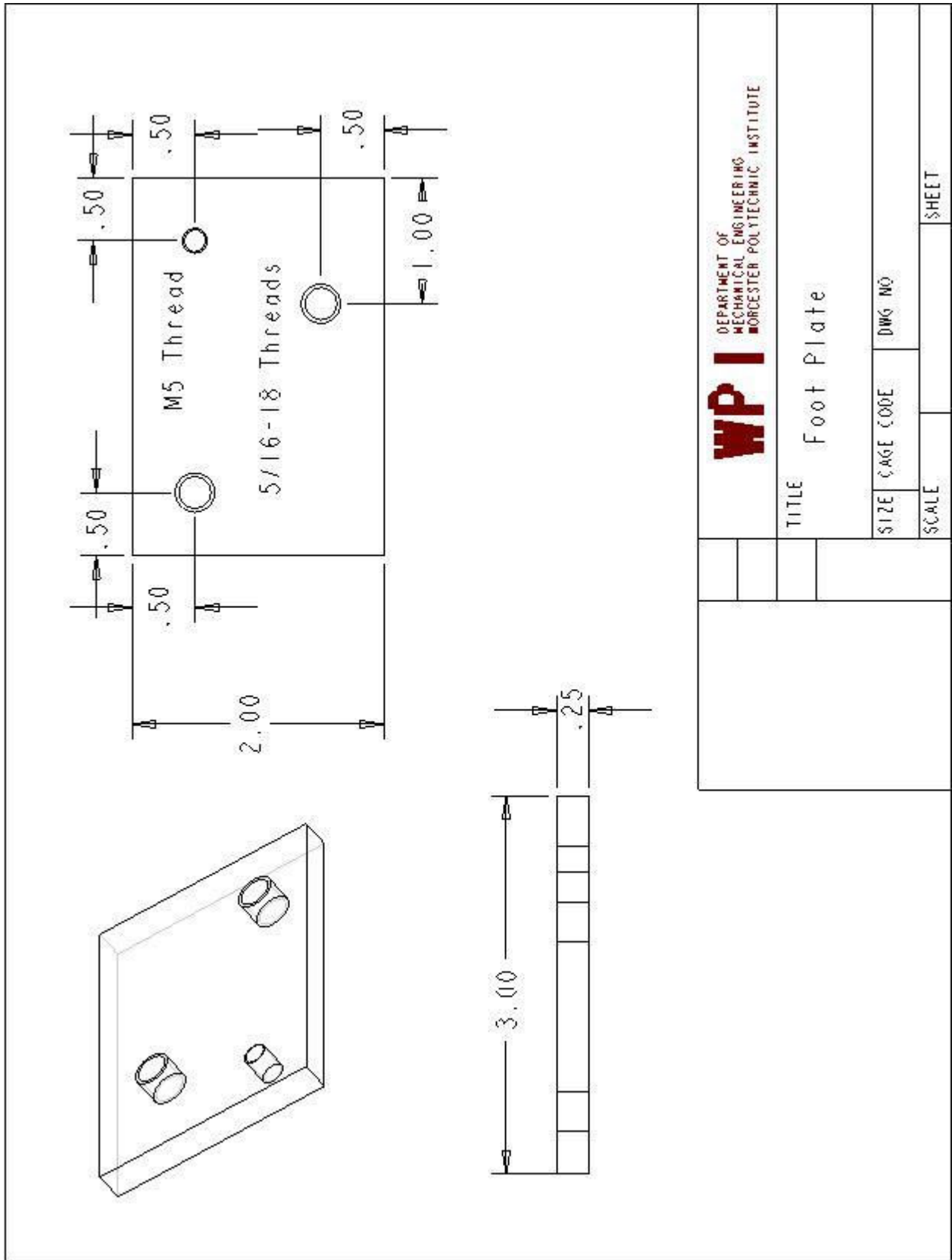



**U-Beam**



 DEPARTMENT OF MECHANICAL ENGINEERING WORCESTER POLYTECHNIC INSTITUTE		TITLE		SHEET	
		U-Beam		SIZE	DWG NO
SCALE		SCALE		SCALE	

**Foot Plate**



 DEPARTMENT OF MECHANICAL ENGINEERING WORCESTER POLYTECHNIC INSTITUTE		TITLE		SHEET	
		Foot Plate		SIZE	DWG NO
SCALE		DWG NO		SHEET	

## ***Appendix L: Methodology Protocols***

### ***Acellular Collagen Gel Contraction***

Purpose: To collect force data on acellular collagen gels, and verify that the load cell could measure forces of collagen retraction during polymerization within an incubator. Experiment also allowed for optimization gel handling procedures.

#### **Materials:**

5mg/ml RTT Collagen

5X DMEM

#### **Procedure:**

1. Followed protocol in laboratory notebook KLB026-004 from the laboratory of Kristen Billiar at Worcester Polytechnic Institute for collagen gel protocol.
2. Porous polyethylene anchors of 38 $\mu$ m porosity were cut into strips and placed into the channel.
3. 4ml of 5 mg/ml collagen was cast into the device
4. Gels were cast into 60mm petri dishes that had PDMS cured with at 25mm channel in which to pour and polymerize the gel.
5. After 5 minutes, gel was topped with 5ml of media.
6. After 3 hours in the incubator the gel was cut from the PDMS channel with a scalped and vascular clamps were attached to the porous polyethylene anchors
7. A Saline bath was prepared and filled into a larger 6 inch Petri dish that was fixed to the device and the clamped gel was placed in the bath

8. Silk sutures connected to the clamps were looped over the ends of the u-beams and the actuator was used to apply pretension to return the gel to 25mm across, including the width of the anchors.
9. Force measurement data was then recorded

### ***Validation of Uniaxial Force Measurement in Cell Populated Collagen Gels***

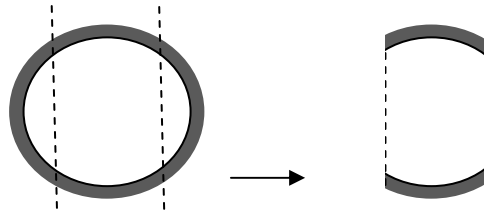
Protocol and procedure for uniaxial validation attempts (Testing protocol adapted from Eastwood, Brown 1994), (Cell seeded collagen gel protocol from Laboratory notebook KLB026-073)

1. Add 0.44 ml of 5X DMEM, 0.34 ml FBS, and 0.88 ml NAOH to a 50 ml conical tube
2. Using a 1 ml pipette, aspirate cell solution at least 20 times to distribute cells homogenously throughout the solution. Solution at  $4.5 \times 10^6$  cells/ml
3. Add 4.4 ml of 5mg/ml collagen and 0.98 ml cell solution simultaneously to the 50 ml conical tube
4. Aspirate the gel mixture using a 10 ml pipette until thoroughly mixed and solution has a homogenous pink color
5. Pull gel mixture into a 10 ml pipette, being careful to avoid excess bubbles, case into petri dish set up in device in the incubator.
6. Start data collection for 1 hour
7. At 1 hour add 5ml of media



***Protocol and Procedure for Fetal Fibroblast vs. IPF***

1. Gels were cut from Flexcell plates and two parallel cuts were made to the circular gels to create 2cm wide samples shown below:



2. A 150 ml saline bath was pured into a 6 inch petri dish. This was used to suspend the gel in a warm bath during testing.
3. The gels were then loaded onto the device by placing vascular clamps on the remaining porous polyethylene anchor, shown above in grey. Styrofoam beads were attached to the anchors to float them in the bath.
4. Samples were stretched to their original diameter for 30 minutes.
5. After 30 minutes, 0.5 mL of 90mM KCL was added to the bath and data was recorded for another 30 minutes.